University of Alberta

Spontaneous Imbibition and Solvent Diffusion in Fractured Porous Media
by LBM

by

Akshay Chandrashekhar Gunde

A thesis submitted to the Faculty of Graduate Studies and Research
in partial fulfillment of the requirements for the degree of

Master of Science

Department of Mechanical Engineering

Abstract

Enhanced oil recovery (EOR) from naturally fractured reservoirs (NFR's) involves the injection of external agents into the fracture networks to extract the resident crude oil in the matrix. Characteristically, these agents displace the oil by diffusion (if miscible) or spontaneous imbibition (if immiscible). The present work performs two-dimensional simulations of these processes at the pore-scale and extends the results to core-scale by using the Lattice Boltzmann method (LBM). Simulations of miscible recovery of kerosene and light mineral oil by injection of pentane are performed to observe the displacement profiles. The LBM model is then extended to simulate the co-current and counter-current spontaneous imbibition of water in a kerosene saturated water-wet sand pack. The oil-water interface development is analyzed at the pore-scale, and the saturation profiles are compared with experiments from literature. Two-phase relative permeabilities of the displacement processes are determined, and their dependence on various physical parameters is studied.

Acknowledgements

Contents

---

[1]Parts of this chapter have been submitted for publication: *(a) A. Gunde, B. Bera, S. K. Mitra, Investigation of Water and CO_2 (carbon dioxide) flooding using micro-ct (micro-computed tomography) images of berea sandstone core using Finite Element simulations. Energy, 35(12): 5209-5216, 2010 (b) A. Gunde, T. Babadagli, and S. K. Mitra. A generic framework to obtain oil-water relative permeability for capillary driven transport in water-wet fractured porous media by LBM (submitted). Water Resources Research (c) A. Gunde, T. Babadagli, S. Roy, and S. K. Mitra. Pore-scale interfacial dynamics and oil-water relative permeabilities of capillary driven counter-current flow in fractured porous media (submitted).*

---

[2]Parts of this chapter have been submitted for publication.

[3]Parts of this chapter have been submitted for publication: *A. Gunde, T. Babadagli, and S. K. Mitra. A generic framework to obtain oil-water relative permeability for capillary driven transport in water-wet fractured porous media by LBM (submitted). Water Resources Research.*

---

[4]Parts of this chapter have been submitted for publication: *A. Gunde, T. Babadagli, and S. K. Mitra. A generic framework to obtain oil-water relative permeability for capillary driven transport in water-wet fractured porous media by LBM (submitted). Water Resources Research.*

[5]Parts of this chapter have been submitted for publication. *A. Gunde, T. Babadagli, S. Roy, and S. K. Mitra. Pore-scale interfacial dynamics and oil-water relative permeabilities of capillary driven counter-current flow in fractured porous media (submitted).*

List of Figures

List of Tables

Chapter 1

Introduction

1.1 Overview

Enhanced oil recovery (EOR) (or tertiary oil recovery) has been the focus of research and development, on account of an incessant increase in oil prices, and a simultaneous advancement in oil extraction technology. Traditional oil recovery techniques such as extraction using natural reservoir pressure (primary) and injection of water and other agents into oil reservoirs (secondary), have been found to leave a majority of the oil in residual form. Hence, after primary and secondary oil recovery techniques are exhausted, EOR techniques are resorted to, to recover certain portion of the residual oil. These techniques include injection of chemicals, gases and solvents into the reservoirs to reduce the interfacial tension, and increasing the mobility of crude oil by reducing its viscosity using methods such as steam injection and CO_2 dissolution.

The injection of external agents into naturally fractured reservoirs (NFR's), as part of the oil recovery process, is more challenging. These reservoirs contain fracture networks, which are formed by natural processes such as chemical dissolution and tectonic activity; and are comprised of fracture channels with dimensions ranging from kilometers to a few microns in width. The injected fluids in these fractures come in contact with porous material of the reservoir rock, and undergo physical interactions with crude oil residing in the pore spaces. These interactions can be immiscible or miscible depending upon the type of injected fluid, resident oil and physical conditions. An important area of study in this respect is the injection of partly miscible CO_2 in the fracture networks; which can serve the dual purpose of oil recovery and CO_2 storage in the reservoir rocks as a means to carbon sequestration.

The fluid transport taking place within a reservoir rock is dependent on the type of porous material, resident oil and injected fluid. In case the two fluids under consideration are immiscible, wettability considerations play an important role in determining the nature of flow and the efficiency of oil recovery. An injected fluid, which is wetting in nature with respect to the porous material, can imbibe into the pore structure from the fracture, on account of capillary forces and displace the resident oil. This process is generally referred to as 'spontaneous imbibition'. In case the two fluids are miscible, the fracture fluid can diffuse into the porous material and expel the resident oil after changing its compositional characteristics. This process is referred to as 'solvent diffusion'. Both these displacement processes can take place while the fluid residing in the fractures is at rest, without any pressure force acting on it, which is described as static condition.

These processes need to be modeled experimentally and numerically not only to assess their applicability in reservoir conditions but also to clarify the physics of the process. The latter requires more pore- (micro) scale simulations and yet models available are limited to capture the complex physical interactions of the EOR processes in NFR's. A number of commercial reservoir simulators and numerical tools have been developed e.g. Eclipse (Schlumberger), CMG (Computer Modeling Group), Visage etc. These tools perform the core- and field- scale analyses of various extraction processes. However, in order to quantify and qualify the actual fluidic mechanisms taking place inside the porous structures, pore-scale numerical simulations have to be performed; which involve multi-phase fluid flow modeling inside the typically micron-sized pores. Such modeling can make use of traditional continuum CFD methods like Finite Element, Finite Volume and Finite Difference. Specialized numerical methods like Random Walk, Invasion Percolation, Diffusion Limited Aggregation are also being used for pore-scale modeling rather than field-scale applications. However, due to the micron-sized dimensions of the flow domains, the intricate physical processes involved, and the highly complex boundaries encountered in a heterogeneous porous reservoir rock, these techniques possess certain limitations for such simulations.

In addition to the continuum models described above, various non-conventional numerical techniques like Lattice Boltzmann method (LBM), Monte-Carlo method, Molecular Dynamics simulations are being increasingly used in order to model fluid flow situations at the micron-scale. The LBM is known as

a meso-scalic technique, since it combines the approaches of continuum and discrete models. In addition to being a simple numerical tool, the LBM has inherent advantages in dealing with the required fluid flow scenario because of its relative ease in dealing with complex boundaries without much additional computational expense, simplicity of the mathematical model, applicability to multi-phase flows and direct inclusion of wettability effects. Hence, the present work uses the LBM as a numerical simulation technique, in order to study spontaneous imbibition and solvent diffusion processes at the pore-scale. The results obtained from the LBM simulations of oil recovery processes have to be analyzed at the pore-scale and extended to the core-scale, so that they can be applied in the case of relevant recovery applications.

1.2   Statement of the problem

Spontaneous imbibition (immiscible) and solvent diffusion (miscible) oil recovery processes constitute an important aspect of tertiary oil recovery. Numerical modeling of these mechanisms has to be performed at the pore-scale using multi-phase fluid flow in a porous geometry which is representative of the actual porous structures found inside a reservoir rock. The mathematical model used for the simulations is required to take into account, physical phenomena encountered in these cases of multi-phase fluid flows, such as interfacial tension and wettability in the case of immiscible, and diffusion characteristics in case of miscible fluids. Results of these simulations should be analyzed at the pore-scale in order to study the nature of fluidic interactions.

Experiments have been performed in literature at the laboratory-scale involving these oil recovery processes, in order to study their quantitative and qualitative nature. These experiments involve the use of artificial sand pack models comprised of glass beads packings. The results obtained from the numerical simulations have to be compared with such experimental results in literature. An important factor considered in these processes is the nature of saturation profile of the invading phase in a two-dimensional displacement scenario. The core-scale saturation profile is a representative of the actual physical processes in the pores and can provide information about the residual oil, and hence the efficiency of the displacement process. Analysis of the saturation profile at different instants of time and for different physical parameters can lead to the characterization of different displacement processes.

Specific to the EOR processes observed in NFR's, it has been observed that the characteristics of oil displacement from a porous matrix depends on various physical parameters such as boundary conditions, fluid properties, matrix orientation with respect to the vertical, matrix shape and size. Two important types of displacement situations have been identified based on the boundary conditions. If the displacement of resident oil takes place through a boundary which is opposite to (or different from) the boundary from which the fluid in the fracture enters the porous matrix, it is called co-current displacement. If the displacement of oil takes place through the same boundary from which the fracture fluid enters the porous matrix (because of the other boundaries being closed), it is called counter-current displacement. These two situations are frequently encountered in actual practice. Hence, the fluid saturation profiles have to be observed for the co- and counter-current displacements, so that a relative comparison can be made.

In immiscible displacement, in order to quantify the nature of oil displacements, two-phase relative permeability analysis is generally performed, which provides important data regarding the mechanism of the processes to be eventually used in field-scale modeling applications. However, there is insufficient literature on the spontaneous imbibition relative permeability analysis using LBM. Also, the effect of physical conditions such as fluid properties, boundary conditions and orientation etc. on the relative permeability curves is not known. Such an analysis can provide important information regarding the nature of spontaneous imbibition process and facilitate the extension of pore-scale results to core- and reservoir-scale.

1.3   Outline of thesis

In light of the described problem statement, the presented work performs multi-phase pore-scale fluid flow simulations of spontaneous imbibition and solvent diffusion oil recovery processes using the numerical methodology of Lattice Boltzmann method.

Chapter 2 contains a review of the existing literature on oil recovery processes and a description of the various LBM techniques used for the simulation of multi-phase flow. In Chapter 3, a single phase LBM algorithm is developed and applied to single-phase flow simulations through porous media, wherein the Darcy's law is verified. A randomly generated porous grid is used, in order

to emulate a two-dimensional sphere packing. The Bhatnagar-Gross-Krook (BGK) approximation is used to determine the collision parameter.

In Chapter 4, the developed LBM model is extended to the simulation of two miscible fluids, with the capability of simulating diffusion and advection transport processes by using two independent collision parameters based on the diffusion co-efficient and viscosity of the fluids, respectively. The model is based on the lines of the methodology proposed by Flekkoy [7]. The algorithm is applied for miscible oil recovery by solvent diffusion in a sand pack model. The displacement profiles of the solvent pentane are observed entering the porous matrix and displacing kerosene and mineral oil under static and dynamic conditions. A vertical simulation is performed incorporating the effect of gravity. The profiles are compared with experimental results from literature and a reasonable agreement is observed.

In Chapter 5, the LBM model is further developed to model two immiscible fluids by the inclusion of interfacial tension and wettability, using the Two-Color model proposed by Gunstensen and Rothman [8] and further improved by Latva-Kokko and Rothman [9], [3]. In Chapter 6, the model is applied to simulate the co-current spontaneous imbibition of water in a kerosene saturated water-wet sand pack for different physical conditions. The saturation profiles observed for gravity-assisted and gravity-opposed configuration are compared with experiments from literature and a reasonable agreement is observed. Pore-scale interfacial dynamics is studied for different contact angles. A relative permeability analysis is performed and the values are compared with literature for a specific case. The relative permeability variation is studied for different values of interfacial tensions, contact angles, viscosity ratios, matrix orientation and matrix shape, and are observed to reflect the physical processes inside the porous medium.

In Chapter 7, the immiscible LBM model is applied to a counter-current spontaneous imbibition of water into a sand pack displacing kerosene in horizontal configuration and the saturation profiles are compared with experiments from literature. The pore-scale interfacial dynamics are observed during the invasion of water and expulsion of kerosene from the same boundary through pores of different sizes. The counter-current relative permeability analysis is performed for different physical parameters and compared with the corresponding co-current values.

Chapter 8 contains a summary of major conclusions from the numerical

analysis of oil recovery processes. A review of undergoing developments in
LBM techniques is discussed and the scope for future advancements is pre-
sented.

Chapter 2

Literature Review [1]

2.1 Oil recovery processes

2.1.1 Flooding

A crude oil reservoir is a naturally formed heterogeneous porous medium in which oil resides inside the pores of the reservoir rock structure. Extraction of oil by primary techniques using natural pressure of reservoirs have been historically used. However, when these recovery processes no longer produce significant results, secondary and/or tertiary oil extraction techniques have been increasingly adopted.

One of the most simple and economical secondary extraction mechanisms is waterflooding where water is injected into a reservoir and it drives the resident oil out of it. Pope (1966) proposed a generalized theory for water flooding based on Buckley-Leverett type of displacement and extended it to polymer flooding, carbonated water flooding or hydrocarbon miscible flooding [10]. Biggs (1970) has shown that the proper implementation of water flooding can actually recover 800 million barrels of secondary oil from 25 producing zones [11]. Craig (1971) has also carried out a detailed study of water flooding with special focus on oil and water properties, efficiency and performance of oil displacement [12]. The process of alkaline water flooding has been discussed

---

[1]Parts of this chapter have been submitted for publication: *(a) A. Gunde, B. Bera, S. K. Mitra, Investigation of Water and CO_2 (carbon dioxide) flooding using micro-ct (micro-computed tomography) images of berea sandstone core using Finite Element simulations. Energy, 35(12): 5209-5216, 2010 (b) A. Gunde, T. Babadagli, and S. K. Mitra. A generic framework to obtain oil-water relative permeability for capillary driven transport in water-wet fractured porous media by LBM (submitted). Water Resources Research (c) A. Gunde, T. Babadagli, S. Roy, and S. K. Mitra. Pore-scale interfacial dynamics and oil-water relative permeabilities of capillary driven counter-current flow in fractured porous media (submitted).*

in detail by Mungan (1981), where the pH of water is increased by injecting relatively inexpensive chemicals in injected water [13]. Water flooding techniques have been studied by both theoretical and numerical approaches. Konoplyov and Zazovsky (1991) have performed simulations of pattern flooding in a fractured porous media [14]. Hadia et al. (2007) and Santhosh et al. (2008) have performed a number of experiments and numerical simulations at laboratory scale to analyze the mechanism of displacement of oil by water [15][16]. In tertiary oil recovery process, miscible and immiscible gases including CO_2 (carbon dioxide) and chemicals are used as flooding phases and even thermal energy is used in some cases to displace the oil. The use of CO_2 has also found applications in carbon sequestration i.e., the reduction of carbon in atmosphere by storing it in oil reservoirs [17].

Due to complex interplay between the fluids in a porous reservoir, the underlying physical processes occurring at the pore scale, need to be understood in detail. The Pore Network Model (PNM) is a commonly used technique to understand the fluid transport at pore-scale. In this model, void space inside the porous rock surface is represented by a network of pores or bulges connected to each other by numerous constrictions or throats. Fatt (1960) proposed such network representation of pore space which later became a widely accepted mode for representation of porous media [18]. Significant progress in this area has been made in recent past, as suggested by the review article by Blunt(2001), where PNM can be used to successfully predict oil recovery [19]. Conventional numerical techniques e.g. Finite Element method have also been used in the simulation of multi-phase flow in porous media [20]. However, these techniques are computationally expensive due to usage of unstructured grids in the complex geometries encountered in porous structures.

2.1.2 Spontaneous imbibition

The spontaneous imbibition process is an important aspect of tertiary oil recovery because of the presence of heterogeneous fracture networks through a typical oil reservoir. It has been studied in literature from the experimental and numerical perspectives.

Mattax and Kyte (1962) performed one of the earliest studies in which the spontaneous imbibition process was defined and formulated [21]. Later, the influence of parameters like wettability and surface tension was analyzed by Babadagli (2002) [22]. Hatiboglu and Babadagli (2007) visually analyzed

porous matrix-fracture interaction in sandpack models for different boundary conditions [5].

The nature and dynamics of counter-current capillary imbibition have been described in literature through experimental observations and simulation results. One of the earliest works explaining the nature of this fluid transport was performed by Indel'man and Katz (1980) [23]. They studied the profile of advancing interface between the two phases for counter-current imbibition and related it to the inhomogeneity in the permeability of the porous system. A comparison of co-current and counter-current imbibition processes was performed by Bourbiaux and Kalaydjan (1988) [6], where they observed that under similar conditions, the counter-current displacement profile shows a more stable saturation growth than the predominantly co-current one. An interesting experimental study of counter-current displacement was performed by Rangel-German and Kovscek (2006), where they observed the imbibition of water in a micro-model and the simultaneous suction and expulsion of fluids through pores of different sizes [24].

In parallel with experimental efforts, analytical and numerical techniques are also applied to understand the capillary displacement in fractured porous media. Silin and Patzek (2004) studied the time scale for counter-current imbibition in regards to storage of liquid waste in rocks and thereby obtained analytical solutions in terms of the volume of displaced fluids [25]. Zeybek et al. (1995) performed a numerical simulation of capillary imbibition in porous structures, where the effect of heterogeneity of permeability and wettability on counter-current and co-current capillary imbibition were considered [26]. Further, a pore-scale numerical simulation was performed by Behbahani and Blunt (2005) using pore-scale network modeling. In their simulations they obtained a semi-empirical relation relating the recovery of imbibition with time for different wettabilities and viscosity ratios [27]. Similarly, the co- and counter-current spontaneous imbibition were illustrated by Unsal et al. (2007) [28]. A semi-analytical solution for co- and counter-current imbibition was also proposed by Schmid et al. (2011) [29].

The existing literature dealing with the pore-scale numerical modeling of spontaneous imbibition process and the subsequent extension to the laboratory-scale is insufficient. Moreover, the characterization of this displacement process in terms of relative permeability is yet to be presented. Recently, the numerical simulation of spontaneous imbibition in porous media has been per-

formed by newer numerical tools such as the Lattice Boltzmann method (LBM) [5].

2.1.3 Miscible flooding

Miscible oil recovery has been studied in literature by using experimental and numerical methodologies under both static and dynamic conditions. Holm (1976) presented a summary of miscible oil recovery mechanisms by the application of CO_2 and hydrocarbons [30]. Paterson (1985) performed a theoretical analysis of the displacements of two miscible fluids [31]. An experimental study of high-pressure miscible displacement was performed by Danesh et al. (1989) [32]. Trivedi and Babadagli (2008) derived dimensionless groups using inspectional analysis in order to gain a better understanding of this process [33]. Hatiboglu and Babadagli performed experiments and simulations of solvent diffusion in a oil saturated glass bead packing under static conditions [1]. Er and Babadagli (2010) performed a similar experimental and core-scale numerical analysis of hydrocarbon oil recovery for a two-dimensional glass bead porous stucture under dynamic conditions [2]. They found the dependence of this process on the physical conditions and geometrical orientation of the porous medium. Miscible oil recovery is an important area because of its potential application in CO_2 sequestration.

2.1.4 Relative permeability analysis

Traditional modeling of oil recovery performance estimation relies on the use of relative permeability curves plotted for the displacement processes. In the case of oil displacement in porous media, a variety of techniques have been suggested to perform these relative permeability analyses. For viscous displacement (pressure driven) dominated flow, measurement techniques and correlations for relative permeabilities are well established. When the process is dominated by capillary (or spontaneous) imbibition, which is commonly encountered in naturally fractured subsurface reservoirs, these measurement techniques are no longer applicable as the displacement process is neither constant rate nor constant pressure. Indirect techniques based on laboratory measurements supported by numerical calculations were applied in a few studies reported so far.

Schembre and Kovscek (2001) calculated relative permeability curves by

using saturation statistics from the results of micro Computer Tomography spontaneous imbibitions experiments [4]. In an earlier study, Bourbiaux and Kalaydjian (1988) matched the laboratory results of co- and counter-current imbibition experiments to numerical models and obtained the relative permeabilities by trial-and-error [6]. Their numerical model was a finite difference solution to continuum equations. Pore scale modeling of this process was suggested to be more useful in understanding the presence of residual oil saturation as shown by Hatiboglu and Babadagli (2007) through their experimental and numerical work [5]. Gunde et al. (2010) adopted a similar system, as used by Hatiboglu and Babadagli, and obtained preliminary results for spontaneous imbibition relative permeability curves for different boundary conditions and fluid wetting properties by applying the LBM method to simulate the process [34]. Similarly, Ramstad et al. (2010) estimated relative permeabilities for viscous displacement in porous media using velocity values obtained from LBM simulations [35].

2.2   Lattice Boltzmann method

2.2.1   Initial development of LBM

The Lattice Boltzmann method (LBM) is one of the recent numerical techniques used to model fluid flow. It has evolved from the original concept of Cellular Automaton Fluids (CAF). Wolfram (1986) explained CAF as a "discrete analogues of Molecular Dynamics" [36], wherein a finite number of fluid particles reside on prespecified locations in space, known as lattice 'sites' or 'nodes', and traverse along the paths by which the sites are connected, with discrete velocity values. He used the kinetic theory of gases and a discrete form of the Boltzmann Transport equation, to discuss the evolution of fluid particles. The Chapman-Enskog expansion was used to derive macroscopic Navier-Stokes equations, and the applicability of automata in fluid flow problems was discussed.

D'Humiares and Lallemand (1988) used the Lattice Gas Automata (LGA) (analogous to CAF), and performed two-dimensional fluid flow simulations [37]. The power of this technique to model complex flow problems was discussed. However, a major drawback of this method was the presence of statistical noise, making its application impractical. Rothman (1988) used the original CAF technique to model fluid flow in a porous medium. An impor-

tant contribution of this work was the validation of Darcy's law through a discrete gas model. The pressure force acting on the fluid was incorporated by the addition of an equivalent change in momentum to the bulk velocity at every lattice at each time step. McNamara and Zanetti (1988) discussed an alternative to the LGA by using the Boltzmann transport equation to evolve particle distribution functions (based on probability) through time [38].This technique eliminated the noise in the original LGA simulations and made the model computationally efficient and suitable for practical fluid flow simulations. The success of their model gave way for further development of the Lattice Boltzmann method.

Succi et al. (1990) performed fluid flow simulations with a Lattice Boltzmann model in two and three dimensions stating the applicability of the technique in a spectrum of areas ranging from laminar to turbulent flows [39]. They applied the LBM in porous media and validated Darcy's law. They further presented a series of numerical simulations for flows in porous media and calculated the permeabilities of the media [40]. Benzi et al. (1990) derived the LBM theory from the dynamics of LGA and discussed its application to specific problems in turbulent fluid flows [41]. Qian et al. (1992) applied the LBM to the study of a one-dimensional diffusion process and reduced the collision operator to a single relaxation parameter [42]. They used the approximation proposed by Bhatnagar-Gross-Krook (BGK) (1954), who presented a kinetic theory based approach to study collision in gases by modifying the collision terms in the Boltzmann Transport equation [43]. This considerably simplified the collision operation and made the LBM computationally efficient. A comparative study was made by Succi et al. (1993) between the conventional LBM and BGK based LBM (also referred to as LBGK) for a single case of fluid flow [44]. They found that although the conventional method was more flexible, LBGK was simpler and more efficient.

A review of the LBM by Succi (1997) further down the line described LBM as having achieved success in the simulation of mesoscopic flows and surpassing the other non-conventional techniques (Direct simulation Monte-Carlo, Molecular Dynamics) by "several orders of magnitude" [45]. The major advantage of the technique being that it fell between the continuum approach of Finite Difference, Finite Volume and Finite Element methods; and the purely non-continuum approach of Molecular Dynamics simulations. However, he also stated the need to overcome the requirement of uniform grid in LBM.

2.2.2 LBM in porous media

One of the most commonly used applications of LBM is to model flow in different types of porous media. After the initial simulations of porous flows by Rothman (1988) and Succi et al. (1990) [46][40], LBM has been consistently used in such flow situations. With the increase in the availability of computational resources and the parallel development of increasingly sophisticated LBM models, it has been applied in increasingly complex porous flow scenarios from the period of its inception.

Chen et al. (1992) performed a three-dimensional computational fluid dynamics (CFD) simulation by using basic principles of LBM [47]. They pointed out that LBM simulations did not require any significant additional resources for dealing with complex boundaries, unlike other techniques. Aharonov and Rothman (1993) proposed a LBM scheme to simulate the flow of non-Newtonian fluids through porous media [48]. They obtained validation of the simulation results by comparing them with theoretical predictions for a simple channel flow. They discussed the advantage of LBM for application to flow situations with intricate geometries, such as those in porous media and further possibilities of simulating multi-phase flow. Grunau et al. (1993) performed a similar LBM modeling for the study of binary fluids in two-dimensional porous media [49]. The porous geometry used in the simulation was randomly generated with an aim of emulating a physical pore structure.

Ferreol and Rothman (1995) performed a realistic LBM simulation by using the three-dimensional reconstructed tomographic images of Fontainebleau sandstone as a porous domain [50]. They calculated the permeability of the rock sample and studied its variation with sample size, LBM grid and resolution and physical model parameters. Their results had a qualitative match with laboratory measurements, which proved an important stepping stone in the applicability of LBM in porous media. Simultaneously, Heijs and Lowe (1995) performed LBM simulations in a porous array of spheres and a clay soil porous structure obtained from tomographic images [51]. They found that the Kozeny-Carman relation provided a reasonable estimate for the prediction of permeability. Similar use of LBM was made to study flow in bidisperse sphere packings by Maier et. al. (1995) [52].

Martys and Chen (1996) performed multi-component flow simulations through a three dimensional porous media by LBM for a viscous displacement case [53].

They obtained relative permeability values for both the phases and compared them with experimental results. Their work opened important possibilities for the simulation of multi-phase flow in porous media. Similar work was carried out by Hazlett et al. (1998) which involved the simulation of immiscible displacement in a reservoir rock[54]. The model obtained porous domains from pore-networks in X-Ray microtomographic images of reservoir rocks and considered the effects of wettability and pressure forces.

LBM models were further applied on complex porous geometries such as those encountered in fracture networks by Eker and Akin (2006), taking into account the multi-scale nature of fracture dimensions [55]. Hatiboglu and Babadagli (2007) performed multi-phase LBM simulations in a laboratory scale fracture-porous matrix system for a spontaneous imbibition and solvent diffusion displacement of kerosene in a water-wet sand pack and compared the core-scale profiles with experimental results [5][1]. However, their work did not provide a pore-scale analysis of the physical processes. Ramstad et al. (2009) performed a relative permeability analysis of viscous displacement in porous media by calculating velocity values using a multi-phase algorithm, and compared the relative permeability values with theoretical predictions [35].

LBM has also been proved a valuable tool in flow modeling through porous materials in areas such as fuel cells and CO_2 sequestration. Joshi et al. (2007) and Park et al. (2007) applied LBM to study fluid flows in fuel cell materials [56][57]. Van Doormal and Pharaoh (2009) studied the anisotropy in the permeability of a randomly generated porous structure of a Proton Exchange Membrane fuel cell using a LBM model [58]. Kang et al. (2010) modeled the flow of CO_2 saturated brine in different porous structures, coupled with the reactive processes in order to study carbon storage phenomenon [59].

The application of LBM in various flow situations in porous media has matured over time. However, tertiary displacement processes such as spontaneous imbibition and miscible diffusion have to be further elucidated at the pore-scale using this technique.

2.2.3   Multi-component flow using LBM

The LBM has been widely applied to simulate fluid flows in porous media. A plethora of these applications involve the simultaneous presence and interaction of two or more phases (or components) e.g. oil displacement by an external agent. In order to deal with these cases, LBM models to simulate

multi-phase flows have been developed.

Immiscible LBM model

Rothman and Keller (1988) initiated the use of multi-phase flows by developing an immiscible flow model in a CAF system [60]. Gunstensen et al. (1991) proposed a model for the flow of two immiscible fluids in LBM [8]. It involved the designation of two colors (say Red and Blue) to the individual fluids. The dynamics of both the fluids were modeled by two separate particle distribution functions, one for each fluid. The LBM governing equations were solved for both the particle distribution functions resulting in two separate solution sets of fluid parameters. A quantity color-gradient (indicating change in color and hence, change in fluid) was formulated and calculated at every lattice at each time step. This enabled the determination of the interface position between the two fluids. An additional force, proportional to the interfacial tension, was added during the collision step, in order to direct the fluid particles at the interface into their respective bulk fluids, thus imitating cohesive forces and keeping the two fluids separate. The authors provided an additional recoloring step after the particles were perturbed in order to maintain a thin interface and prevent the diffusion of one fluid into the other. The major disadvantages of the Two-Color method were the increased computational requirement due to color-gradient calculation, a complex recoloring step and the inability to deal with fluids having different viscosities due to a thin and rigid fluid interface.

Shan and Chen (1993) proposed a generalized LBM model for the simulation of multiple immiscible phases. It involved the solution of LBM governing equations for all the present phases. An additional force term was included during the collision step, denoting the non-local interactions of a fluid particle with particles of other phases in its vicinity. Hence, an interaction potential (called pseudo-potential) was formulated based on the number density of the interacting particles. For the purpose of computational efficiency, only nearest neighbor interactions i.e. interactions with particles on adjacent lattice sites were considered. The advantages of the pseudo-potential model over the Two-Color model included the simulation of more than two phases, relatively less computational requirement and an ability to deal with fluids having different viscosities. However, an inherent demerit of this technique was the formation of spurious velocities at the interface due to non-conservation of local momentum [61].

Tolke et al. (2002) further improved the Two-Color model by implementing a simplified form of the original recoloring step and analyzed the flow of binary fluids in porous media [62]. Although this work made the model more practically applicable, it still could not deal with viscosity ratios other than 1. Latva-Kokko and Rothman (2006) proposed a variant of the Two-Color model in which the separation scheme was dependent on an interface parameter β, which controlled the diffusion of the phases at the interface [9]. By having values of β less than 1.0, it was possible to introduce a slightly diffusive nature in the fluids, leading to a relatively thick interface. This provided the interface with the flexibility to deal with fluids having viscosity ratios till 10.

Latva-Kokko and Rothman (2006) further proposed a scheme to introduce perturbation in the force balance at a fluid-solid surface, by preferentially assigning the sites at the solid boundary with the particles of one of the two fluids. This created an inclination for the particles of one of the phases to be directed towards the solid surface, mimicking preferential affinity by the solid. Hence, this model could be used to include capillarity and wettability effects in the system, and could deal with different contact angles depending on the number density of the wetting fluid at the solid sites.

Swift et al. (1996) proposed a sophisticated LBM technique for the modeling of immiscible fluids by dealing with the free energy of the fluid particles and relating it to the pressure tensor. A major advantage of this model was the ability to deal with fluids having high viscosity ratios. However, considering the simplicity and the applicability of the Two-Color model, the LBM in the present work uses the Two-Color scheme with the modifications done by Latva-Kokko and Rothman to model the capillary (or spontaneous) imbibition of a wetting fluid into an oil saturated porous matrix.

Miscible LBM model

Simulation of solvent diffusion in porous media requires a LBM model dealing with miscible fluids. Flekkoy (1994) proposed a miscible LBM model based on the usage of two separate particle distribution functions, one for the total fluid mass and other for the information of relative presence of the fluids at a lattice site. Both the functions are solved using the LBM governing equations. The BGK relaxation parameter of distribution function representing the total mass depends on the kinematic viscosity of the mixture; while that of the function representing the relative presence depends on the diffusion coefficient

of the two fluids. The simultaneous use of two different relaxation parameters, leads to independent solutions of the particle distribution functions. In this way, the independent transport processes of diffusion and convection can be modeled. The advantages of the proposed model are computational efficiency and simplicity in implementation. This technique proved to be an important tool in the further study of miscible flows in varied situations [63], [64], [1].

The LBM performed in the present work uses the Flekkoy model for static and dynamic miscible flooding of resident oil by external solvents in a two-dimensional sand pack.

Chapter 3

Single-phase LBM model

3.1 Introduction

Analytical and numerical approaches towards the study of fluid flow have been primarily comprised of two different perspectives - continuum and non-continuum. While following the continuum approach, a fluid can be viewed as a single entity with properties varying continuously through the material volume. Analytical solutions of the property values are obtained by dealing with a control volume and applying the laws of conservation of mass and momentum on macro-scale. This has resulted in the formulation of a set of governing equations known as continuity equation and Navier-Stokes equations for fluid flow [65]. A number of iterative solution schemes have been developed in order to obtain the numerical solution of the mathematical model comprising these equations, like the Finite Difference method, Finite Element method and Finite Volume method [66].

On the contrary, a non-continuum approach consists of visualizing a fluid as a collection of particles. Properties of a system are determined by summation of the properties of individual particles. Numerical techniques developed for solution of mathematical models through this approach include Molecular Dynamics simulation and the Monte Carlo method, which are generally applied for micro-scale fluid flow situations. However,the computational requirements for these numerical schemes have proven to be highly expensive [67][68]. Hence an optimum balance between the micro- and macro-scale approaches is required.

3.2 Particle distribution function

While dealing with a system containing a large number of fluid particles, it is more convenient to group them in suitable collections and deal with the collections instead. The particle distribution function (f) has been used for this purpose. It indicates the fraction of particles in a fluid volume possessing momenta within a certain range at a time instant. For instance, in a system containing a total number of M particles, if the value of the distribution function for a momentum range of **p** and **p+dp** at a certain instant of time is f, then the number of particles in the specified range is given by $Mf(\mathbf{p}, t)d\mathbf{p}$ [69].

3.3 Boltzmann Transport Equation

As described in section 3.2, a unique method of dealing with group of particles in the form of particle distribution function f has been developed. Boltzmann developed a relation between the change of particle distribution f and the collision operator Ω in absence of an external force. It states that "Total rate of change of particle distribution function is equal to the rate of change of collision in absence of an external force." [69]

$$\frac{\partial f}{\partial t} + \mathbf{c}\nabla f = \Omega \tag{3.1}$$

This is known as the Boltzmann transport equation and forms the mathematical basis for the Lattice Boltzmann method. In this equation **c** denotes the velocity of the particles and Ω is the collision operator. The main task in hand is the calculation of the collision operator and a number of schemes have been proposed for this very purpose.

3.4 BGK approximation

The Bhatnagar-Gross-Krook approximation [43] proposed in 1954 is a method of calculating the collision operator Ω. According to this scheme, the collision operator is replaced by a term containing the equilibrium distribution function and a relaxation parameter.

$$\Omega = -\omega(f - f_{eq}) = -\frac{f - f_{eq}}{\tau} \tag{3.2}$$

Here, f_{eq} is the equilibrium distribution function which represents the value of the distribution function when the system is in equilibrium, ω is the relaxation parameter and τ is the relaxation time. Hence, it can be said that a system attempts to approach equilibrium due to every collision and its rate of approach is governed by the relaxation parameter ω or the relaxation time τ. With the application of the BGK approximation, the Boltzmann transport equation can be written as,

$$\frac{\partial f}{\partial t} + \mathbf{c}\nabla f = -\omega(f - f_{eq}) = -\frac{f - f_{eq}}{\tau} \qquad (3.3)$$

3.5 Discretization of particle states

Typically, a fluid particle can possess any spatial position and momentum (in terms of magnitude and direction) inside the fluid volume. However, the LBM discretizes the positions and momenta (collectively referred as 'states') of particles by allowing them to attain certain predefined values. Such a methodology forms the basis of formation of a deterministic system of fluid particles. Rothman (1988) summarized this approach as [46]

"...instead of simplifying the medium and solving for the flow, I employ a simplified (but accurate) model for the flow that allows the medium to be as complex as desired."

3.6 Particle transport in lattices

A typical fluid system is divided into a finite number of lattices, while implementing the LBM. Different models of such discretization have been discussed in section 3.7. Consider the example of a D2Q9 lattice structure shown in Fig. 3.1. In this lattice system, each lattice has a lattice site (or node) at its center. Each site has 9 velocity configurations associated with it. These are numbered from 0 to 8 and shown in Fig. 3.2. 0 refers to the configuration of particles which are stationery on the lattice site. For a particular lattice node denoted by its position vector, $\mathbf{r}$, at any instant of time t, the particles transported in one of its associated configurations i are represented by the distribution function $f_i(\mathbf{r}, t)$.

Fluid particles in a lattice system undergo two transport processes in a specified lattice time dt_l. In the LBM simulations performed in this work,
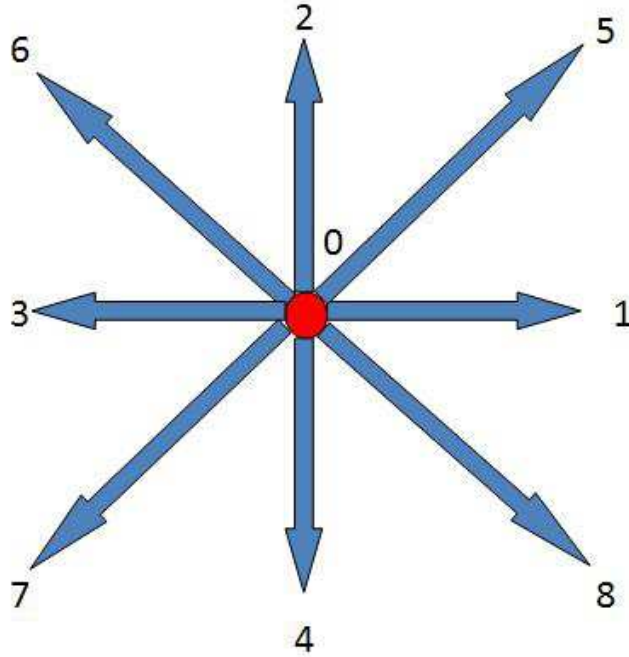
Figure 3.1: A typical D2Q9 lattice. Arrows denote 8 velocity directions and an additional stationary state is included.

each lattice is assumed to be 1 *lattice units* in dimension. Also, a particle transport process is assumed to take place in a single time step ($dt_l = 1$). Hence, the velocity of particles in a particular direction i, $\mathbf{c}_i$, is also the displacement vector in that direction. A particle population f at a node $\mathbf{r}$ at time t_l associated with direction i advects to its adjacent node in its associated direction. This process is known as 'streaming'.

$$f_i(\mathbf{r}, t_l) = f_i(\mathbf{r} + \mathbf{c}_i, t_l + dt_l) \tag{3.4}$$

When more than one particle populations meet at any specific node at any instant of time due to advection from their adjacent nodes or their stationary residence at that node, then they get redistributed in various associated directions of the node. This process is called 'collision'.

$$f_i(\mathbf{r}, t_l + dt_{l,c}) = f_i(\mathbf{r}, t_l) + \Omega \tag{3.5}$$

In the presence of an external force, the collision equation is modified as:

$$f_i(\mathbf{r}, t_l + dt_{l,c}) = f_i(\mathbf{r}, t_l) + \Omega + F_i \tag{3.6}$$
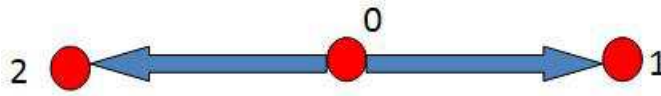
Figure 3.2: A typical D1Q3 lattice. Particles can traverse in the two available directions or stay at rest at a lattice site.

Here, $dt_{l,c}$ is the time required for collision ideally assumed to be zero, F_i denotes an external force acting on the fluid particles for the state i. It can be observed that the Boltzmann Transport equation 3.1 can be obtained by summing up the two equations of streaming and collision. In other words, streaming and collision processes together describe the particle transport in a Lattice Boltzmann system and constitute the mathematical model for such systems. These equations can be said to be the governing equations for a LBM model.

3.7 Lattice structures

This section introduces some typical lattice structures that are used for spatial discretization of a LBM system.

3.7.1 One dimensional lattice structures

Typically, in the case of one-dimensional transport processes, the D1Q3 and D1Q5 lattice structures have been used.

D1Q3

The D1Q3 lattice structure involves the assignment of 3 different velocity configurations to each lattice site. A particle on any site can either traverse in one of the two available directions or stay stationary on the site in the streaming process according to Eq. 3.4. Also various particles meeting at a single site undergo collision according to Eq. 3.5.

An important aspect during the calculation of equilibrium distribution function during the collision process is the assignment of weight factor to every velocity configuration. The weight factors assigned to velocity configurations can be stated as:
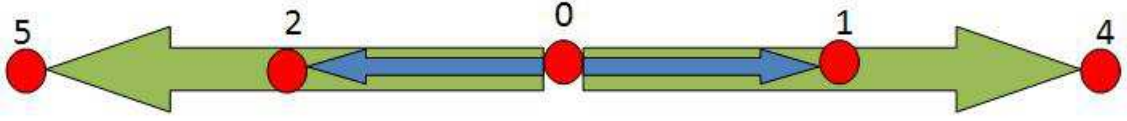
Figure 3.3: A typical D1Q5 lattice. Particles can traverse in the two directions with different velocities to reach the adjacent or next-to-adjacent sites.

$$W_0 = \frac{4}{6}$$
$$W_1 = \frac{1}{6}$$
$$W_2 = \frac{1}{6}$$

$$(3.7)$$

D1Q5

A transport process considered to be taking place in a single dimension can also be modeled by using the D1Q5 lattice model. This involves the assignment of 5 different velocity configurations to every node as shown in Fig. 3.3. A particle can be considered to advect to its next-to-adjacent node in addition to its adjacent node in such a case. The respective weight factors associated with various velocity configurations can be listed as:

$$W_0 = \frac{6}{12}$$
$$W_1 = \frac{2}{12}$$
$$W_2 = \frac{2}{12}$$
$$W_3 = \frac{1}{12}$$
$$W_4 = \frac{1}{12}$$

$$(3.8)$$

3.7.2   Two dimensional lattice structure

A property transport considered to be taking place in a plane can be modeled by using two-dimensional lattice structures.
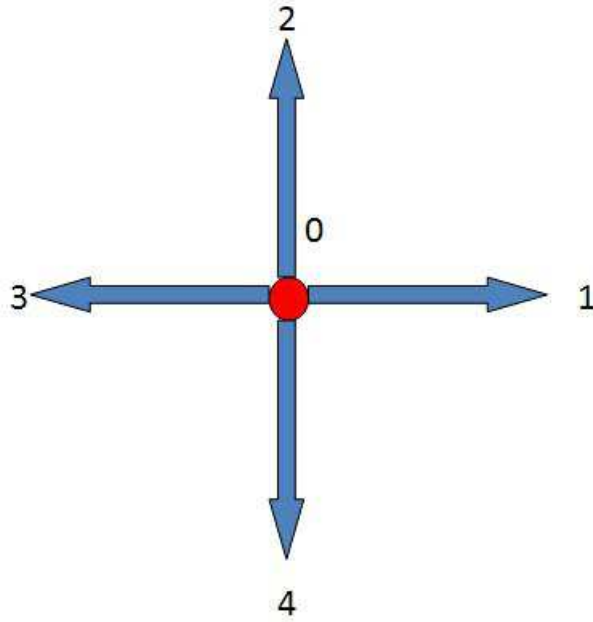
Figure 3.4: A typical D2Q5 lattice. Particles can traverse in any of the 4 directions or stay at rest at a lattice site.

D2Q5

A typical D2Q5 lattice structure has 5 different velocity configurations assigned to every lattice. A particle can traverse in any of the four directions shown in Fig. 3.4 in addition to reside as stationary on the site itself. The weight factors associated with each velocity configuration can be listed as:

$$
\begin{aligned}
W_0 &= 0 & W_1 &= \frac{1}{4} \\
W_2 &= \frac{1}{4} & W_3 &= \frac{1}{4} \\
& & W_4 &= \frac{1}{4}
\end{aligned}
$$

(3.9)

D2Q9

The D2Q5 lattice model described in previous section is generally used for cases involving two-dimensional transport like heat transfer by conduction. However, in the case of two-dimensional fluid flow simulations, satisfactory results have not been obtained by this lattice structure since the number of

states assigned in the model prove insufficient to describe a typical fluid system [70]. Hence in order to conserve isotropy observed in the case of a fluid flow, the D2Q9 model is generally used. In this model a typical lattice can be visualized as a square with a lattice site stationed at the centroid. A particle on the site can advect along any of the 8 different directions surrounding it or reside stationary at the site itself, giving rise to 9 different velocity configurations which have been presented in Fig. 3.1. Similar to other lattice structures, the mathematical model is governed by the streaming and collision equations. The weight factors associated with the velocity configurations can be listed as:

$$
\begin{aligned}
W_0 &= \frac{4}{9} \quad W_1 = \frac{1}{9} \\
W_2 &= \frac{1}{9} \quad W_3 = \frac{1}{9} \\
W_4 &= \frac{1}{9} \quad W_5 = \frac{1}{36} \\
W_6 &= \frac{1}{36} \quad W_7 = \frac{1}{36} \\
W_8 &= \frac{1}{36}
\end{aligned}
$$

(3.10)

3.7.3 Three dimensional lattice structures

The two-dimensional lattice models described in section 3.7.2 can be extended to three dimensional lattice structures in order to analyze the transport of a property in space.

D3Q15

This structure consists of velocity configurations extending in all three dimensions. Each lattice can be visualized as a cube with particles directed towards vertices and face centers as shown in Fig. 3.5. This results in 14 velocity configurations for populations at the lattice site in addition to the stationary one. The weight factors assigned to all the velocity configurations can be listed as:
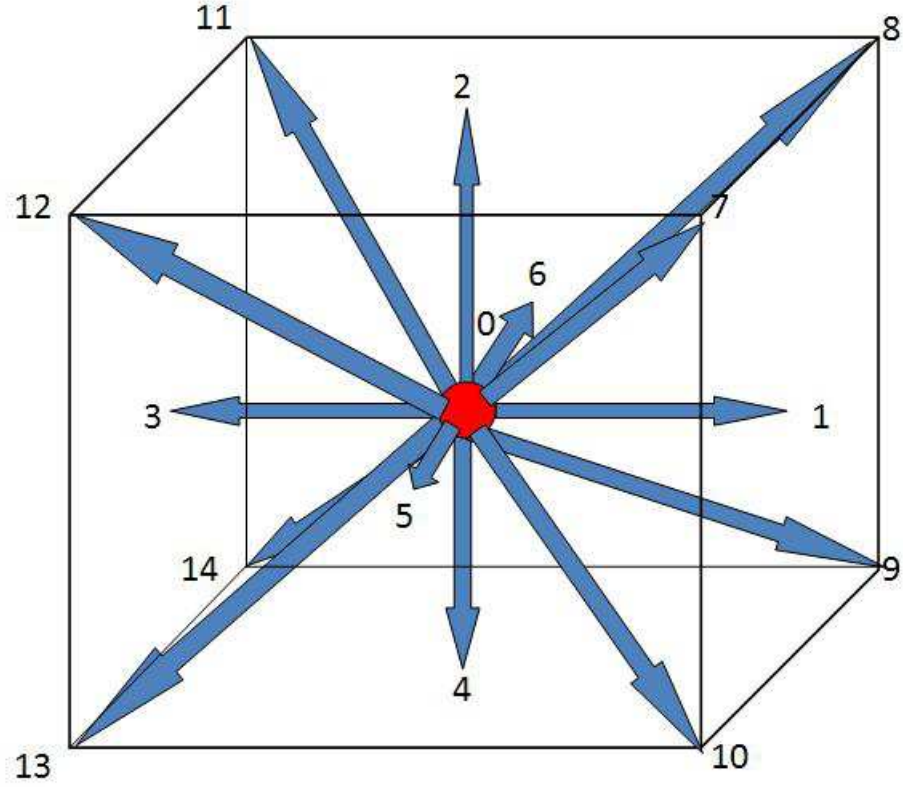
Figure 3.5: A typical D3Q15 lattice. Particles at a lattice site can traverse in 3 dimensions along 14 directions along the face centers or vertices of the lattice cube.

$$
\begin{aligned}
W_0 &= \frac{16}{72} & W_1 &= \frac{8}{72} & W_2 &= \frac{8}{72} \\
W_3 &= \frac{8}{72} & W_4 &= \frac{8}{72} & W_5 &= \frac{8}{72} \\
W_6 &= \frac{8}{72} & W_7 &= \frac{1}{72} & W_8 &= \frac{1}{72} \\
W_9 &= \frac{1}{72} & W_{10} &= \frac{1}{72} & W_{11} &= \frac{1}{72} \\
W_{12} &= \frac{1}{72} & W_{13} &= \frac{1}{72} & W_{14} &= \frac{1}{72}
\end{aligned}
$$

$$(3.11)$$

D3Q19

This lattice structure consists of lattices extending in all three dimensions, each one of which can be visualized as a cube with velocity configurations towards edge centers and face centers. This results in a total of 19 velocity configurations. The weight factors assigned to all the velocity configurations can be listed as:

$$
\begin{aligned}
W_0 &= \frac{12}{36} & W_1 &= \frac{2}{36} & W_2 &= \frac{2}{36} \\
W_3 &= \frac{2}{36} & W_4 &= \frac{2}{36} & W_5 &= \frac{2}{36} \\
W_6 &= \frac{2}{36} & W_7 &= \frac{1}{36} & W_8 &= \frac{1}{36} \\
W_9 &= \frac{1}{36} & W_1 0 &= \frac{1}{36} & W_1 1 &= \frac{1}{36} \\
W_1 2 &= \frac{1}{36} & W_1 3 &= \frac{1}{36} & W_1 4 &= \frac{1}{36} \\
W_1 5 &= \frac{1}{36} & W_1 6 &= \frac{1}{36} & W_1 7 &= \frac{1}{36} \\
& & & & W_1 8 &= \frac{1}{36}
\end{aligned}
\tag{3.12}
$$

3.8 LBM in Fluid Flow

The LBM is applied to fluid flow problems by following the principles of conservation of mass and momentum.

3.8.1 Calculation of mass

Lattice Boltzmann method applies the principle of conservation of mass at every lattice at each time step site in the entire grid, which can be summed up to be realized as the conservation of mass for the entire fluid volume. The number density of fluid particles at each lattice site is calculated as:

$$
\rho_l = \sum_{i=0}^{n} f_i
\tag{3.13}
$$

Here the value of i ranges over all the velocity states (n) at the site.

3.8.2 Calculation of momentum

The fluid velocity is calculated at every lattice site after each time step in the fluid volume.

$$\mathbf{u}_l = \frac{1}{\rho_l} \sum_{i=0}^{n} f_i \mathbf{c}_i \qquad (3.14)$$

In case of two dimensional fluid flow discretized by D2Q9 model shown in Fig. 3.1, the velocity components can be calculated as listed in Eq. 3.15

$$v_x = f_1 + f_5 + f_8 - f_3 - f_6 - f_7 \qquad (3.15)$$
$$v_y = f_2 + f_5 + f_6 - f_3 - f_7 - f_8$$

3.8.3 Collision operator and equilibrium distribution

The BGK approximation stated in Eq. 3.2 is used for calculation of collision operator in case of fluid flow. The relaxation parameter ω is related to the kinematic viscosity of the fluid by [46]

$$\omega = \frac{1}{3\nu_l + 0.5} \qquad (3.16)$$

Equilibrium distribution function in case of fluid flow is calculated by using the Chapman-Enskog expansion to obtain the distribution function in terms of velocity [70].

$$f_{i,eq} = W_i \rho_l \left(1 + \frac{\mathbf{c}_i \cdot \mathbf{u}_l}{c_s{}^2} + \frac{1}{2} \frac{(\mathbf{c}_i \cdot \mathbf{u}_l)^2}{c_s{}^4} - \frac{1}{2} \frac{\mathbf{u}_l^2}{c_s{}^2} \right) \qquad (3.17)$$

Here c_s denotes the velocity of sound in the fluid which is given as:

$$\mathbf{c}_s = \frac{\mathbf{c}_i}{\sqrt{3}} \qquad (3.18)$$

3.8.4 Physical system vs. lattice system

A physical fluid flow is imitated by the LBM by simulating a dimensionally similar fluid flow in a lattice system. In order that such a lattice system is able to represent the original fluid system, certain ground rules have been laid down which are to be followed during its formulation [69],[70],[71]:

- Non dimensional quantities characterizing the fluid flow of the actual system and that of the lattice fluid system are equal.

- The actual fluid flow domain and the lattice domain possess geometrical similarity.

- Since the LBM is essentially a weakly compressible technique, the Mach number of the lattice system is less than 0.3 in order to model an incompressible flow. Typically for this purpose, the value of characteristic flow velocity in the lattice system is less than 0.1 $lattices/s$.

3.8.5   Boundary conditions in LBM

Application of fluid flow boundary conditions in terms of LBM parameters has been presented here.

No-slip boundary condition

A general fluid-solid interface is considered to follow the no-slip boundary condition i.e., relative flow velocity at the interface between fluid and solid is zero since the fluid particles at the interface are assumed to possess the velocity of solid itself [65]. This condition is implemented in LBM by the bounce-back scheme [70].

Simple bounce-back   Simple bounce-back scheme involves the physical consideration that the edge of the solid wall is aligned with the lattice grid and lies on a row (or column) of lattice sites. Fluid particles reaching these fluid-solid interfacial sites from the sites in the bulk fluid are assumed to 'bounce-back' in the opposite direction without any loss of momentum. This is achieved by reversing the particle distribution values into the incoming velocity configurations at these sites at each time step. The particle distribution functions oriented to traverse along the edge of the walls are not allowed to participate in any transport process, thus maintaining their values to the initial ones. Thus, these assumptions ensure that the resultant velocity calculated at the interfacial sites according to Eqn. 3.15 is zero throughout the simulation.

The application of this boundary condition has been explained in Fig. 3.6(a). In this case, the wall position coincides with the boundary site (green). Hence, in a single time step, the particle distribution from the interior fluid

node (blue) streams to the wall node and its value is assigned to the incoming particle distribution. Similarly, other particle distributions arriving at the boundary site are reversed, so that the net velocity at the wall is zero. A disadvantage of the simple bounce-back technique is its first order accuracy.

Interpolated bounce-back Interpolated bounce-back condition is based on the lines of the methodology described by Pan et al. (2006) [72]. It is used in case the wall position does not coincide with the boundary lattice sites and is at a certain distance away from it. In this case, the incoming particle distribution functions at the boundary sites are not assigned the values of those streamed from the interior fluid sites. They are assigned linearly interpolated values between the boundary sites and the interior fluid sites.

The application of the interpolated bounce-back scheme is described in Fig. 3.6(b). In this case, the wall position does not coincide with the boundary site (green) and is further away from it. The particle distribution from the interior site (blue) streams to the boundary site (green) but is not reversed. Instead the value of the incoming particle distribution is a linearly interpolated value obtained from a position between the wall and interior site. This scheme provides the ability to deal with curved boundaries by using an uniform lattice grid for a irregular boundary system such as a porous medium. The value of the incoming particle distribution can be calculated as:

$$d = \frac{x_l - 2x_e}{x_l} \tag{3.19}$$

$$f_{g,i}^{n+1} = f_b^n(d) + f_{g,o}^n(1 - d) \tag{3.20}$$

Here, x_l is the distance between two lattice sites, x_e is the distance of the wall from the boundary site, f_b^n is the particle distribution at the interior site before streaming to the boundary site, $f_{g,o}^n$ is the outgoing particle distribution function at the boundary site before streaming takes place.

Constant velocity boundary condition

The constant velocity boundary condition is typically used at inlets where the velocity is known and has a constant value. Consider a D2Q9 site (such as the one shown in Fig. 3.1), on an inlet boundary with constant inlet velocity U_{in}, and fluid region on the right. While the outgoing populations at the

(a)

(b)
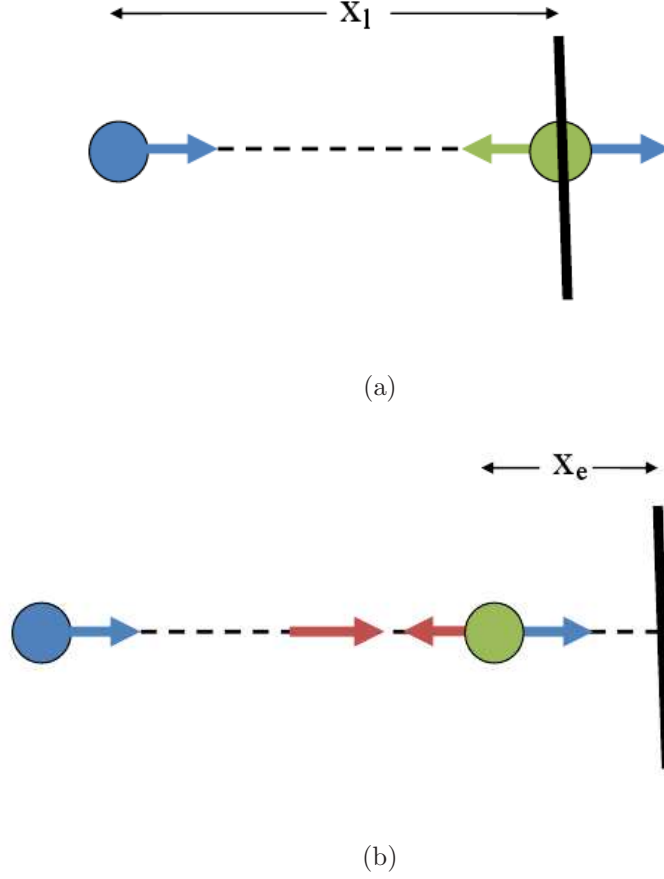
Figure 3.6: (a) Simple bounce-back boundary condition. Particle distribution at the interior site (blue) streams to the boundary site (green) and is reversed. (b) Interpolated bounce-back boundary condition. Wall is at a distance from the boundary site. A linearly interpolated value between the outgoing particle distribution functions of the interior and boundary sites is used as the incoming function at the boundary site.

boundary i.e.,f_3, f_6 and f_7 can be implicitly determined by the streaming process, the incoming populations i.e., f_1, f_5 and f_8 are obtained by the Inamuro method. This involves the assumption of equilibrium at the boundary and the calculation of a pseudo number density (ρ_s). The equations are given as [69]:

$$\rho_s = \frac{1}{1 - U_{in}}(f_0 + f_2 + f_4 + 2(f_6 + f_7 + f_3)) \tag{3.21}$$

$$f_1 = f_3 + \frac{2}{3} + \rho_s U_{in}$$

$$f_5 = f_7 - \frac{1}{2}(f_2 - f_4) + \frac{1}{6}\rho_s U_{in}$$

$$f_8 = f_6 + \frac{1}{2}(f_2 - f_4) + \frac{1}{6}\rho_s U_{in}$$

$$\tag{3.22}$$

Periodic boundary conditions

Periodic boundary conditions are applied in case the computational domain is an individual part of a recurring system. In this case, the incoming particle distribution functions of one boundary are assigned the corresponding values of the outgoing particle distribution functions of the opposite boundary and vice versa. Periodic boundary conditions provide an implicit ability to conserve the mass of a lattice system.

3.8.6 Incorporation of external forces

The LBM model used in this work incorporates external forces such as pressure gradients and gravity on the fluid, by the addition of an equivalent change in momentum to the calculated velocity of the fluid [70], before it is used to determine the equilibrium distribution function. In case of a pressure gradient, the perturbed velocity is determined as:

$$\mathbf{u}_{f,l} = \mathbf{u}_l + \tau \frac{\mathbf{p}_g}{\rho_l^{eff}} \tag{3.23}$$

Here, $\mathbf{u}$ is the velocity determined from Eq. 3.14, $\mathbf{p}_g$ is the pressure gradient, ρ_l^{eff} is the density of the fluid in lattice units and $\mathbf{u}_{f,l}$ is the velocity used to calculate the equilibrium distribution function in Eq. 3.17.

Similarly, gravity is incorporated as:

$$\mathbf{u}_{f,l} = \mathbf{u}_l + \tau \mathbf{g}_l \tag{3.24}$$

Here, $\mathbf{g}_l$ is the acceleration due to gravity in lattice units.
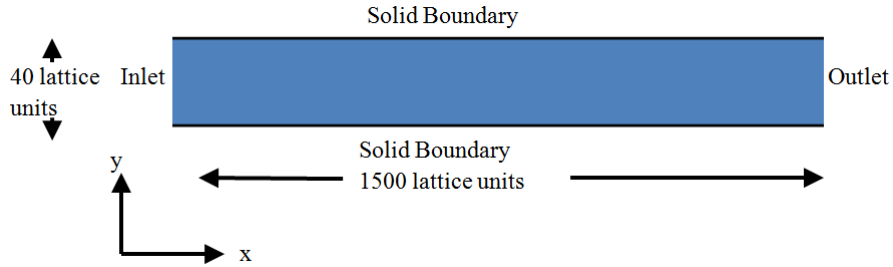
Figure 3.7: Schematic of channel for poiseuille flow simulation. The channel has length 1500 *lattice units* and width 40 *lattice units*. Fluid enters the channel along the x direction from the inlet, with a constant velocity of 0.02 *lattices/s*.

3.9   Poiseuille Flow

The application of the developed single-phase LBM model to the case of a Poiseuille flow is presented in this section. Appendix 8.4 shows a flow-chart of the LBM algorithm. A schematic of the flow domain has been shown in Fig. 3.7. It consists of a two dimensional channel with a length of 1500 *lattice units* and a constant width (H) of 40 *lattice units*. Fluid enters through left boundary (inlet) and exits through the right (outlet). Upper and lower surfaces are solid walls where the no-slip condition is assumed.

Application of LBM to the problem involves discretization of the fluid volume into a D2Q9 lattice structure. Governing equations are streaming and collision equations stated in Eq. 3.4, 3.5. In case of velocity inlet, velocity boundary condition, explained in section 3.8.5 have been imposed at the inlet boundary in order to maintain a constant velocity of 0.01 *lattice/s*. Upper and lower boundaries are considered to be solid walls and simple bounce-back scheme has been applied on them so that a zero velocity is maintained at every time step. Number density of the fluid has been assumed to be 1.0 *lattice unit* and kinematic viscosity of fluid has been assumed to be 0.02 *lattice units*. Reynolds number has been calculated for the velocity inlet boundary condition in Eq. 3.25 as 20. It can be said that fluid flow lies in laminar regime.

$$Re = \frac{U_{in}H}{\nu_l} = 20 \tag{3.25}$$

Primary aim in the simulation of such a fluid flow problem is the variation of velocity throughout the fluid volume. Theoretically, variation of velocity across the channel width is parabolic in the bulk fluid [65]. It is observed that,
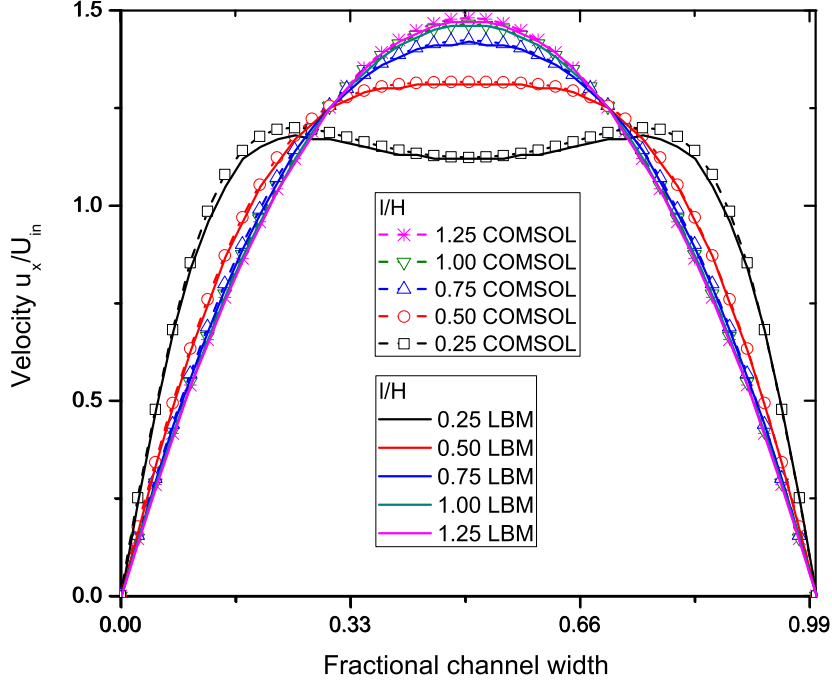
Figure 3.8: Comparison of results for profile development of v_x for COMSOL and the developed LBM code for Poiseuille flow.

a gradual velocity profile development takes place from the inlet until it attains the parabolic profile at a certain distance. This region is called the entrance region for a Poiseuille flow. Maximum value of velocity attained in this flow is about 1.5 *lattice units/s* which is equal to 1.5 times the inlet velocity as predicted by theory. [65].

In order to validate the developed LBM model, the profile development in the entrance length region has been studied by plotting the velocity profile across the channel length at various values of l/H where l is the distance of the cross section for which the velocity profile is plotted from the inlet boundary. Similar velocity profiles have been plotted for flow under similar conditions through a channel with equal aspect ratio and Reynold's number by using Finite Element Method in commercial software COMSOL Multiphysics developed by COMSOL Inc. Comparison of flow development observed for the methods has been shown in Fig. 3.8. It can be observed that both the results are in close agreement with other and LBM is successfully able to capture the longitudinal velocity profile development in the entrance length regime of a
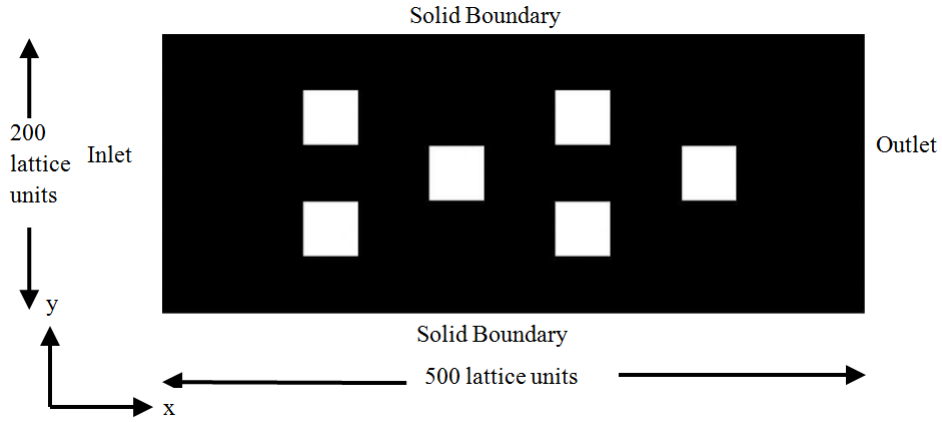
Figure 3.9: Schematic for the simulation of flow through porous medium. White regions depict solid bodies and black regions depict fluid volume.

Poiseuille flow.

3.10   Flow in simple porous medium

The Lattice Boltzmann model developed for Poiseuille flow described in section 3.9 has been extended in this section to pressure driven flow in a simple two dimensional porous medium by inserting solid bodies in the flow path.

A schematic of the flow domain has been shown in Fig. 3.9. It consists of a two dimensional channel with length 500 *lattice units* and a width 200 *lattice units*. Six solid bodies have been inserted in the flow domain in order to study the effect of flow of fluid around them. This geometry can be loosely referred to as a porous medium where the solid bodies represent solid grains and fluid space represents pore volume. Fluid enters through the left boundary (inlet) and exits through the right (outlet). The fluid flow is pressure driven with a constant pressure gradient applied across the channel. Upper and lower boundaries have been considered to be solid walls and no-slip conditions have been assumed over them.

Application of LBM to the problem involves discretization of the fluid volume into D2Q9 lattice structure. Governing equations are streaming and collision equations stated in Eq. 3.4, 3.5. A constant pressure gradient is maintained across the fluid volume by the addition of pressure force (p_g) to the calculated momentum before collision at every time step. Upper and lower boundaries are considered to be solid walls and simple bounce-back scheme has

35
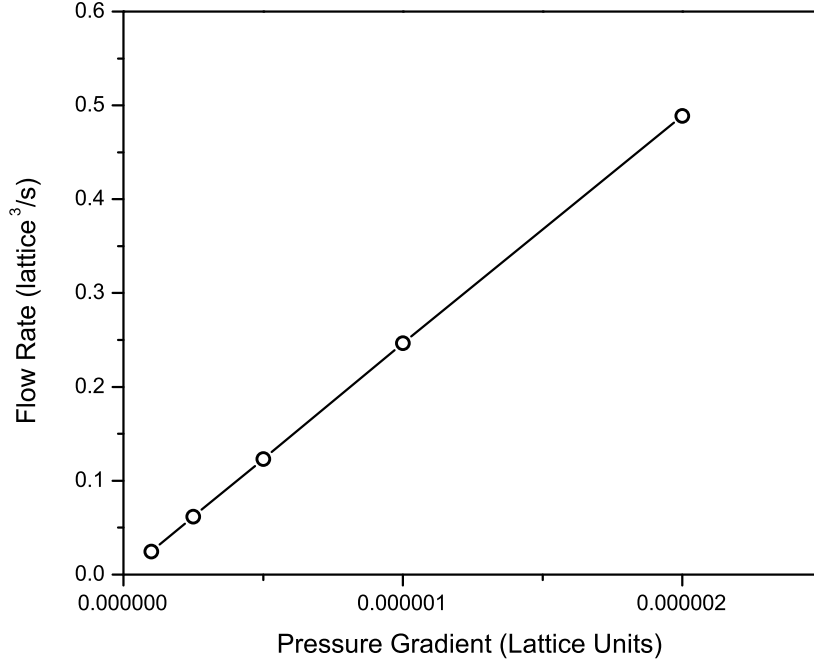
Figure 3.10: Plot of flow rate vs. pressure gradient for flow through porous medium. Linear relationship is observed, which verifies the Darcy's law.

been applied on them in order to maintain zero velocity at every time step. Similarly bounce back scheme has been implemented on the surface of the solid bodies so that they are treated as pore surfaces and no slip condition holds throughout. Density of fluid has been assumed to be 1 lattice unit and kinematic viscosity of fluid has been assumed to be 0.02 *lattice units*.

In order to validate the model developed, the flow analysis has been carried out for various values of pressure gradient applied and the flow rate has been measured for each. Plot of the two quantities has been shown in Fig. 3.10. It can be observed that the two quantities vary linearly with each other. This relationship verifies the simplified form of the Darcy's law across a porous medium which has been stated in Eq. 3.26 [46].

$$q = -\frac{k}{\mu}p_g \tag{3.26}$$

Here, q is the flow rate across the porous medium , μ is the viscosity of the fluid, p_g is the pressure gradient applied across the porous medium and k is

the absolute permeability along the direction of the pressure gradient.

3.11   Concluding remarks

In this chapter, the theory of the LBM was studied and the Boltzmann transport equation was broken down into two separate equations to formulate the streaming and collision equations respectively. The two equations form the mathematical model of the LBM. Preliminery simulations of a single-phase flow in a two-dimensional channel and a simple porous medium were performed using the LBM model and boundary conditions. It was found that the LBM model successfully captures the gradual development of transverse velocity profile in the entrance length region of a Poiseuille flow. Also, the Darcy's law was verified for the porous medium using the LBM model. This model is further developed to handle the flow of two miscible fluids and then applied to the miscible oil recovery process in a two-dimensional sand pack in the next chapter.

Chapter 4

Miscible oil recovery by LBM [1]

Enhanced oil recovery (EOR) involves the injection of various external agents into the fracture networks of reservoir rocks enabling them to come in contact with the porous matrices within these structures. In case of miscible oil recovery, these agents act as solvents and the oil-solvent mixture may be recovered from the reservoirs on account of the diffusive transport (static condition), or in conjunction with an advective transport which occurs due to externally applied pressure gradient (dynamic condition). This chapter extends the single-phase LBM model described in Chapter 3 to model miscible oil recovery from porous media under static and dynamic conditions. Simulations are performed for oil recovery from two-dimensional sand pack models which represent porous matrices in contact with reservoir fractures. Randomly generated porous structures are used as geometrical domains which are initially saturated with oil. Kerosene and light mineral oil are used as oleic phases and hydrocarbon pentane as miscible solvent. The displacement profiles of the two phases obtained from LBM simulations are compared with experimental results from literature [1] [2]. Further simulation is performed with vertical orientation of the sand pack introducing the effect of gravity. These simulations can be used as a basis to study the effect of physical and geometrical parameters on the modes of miscible oil recovery and further, in the understanding of CO_2 storage processes.

---

[1]Parts of this chapter have been submitted for publication.

4.1 Lattice Boltzmann Model

The simulations performed in this chapter use the miscible modeling method proposed by Flekkoy [7]. The fluid volume under consideration is discretized into individual lattices, each with a lattice site. The D2Q9 model [71] is used in these simulations. In order to deal with the simultaneous presence of two different fluids in the computational domain, each fluid is assigned a separate particle distribution function (say R_i and B_i). The number densities of both fluids at a lattice site are given by:

$$R = \sum_{i=0}^{8} R_i \tag{4.1}$$

$$B = \sum_{i=0}^{8} B_i \tag{4.2}$$

The total number density at a lattice site is given by:

$$N = R + B \tag{4.3}$$

Also, the difference in the number densities is given by:

$$\delta = R - B \tag{4.4}$$

Here, the quantities N and δ are associated with the total mass and relative presence of the two fluids at a particular lattice. Hence, the LBM governing equations stated in Eqs. 3.4 and 3.5 are solved for the quantities N_i and δ_i such that,

$$N_i = R_i + B_i \tag{4.5}$$

$$\delta_i = R_i - B_i \tag{4.6}$$

Here, N_i and δ_i denote the transport of mass and information through the computational domain. The BGK approximation given in Eq. 3.3 is used to determine the collision parameters. The relaxation parameters of the two distribution functions depend on the equivalent viscosity at the lattice site $\nu_{l,m}$ and the diffusion coefficient D_l of the two fluids, respectively [7].

$$\omega_\nu = \frac{1}{(3\nu_{l,m} + 0.5)} \tag{4.7}$$

$$\omega_D = \frac{1}{(3D_l + 0.5)} \tag{4.8}$$

The equilibrium particle distribution functions for N_i and δ_i are given as [69]:

$$N_{i,eq} = W_i N \left(1 + \frac{\mathbf{c}_i \cdot \mathbf{u}_l}{c_s{}^2} + \frac{1}{2} \frac{(\mathbf{c}_i \cdot \mathbf{u}_l)^2}{c_s{}^4} - \frac{1}{2} \frac{\mathbf{u}_l^2}{c_s{}^2} \right) \tag{4.9}$$

$$\delta_{i,eq} = W_i \delta \left(1 + \frac{\mathbf{c}_i \cdot \mathbf{u}_l}{c_s{}^2} \right) \tag{4.10}$$

Here, W_i is the weight factor. N and δ are calculated on the lines of Eq. 3.13:

$$N = \sum_{i=0}^{8} N_i \tag{4.11}$$

$$\delta = \sum_{i=0}^{8} \delta_i \tag{4.12}$$

The simultaneous propagation of both distribution functions through time provides a solution for the advection and diffusion transport processes in the miscible fluids case. Gravitational forces are incorporated in the two-fluid system by using the Boussinesq approximation by calculating an equivalent lattice density as:

$$\rho_{m,l}^{eff} = \frac{R \times \rho_{R,l}^{eff} + B \times \rho_{B,l}^{eff}}{R + B} \tag{4.13}$$

Here, $\rho_{m,l}^{eff}$ is the equivalent lattice density calculated at a site, and $\rho_{R,l}^{eff}$ and $\rho_{B,l}^{eff}$ are the lattice densities of the two fluids scaled from their physical values. These are used to calculate the lattice gravity which is then added to the velocity.

$$\mathbf{u}_{f,l} = \mathbf{u}_l + \mathbf{g}_l \times \frac{\rho_{m,l}^{eff} - \rho_0}{\rho_0} \tau \tag{4.14}$$

Here, ρ_0 is the reference density, considered to be the density of the lighter fluid. $\mathbf{u}_{eq}$ is then used in Eqs. 4.9 and 4.10.
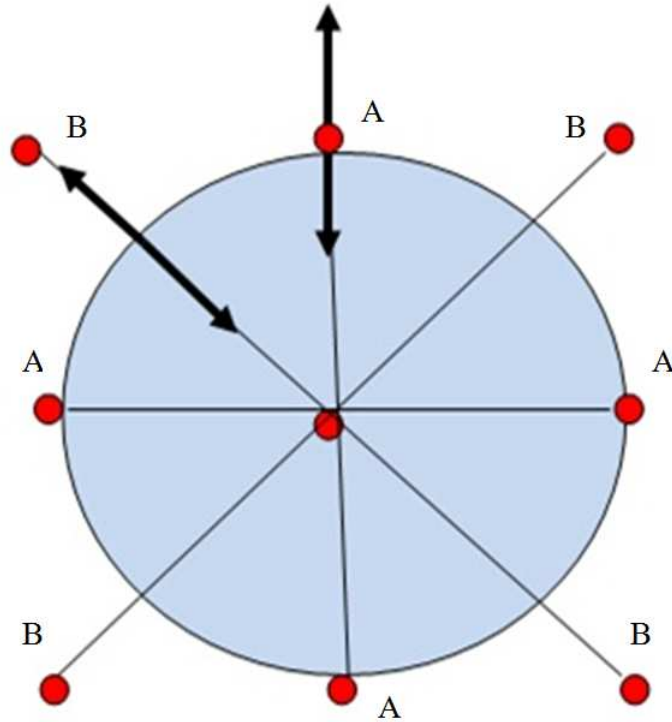
Figure 4.1: A solid spherical cross section present in the lattice grid. The diameter of the solid is 2 *lattice units*. Simple bounce-back rule can be applied to nodes of type A, however interpolated boundary conditions have to be applied at nodes of type B. This technique enables the model to deal with curved solid surfaces without the use of an unstructured grid.

The following are the different types of schemes used for implementing boundary conditions:

- Simple bounce-back [70] - Used to implement no-slip boundary condition on the fluid-solid boundary.

- Interpolated bounce-back [72] - Used to implement no-slip boundary condition on curved surfaces. The application is shown in Fig. 4.1. Here, a spherical cross-section is present in the system with its center at a lattice site and radius equal to the lattice spacing. A simple bounce-back rule can be applied at boundary nodes of type A, however an interpolated bounce-back rule has to be applied at boundary nodes of type B.

- Inamuro [69] - Used to maintain a constant velocity at a fracture inlet.

In order to obtain a quantitative and qualitative comparison between the results of the experiments and simulations, the values for the parameters used

Table 4.1: Properties of fluids

Property	Pentane	Kerosene	Light mineral oil
Density (g/cm^3)	0.63	0.79	0.83
Viscosity (cp)	0.38	2.9	36.32
Diffusion coefficient (cm^2/s)		4×10^{-4}	2.5×10^{-4}

in the simulations have to be scaled from the physical values. The following dimensionless parameters have to maintained same for both the systems:

- Aspect ratio of the porous matrix.

- Ratio of matrix and solid grain size in a sand pack model.

- Viscosity ratio of the two miscible fluids. (ν_1/ν_2)

- Schmidt number. (ν/D)

- Reynold's number $(U_{in}\ L_c/\nu)$ in case of dynamic flooding with a known fracture inlet velocity. L_c is the characteristic length considered to be the average size of a solid grain.

4.2 Results and discussion

The various results obtained from the LBM simulations are presented and discussed in this section.

4.2.1 Static miscible flooding

The LBM model developed in section 4.1 is applied to a case of miscible oil recovery under static conditions. Experiments involving the recovery of kerosene and mineral oil from a two-dimensional sand pack performed by Hatiboglu and Babadagli [1] are chosen from literature to compare the results from simulations. The solvent used in these experiments is pentane. The setup consists of a glass bead packing compressed between two sheets of acrylic giving it the ability to observe the two-dimensional displacement profiles with time. The average glass bead diameter is 0.1 mm and the sand pack is 5 cm × 5 cm in dimensions.
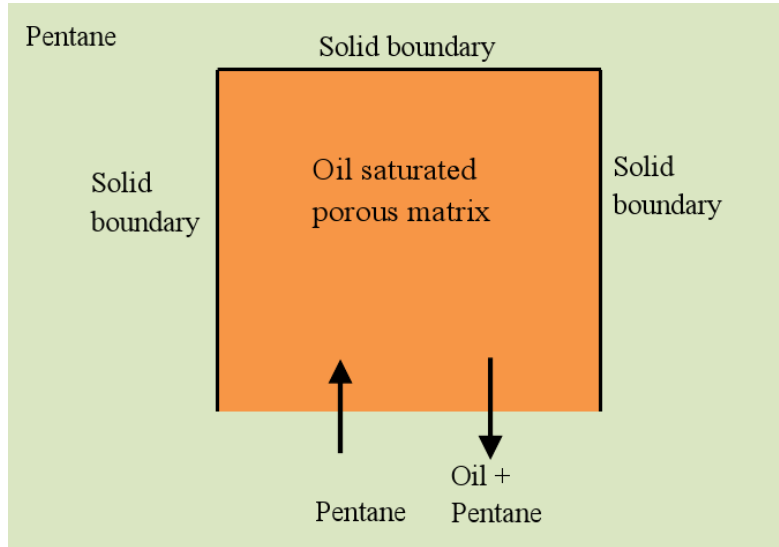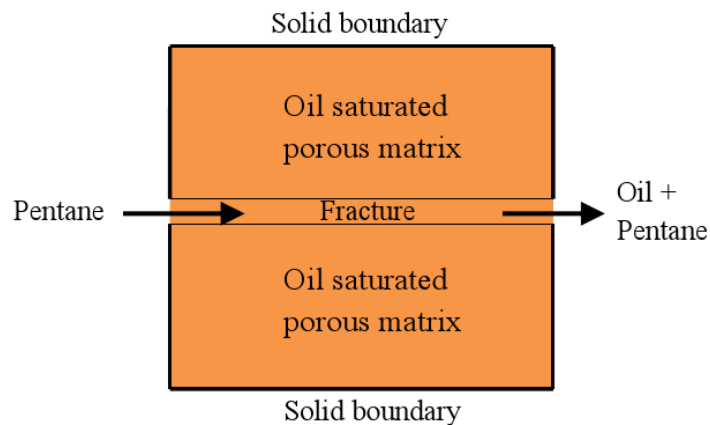
Figure 4.2: (a) Schematic of the porous system obtained from static miscible displacement experiments in literature [1]. It consists of a glass bead packing of dimensions 5 cm × 5 cm, with the average size of the glass bead 0.1 mm. The glass bead packing is initially saturated with and immersed in solvent pentane with one open boundary. (b) Schematic of the porous system obtained from dynamic miscible displacement experiments in literature [2]. It consists of a glass bead packing of dimensions 10 cm × 15 cm, with the average size of the glass bead 0.5 mm, with a channel passing through the center. The channel is connected to the inlet and outlet ports through which pentane is injected in the system and the mixture of pentane and oil is recovered respectively.

The pore space is initially saturated with an oleic phase and then horizontally immersed in the solvent. Three boundaries of the porous model are closed, and one boundary kept open, giving it a nature of counter-current displacement [5]. A schematic shown in Fig. 4.2 represents the physical orientation of their orientation cell. Properties of the relevant fluids are given in Table 4.1.
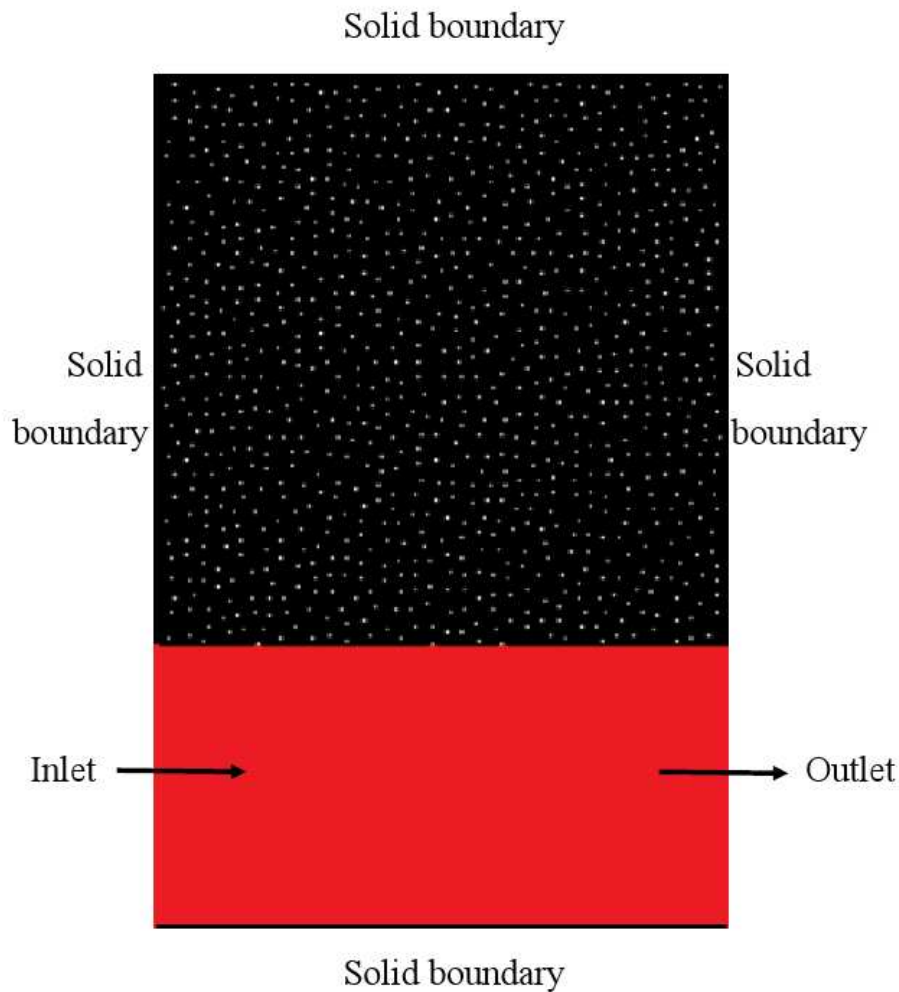
Figure 4.3: The LBM porous system generated for static miscible flooding simulations. A 200 × 200 lattice grid is generated as a porous matrix by random assignment of lattices as solid grains (white) and the pore space (black) is considered to be saturated with the oleic phase. A reservoir (red) of width 100 lattices is assumed to be located beside the open boundary of the porous matrix and contains the solvent pentane. A continuous supply of the solvent is maintained at the inlet and the diffused oil is expelled through the fracture outlet.
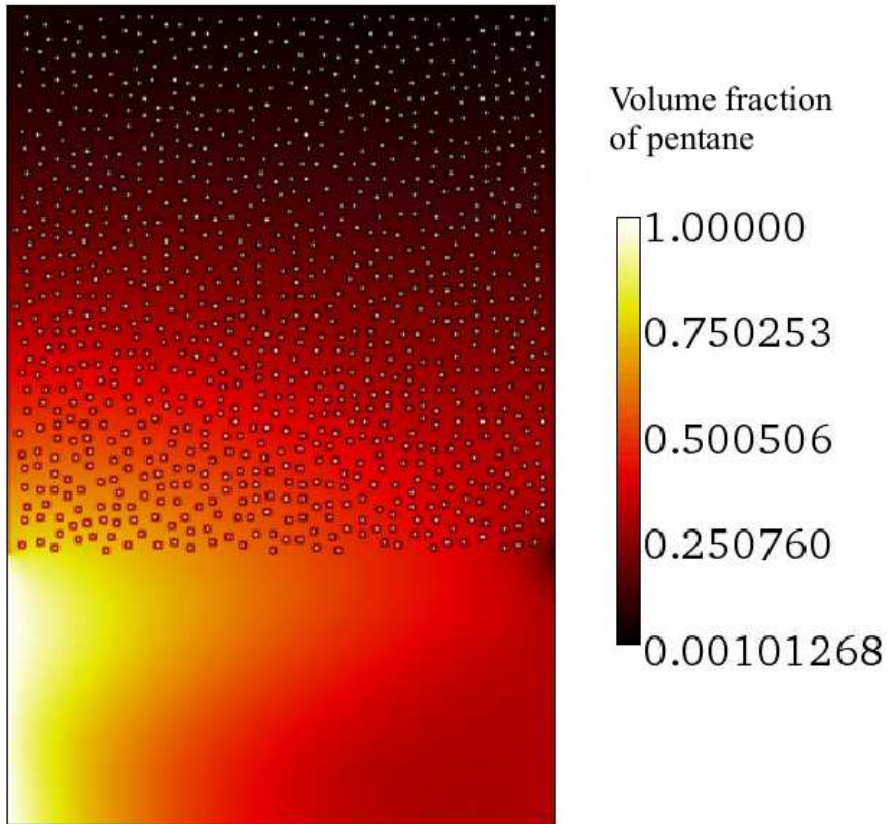
Figure 4.4: LBM result showing simultaneous diffusion of solvent pentane and kerosene into the pore matrix and fracture respectively leading to oil recovery from the outlet, for the static miscible displacement case. Color variation representing the volume fraction of pentane is displayed. The gradual diffusion of the solvent into the porous medium can be observed.

A 200 × 200 lattice grid is chosen for the purpose of the simulation of the described experiment. Some of the lattices are randomly assigned as solid grains, while the rest of the volume is considered to be pore space. The size of each solid grain is 2 *lattices* and the application of simple and interpolated boundary conditions is made on these grains so that the circular profile of the grains is dealt with. A distance of minimum 3 *lattices* is maintained between any two solid grains a stable LBM simulation can be performed. The domain geometry can be further improved by using an actual representation of a physical porous medium and increasing the computational resources. Similar to the experimental setup, three boundaries of the porous matrix are considered to be solid walls with simple bounce-back condition applied on them. An additional reservoir of 100 lattice width is considered to be in contact with the fourth open boundary imititating the presence of a fracture. The pore space

is initially assumed to be filled with kerosene or mineral oil and the reservoir with pentane, by assuming values of viscosity and density keeping in mind the requirements stated in section 4.1. The porous matrix-reservoir system used for LBM simulations is shown in Fig. 4.3. A constant mass flux is maintained at the reservoir inlet so that a continuous supply of solvent is maintained and the displaced oil entering the reservoir is removed via the reservoir outlet.

The LBM simulation is performed for kerosene and mineral oil for the described conditions. The contact of two miscible fluids results in mass diffusion across the matrix-fracture boundary causing the resident oil in the pore space to collect in the reservoir and be eventually recovered from the outlet. A relative variation of the volume fraction of pentane throughout the porous matrix for kerosene displacement is shown in Fig. 4.4. Here, the gradual diffusion of pentane in the pore matrix can be observed. The kerosene diffusing into the reservoir can be observed to undergo a continuous expulsion from the outlet. In order to compare such displacement profiles with experimental results a threshold value of 0.1 is chosen for the mass fraction and used in the simulation results. A lattice possessing a mass fraction of pentane greater than the threshold value is assigned as pentane and less than the threshold as the oleic phase. A small value of the assumed threshold is in terms with our intention of observing the actual presence of the solvent in the porous matrix, which is visualized in the experimental results.

For a qualitative comparison of the LBM and experimental results, the displacement profiles from both these methodologies are compared against each other at equal instants of time. Fig. 4.5 shows the snapshots of solvent displacements for kerosene displacement experiment. It can be observed that there is a reasonable agreement between the areas swept by the solvent obtained from both sources. Also, the time required for the solvent to reach the opposite boundary is approx. 600 mins in the LBM simulations. Similar comparison for light mineral oil displacement is shown in Fig. 4.6. It can be observed that mineral oil shows a similar diffusion trend for the LBM simulations, with longer time for the solvent to diffuse to the opposite boundary, owing to the higher viscosity of the oleic phase. The non-uniform displacement front observed in the experiments is not reproduced in the LBM results. This can be further improved if an actual representation of the porous structure is used for the simulations by using an actual image of the sand pack detailing the solid grain positions. The displacement simulations performed under static
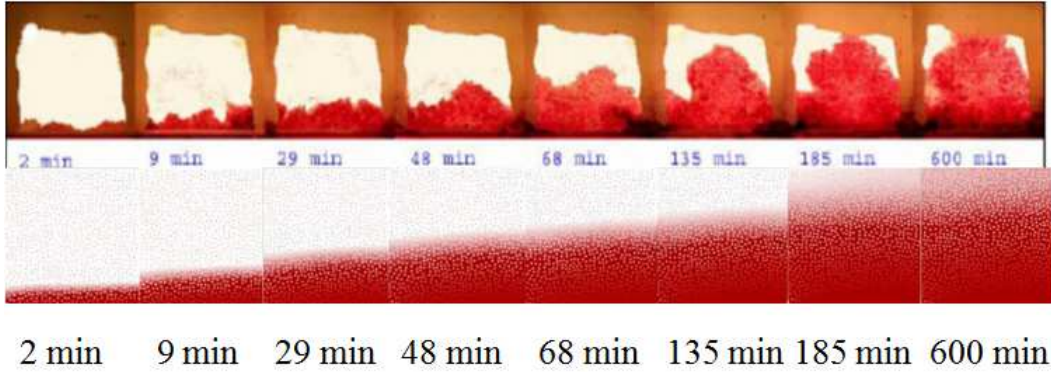
Figure 4.5: Comparison of displacement profiles at different time instants for the horizontal displacement of kerosene from a glass bead packing under static conditions. Upper snapshots show the displacement profiles of oil(light) and pentane(dark) obtained from experiments in literature [1], while the lower snapshots show profiles of oil(white) and pentane(dark) obtained from LBM simulations. The areas swept by the solvent are observed to be in agreement in both cases.

conditions can be used as a basis to simulate dynamic flooding of kerosene and light mineral oil in the next section.

4.2.2 Dynamic miscible flooding

The developed LBM model is applied to simulations of miscible displacement of kerosene and light mineral oil by using solvent pentane under dynamic conditions. Experiments under these conditions are performed by Er and Babadagli [2] and the corresponding simulation results are provided here. A glass bead packing, similar to the static case, is considered as a two-dimensional porous matrix to observe the displacement profiles at different instants of time. Average size of glass bead diameter is $0.5\ mm$. The dimensions of the sand pack are $10\ cm\ \times\ 15\ cm$. A channel runs through the center of the glass bead packing, which serves the purpose of a fracture in contact in two porous matrices in a symmetrical manner. The channel is connected to the inlet and outlet ports, and a micropump is used to maintain a continuous injection of solvent into the channel at a constant flow rate of $15\ ml/hr$. Due to this, in addition to the diffusive transport process given rise by the mixing of oleic phase and solvent, there is an advective transport of the mixture recovered from the outlet port. All other boundaries of the matrix are closed. The schematic shown in Fig. 4.2(b) represents the matrix-fracture configuration.
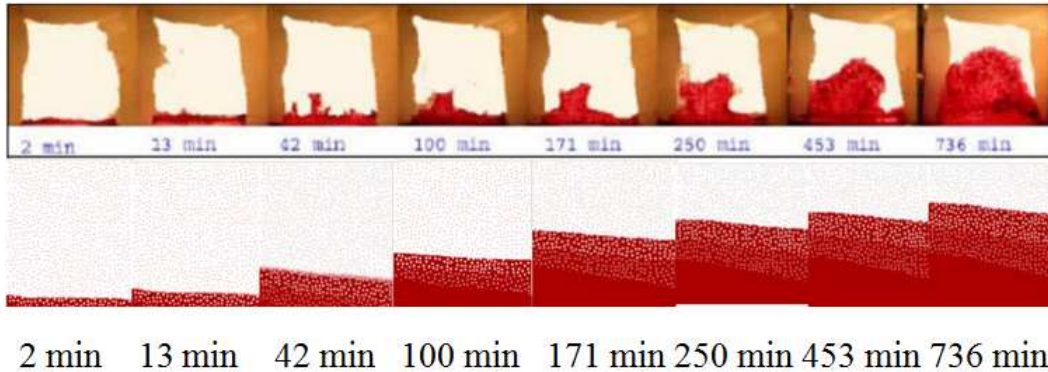
Figure 4.6: Comparison of displacement profiles at different time instants for the horizontal displacement of light mineral oil from a glass bead packing under static conditions. Upper snapshots show the displacement profiles of oil(light) and pentane(dark) obtained from experiments in literature [1], while the lower snapshots show profiles of oil(white) and pentane(dark) obtained from LBM simulations. The areas swept by the solvent are observed to be in agreement in both cases.

A porous system, consisting of a 200 × 300 lattice grid is considered for simulation of the dynamic miscible displacement. Similar to the static case, a randomly generated porous structure is used. The fracture channel is assumed to be 12 lattices in width. Bounce-back schemes are used on all solid boundaries. The pore space is initially considered to be filled with the oleic phase and the channel is assumed to contain pentane. The Inamuro boundary condition [69] is used to maintain a constant mass flux at the fracture inlet. The porous lattice system is shown in Fig. 4.7. The LBM model described in section 4.1, is modified with the scaled values of physical parameters, as reported in experimental work [2].

In the case of kerosene displacement by pentane in a horizontal configuration at an injection rate of 15 ml/hr, a simultaneous diffusion and advection is observed as in the experimental case. The solvent displacement profiles are observed for different time instants and a comparison is made with the experimental results, as shown in Fig. 4.8. A threshold of 0.1 for the volume fraction of pentane is used for the visualization of presence of solvent phase in a lattice similar to that considered for the static case. It can be observed by comparing snapshots at equal time instants that the solvent displacement profile is very well reproduced by the LBM model, with substantial agreement between the results. The wavy nature of the solvent profile is observed in the LBM results.
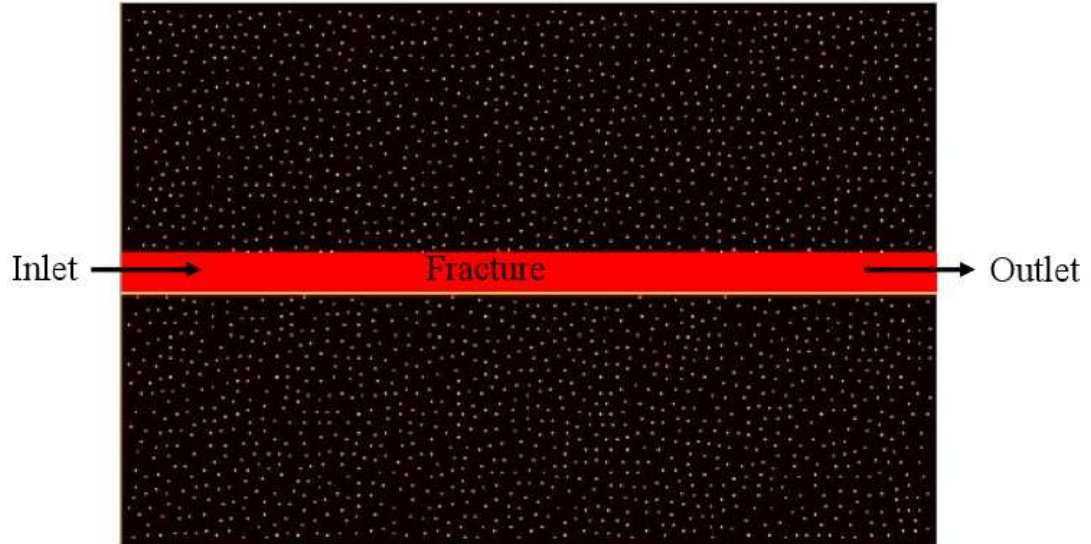
Figure 4.7: The LBM porous system generated for dynamic miscible flooding simulations. A 300 × 200 lattice grid is generated as a porous matrix by random assignment of lattices as solid grains (white) and the pore space (black) is considered to be saturated with the oleic phase. A channel (red) with a width of 12 lattices passes through the center and contains the solvent pentane. All the boundaries of the porous matrix are closed except the inlet and outlet as shown, through which the solvent is injected and the oil-solvent mixture is recovered respectively.

The pore spaces near the fracture inlet show the fastest diffusion of solvent. A comparison of light mineral oil displacement with experimental results under similar conditions is shown in Fig. 4.9. Mineral oil shows a similar solvent displacement pattern as kerosene, but requires a larger displacement time due to relatively higher viscosity.

In order to study the efficiency of this displacement process, the displacement profiles are studied at different amounts of injected solvent, measured in terms of the pore volume of the matrix. Fig. 4.10 shows a comparison between experiment and simulation for the kerosene displacement case, at different amounts of injected solvent. A reasonable agreement is observed, which provides an estimate of the actual amount of solvent required to completely recover the resident kerosene in the pore volume.

Further, a kerosene displacement simulation is performed with the vertical orientation of the bead packing, taking into account the effect of buoyancy

49
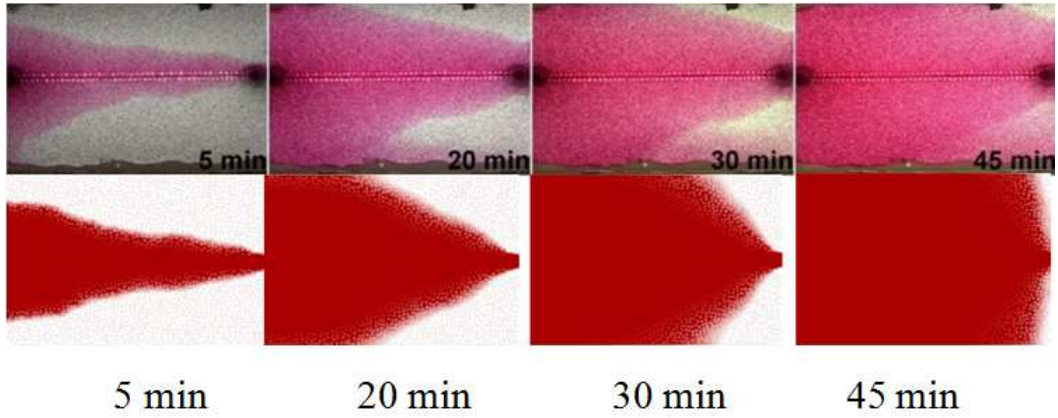
Figure 4.8: Comparison of displacement profiles at different time instants for the horizontal displacement of kerosene from a glass bead packing by the injection of solvent pentane at a constant rate of 15 ml/hr. Upper snapshots show the displacement profiles of oil(light) and pentane(dark) obtained from experiments in literature [2], while the lower snapshots show profiles of oil(white) and pentane(dark) obtained from LBM simulations. Both the results are observed to be in agreement.

forces arising in the two-fluid system. The acceleration due to gravity is scaled from its physical value and used to calculate the buoyancy forces on the fluids, which are included in the LBM equations according to the method described in section 4.1. The resulting displacement profiles are studied and compared with experiment in Fig. 4.11. The change in the displacement patterns is observed in both cases, due to the tendency of the lighter solvent fluid to stay on top of the heavier oleic phase. This situation is especially relevant in practice with vertically oriented fractures in porous reservoirs. However, the developed LBM model shows limitations in reproducing the finger-like profiles displayed the solvent during diffusion, which can be seen in the experimental results. The LBM simulations with heavy mineral oil were computationally unstable due to a large viscosity ratio of about 400 between the two fluids. Also, the simulations performed for higher flow rates of the solvent were found to be computationally unstable because of the characteristic velocity exceeding the required value described in section 3.8.4. This LBM model, with further improvements, can be used to study the displacement process with a similarly lighter CO_2 injected in the reservoir rocks, which can lead to further applications in geological CO_2 storage and carbon sequestration.
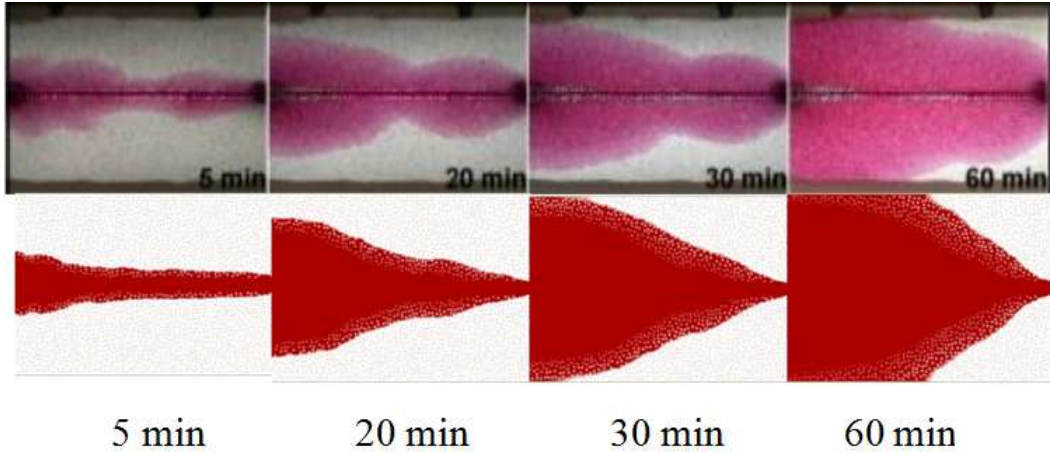
Figure 4.9: Comparison of displacement profiles at different time instants for the horizontal displacement of light mineral oil from a glass bead packing by the injection of solvent pentane at a constant rate of 15 ml/hr. Upper snapshots show the displacement profiles of oil(light) and pentane(dark) obtained from experiments in literature [2], while the lower snapshots show profiles of oil(white) and pentane(dark) obtained from LBM simulations. Both the results are observed to be in agreement.

4.3 Conclusion

Displacement of resident oil in porous media by the injection of miscible agents in adjoining fracture networks by numerical modeling using the Lattice Boltzmann method is studied. The method proposed by Flekkoy [7] is used for the modeling of mass diffusion and advection transport processes in the recovery of kerosene and light mineral oil by hydrocarbon pentane. The porous systems under consideration involve glass bead packings compressed between two acrylic sheets in order to study the displacement profiles of diffused solvent in the pore matrix with time. They are attempted to be simulated by a randomly generated lattice grain structure, with equivalent boundary conditions.

The oleic phases are displaced under static conditions by the presence of a reservoir filled with the injected solvent, which causes simultaneous diffusion and subsequent recovery. In case of horizontal displacement processes, the solvent pentane diffuses into the porous matrix gradually. The comparison of numerical and experimental results from literature [1] for the observed solvent displacement profiles indicate approximately equal areas swept by pentane at same time instants. The time required for complete displacement of the pore matrix is higher in the case of mineral oil than kerosene, due to relatively
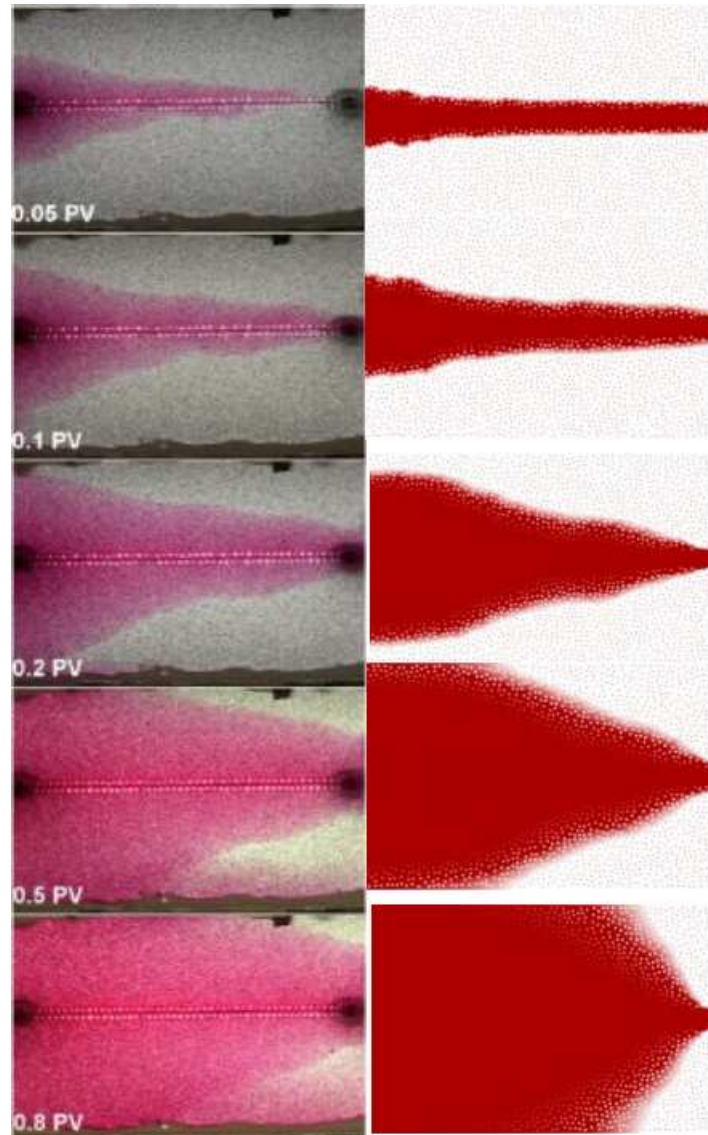
Figure 4.10: Comparison of displacement profiles at different amounts of injected solvent pentane for the horizontal displacement of kerosene from a glass bead packing at a constant rate of 15 ml/hr. The injection amount is measured in terms of pore volume. Snapshots on the left show the displacement profiles of oil(light) and pentane(dark) obtained from experiments in literature [2], while those on the right show the displacement profiles of oil(white) and pentane(dark) obtained from LBM simulations. Both the results are observed to be in agreement.

higher viscosity. The non-uniform nature of the displacement front observed in case of experimental observations is not reproduced by the LBM simulations and can be improved by the use of actual porous structure in the sand pack
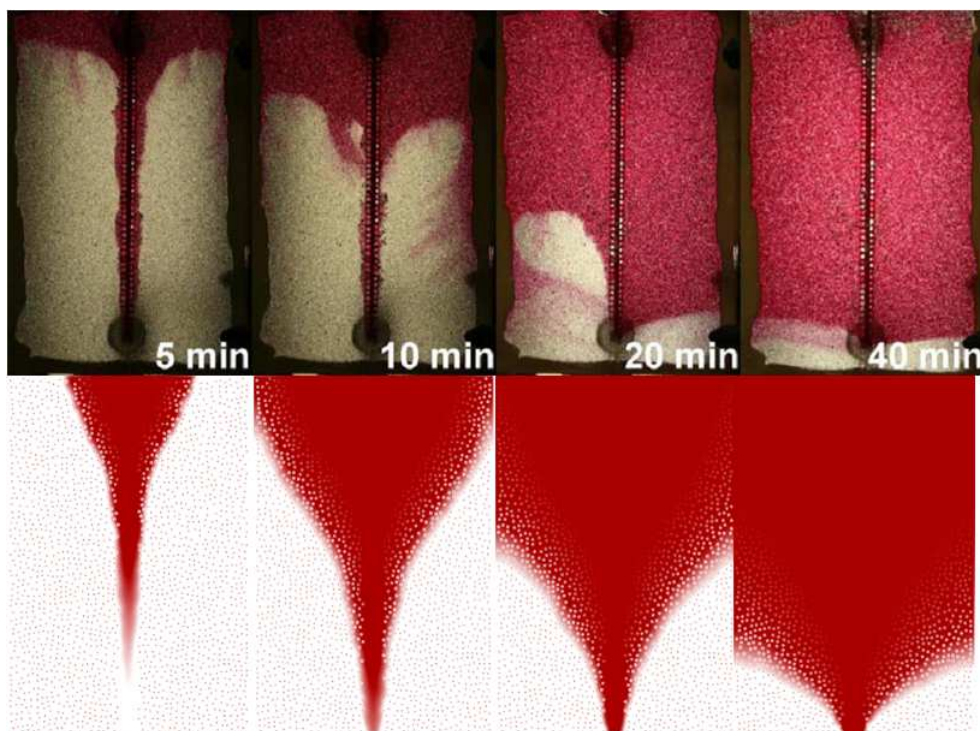
Figure 4.11: Comparison of displacement profiles at different time instants for the vertical displacement of kerosene from a glass bead packing by the injection of solvent pentane at a constant rate of 15 ml/hr. Upper snapshots show the displacement profiles of oil(light) and pentane(dark) obtained from experiments in literature [2], while the lower snapshots show profiles of oil(white) and pentane(dark) obtained from LBM simulations. Both the results are in agreement. However, the finger-like profiles observed in case of experimental results are not completely reproduced by the LBM simulations.

model.

The simulations of kerosene and mineral oil miscible displacement are performed under dynamic conditions by the constant injection of solvent through the inlet port of the fracture passing through a porous matrix. The fluidic system undergoes simultaneous diffusion and advection resulting in a mixture of the solvent and oleic phases to be recovered from the outlet port. The solvent displacement profiles show a substantial agreement when compared with results obtained from experiments in literature [2] under similar conditions. The efficiency of displacement process can be understood from the comparison for equal amounts of injected solvent, which shows good agreement as well. The nature of the displacement profile is reproduced in the LBM simulations at equal time instants, with greater displacement time required by pentane

in the case of light mineral displacement similar to the case of static recovery. Further simulations are performed with a vertical orientation of the sand pack, displaying a change in the displacement profile trend due to additional buoyancy forces in the system, which agrees with experimental observations.

The performed simulations can be used to analyze oil recovery processes by the injection of miscible solvents under static and dynamic conditions. However, the developed LBM model is not able to satisfactorily produce finger-formations observed in the experimental results. These studies can have a further application in CO_2 sequestration, wherein a similar injection of CO_2 takes place in order to recover the resident oil and store carbon in geological reservoirs.

Chapter 5

Immiscible LBM model [1]

Spontaneous imbibition process involves the displacement of oil residing in a porous matrix by a wetting fluid with respect to the matrix solid due to capillary forces. In order to model the immiscible interaction of the two phases, the single-phase LBM model developed in Chapter 3 has been extended further.

5.1 Multi-component modeling technique

The LBM model in this work uses the two-color approach initially proposed by Gunstensen and Rothman [8], and later developed by Latva-Kokko and Rothman [9][3]. The two-color model involves the consideration of two separate fluids in the porous region (say R and B). The governing equations (Eqs. 3.4, 3.5) are applied to both the fluids according to their respective relaxation parameters (ω_R, ω_B). The fluids interact with each other at their interface to maintain immiscibility. The total distribution function at a site for a particular direction is calculated as $N_i = R_i + B_i$.

5.1.1 Interfacial tension

Interfacial tension is incorporated in the LBM model by addition of an external force to each fluid at the interface, which is determined by formulating a quantity Color Gradient as [8]:

$$\mathbf{G} = \Sigma \mathbf{c}_i [R(\mathbf{r} + \mathbf{c}_i) - B(\mathbf{r} + \mathbf{c}_i)] \tag{5.1}$$

---

[1]Parts of this chapter have been submitted for publication: *A. Gunde, T. Babadagli, and S. K. Mitra. A generic framework to obtain oil-water relative permeability for capillary driven transport in water-wet fractured porous media by LBM (submitted). Water Resources Research.*

Here, R (or B) is the lattice number density calculated individually for Red (or Blue) fluid using Eq. 3.13. It can be given as:

$$R = \sum_{i=0}^{8} R_i \tag{5.2}$$

$$B = \sum_{i=0}^{8} B_i \tag{5.3}$$

The Color Gradient is then incorporated in the interfacial tension force which is added to the total distribution function N_i of the two fluids during collision. This force is given as:

$$F_{l,i}^{ift} = |\mathbf{G}|Acos[2(\theta_i - \theta_f)] \tag{5.4}$$

Here θ_f denotes the direction of the color gradient and θ_i denotes the direction of velocity state. The parameter A is related to the interfacial tension according to [35]:

$$\sigma_l^{ift} = -\frac{192\rho_l^{eff}A}{\omega} \tag{5.5}$$

The cosine term in Eq. 5.4 orients the distribution functions of the individual fluids into their bulk and incorporates cohesion. In addition to the inclusion of interfacial tension force in the collision equation, a redistribution scheme has to be incorporated in order to ensure immiscibility. The method proposed by Latva-Kokko and Rothman is used for this purpose [9], which can be written as:

$$R_i = \frac{R}{R+B}N_i + \text{ß}\frac{RB}{(R+B)^2}N_{i,eq}^0 cos(\theta_i - \theta_f) \tag{5.6}$$

$$B_i = \frac{B}{R+B}N_i - \text{ß}\frac{RB}{(R+B)^2}N_{i,eq}^0 cos(\theta_i - \theta_f) \tag{5.7}$$

Here, $N_{i,eq}^0$ is the zero velocity equilibrium distribution function determined for the total distribution function N_i using Eq. 3.17 as:

$$N_{i,eq}^0 = W_i(R + B) \tag{5.8}$$

The interface thickness is determined by the diffusive parameter ß, which has to be less than 1.0 for a mildly diffusive interface in order to incorporate
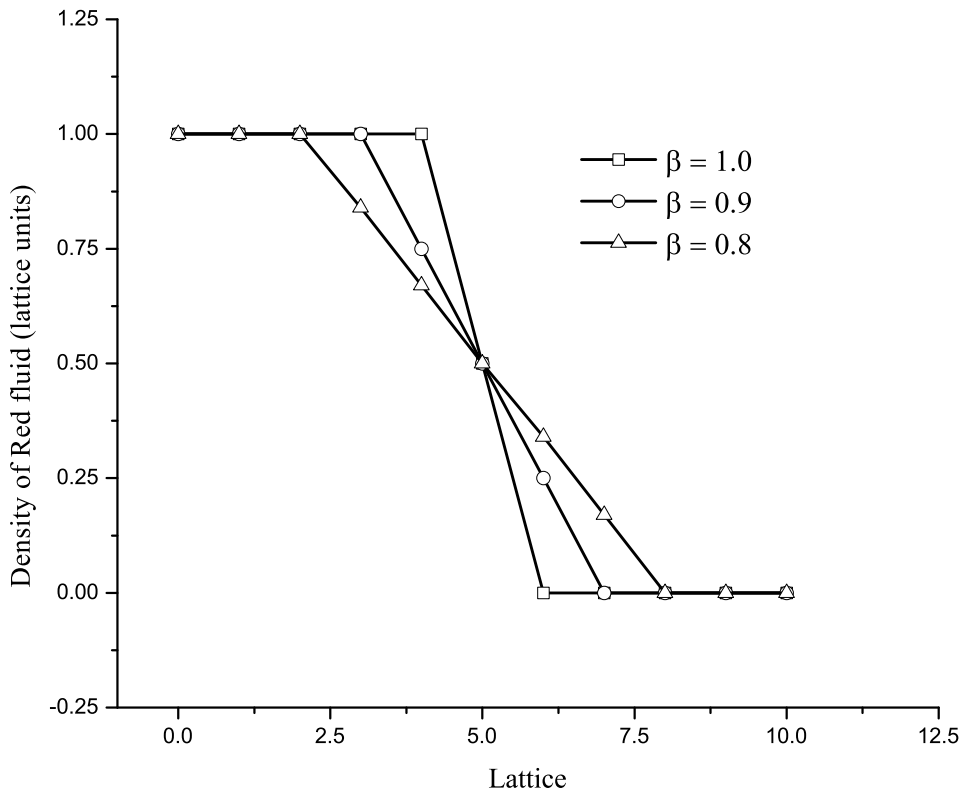
Figure 5.1: Plot of lattice density of one of the components (R) along the lattice length, indicating the dependence of interface thickness of two immiscible fluids on separation parameter ß. As ß approaches 1.0, the interface tends to its sharpest form.

two fluids of different viscosities. Fig. 5.1 shows the variation of interface thickness with respect to ß. As the value of ß approaches 1.0, the interface tends to attain its sharpest form. Values of greater than 1.0 may induce negative values in the particle distribution functions of the fluids.

5.1.2 Wettability

Wettability of the fluids has to be taken into account in order to consider the contact angle dependent surface tension forces driving the spontaneous imbibition flows. This has been done by considering the nodes on the solid boundary to be assigned with the presence of the wetting fluid by providing a finite density value of the fluid [3]. This assignment is only for the purpose of calculating the color gradient. The color gradient at the corresponding fluid nodes is perturbed due to such considerations, which in turn leads to

a modification of the distribution function values, mimicking the preferential affinity. The resulting equilibrium contact angle is related to the assigned wetting fluid density by,

$$\rho_w = cos(\theta_{eq}) \times 1 \; lattice \; number \; density \qquad (5.9)$$

Here ρ_w denotes the value of assigned wetting fluid density to the solid nodes and θ_{eq} denotes the equilibrium contact angle. The equation is dimensionally balanced by multiplication with the unit of number density.

5.2 Capillary imbibition in a two-dimensional channel

The surface tension LBM model was validated using a spontaneous imbibition displacement process in a two dimensional channel. The walls of the channel are considered to be solid boundaries and periodic boundary conditions are assumed at the open boundaries. The non-wetting fluid is assumed to be present in the channel between the wetting fluid as shown in Fig. 5.2. Different values of number densities are assigned for the wetting fluid at the wall sites and the corresponding equilibrium contact angles are obtained. Thus, the assignment of appropriate number densities at the wall sites can take the wettability considerations into account for a range of contact angles.

Further simulations were performed for the imbibition of a wetting fluid into a channel initially filled with a non-wetting fluid. The wetting fluid forms a concave meniscus as shown in Fig. 5.3(a), and enters the channel displacing the non-wetting fluid from the opposite boundary. The fluids assumed to have an equal density and gravitational force is assumed to act in the direction opposite to imbibition according to Eq. 3.24. Hence, it is observed that the imbibing fluid comes to rest after a certain imbibition distance (distance of the meniscus from the inlet when it comes to rest). Different values of number densities of the wetting fluid are assigned to the wall sites, to obtain different imbibition distances. The variation of imbibition distance with respect to the cosine of the equilibrium contact angle used for the imbibition is shown in Fig. 5.3(b). The imbibition distance is found to have a linear relationship with the cosine of the contact angle used, as observed in the literature [3].

5.3 Concluding remarks

An immiscible fluid flow model for the LBM has been developed based on the two-color scheme, along with the inclusion of an interface parameter (ß). The model is observed to maintain a reasonably thin interface for values of ß close to 1.0. The wettability effects are incorporated by assigning biased number densities of the wetting fluid on the walls, their values depending on the equilibrium contact angle. A range of equilibrium contact angles were obtained by using different values of the wetting fluid number density. A spontaneous imbibition of a wetting fluid into a channel filled with non-wetting fluid was simulated, and the imbibition distance was found to be directly proportional to the cosine of the contact angle. In the next chapter, this model is used in the complex porous geometry of a sand pack to simulate the co-current spontaneous imbibition of water in a oil-saturated water-wet sand pack.
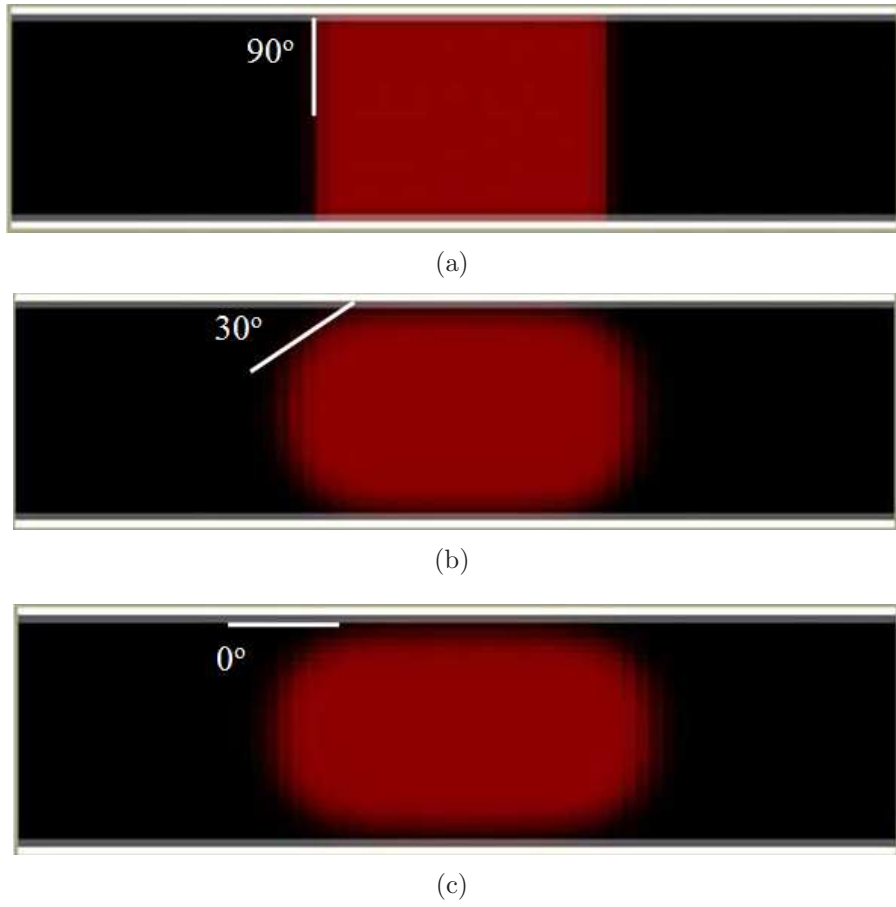
Figure 5.2: Equilibrium contact angles of (a) 90° (b) 30° and (c) 0° obtained by the preferential coloring of solid sites by number density of the wetting fluid. The non- wetting (red) fluid is initially positioned between wetting (black) fluid touching the solid walls on both sides. A meniscus is gradually obtained depending on the value of density of colored fluid on walls.
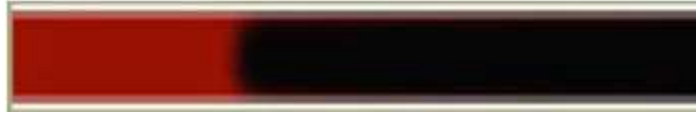
(a)
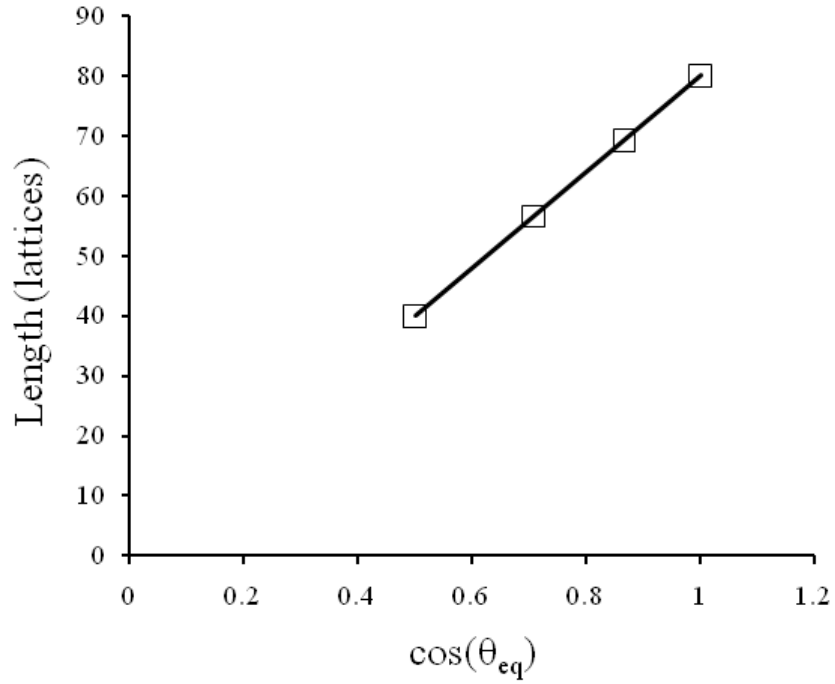
(b)

Figure 5.3: (a) A spontaneous imbibition displacement of non-wetting (black) fluid by wetting (red) one. Preferentially wettability gives rise to a meniscus and a surface tension force. The interface velocity asymptotically approaches zero after a certain time. (b) Validation of surface tension model by plotting the length of imbibition against cosine of the contact angle. The linear variation obtained agrees with the literature [3].

Chapter 6

Co-current spontaneous imbibition by LBM [1]

The LBM model developed in Chapter 5 is applied in this chapter to simulate the co-current spontaneous imbibition (or capillary imbibition) of water in a kerosene saturated two-dimensional sand-pack. The objectives of this chapter are two-fold: (1) An extensive and critical analysis of application of the LBM technique to model spontaneous imbibition and understand the pore-scale displacement, and (2) to obtain capillary imbibition relative permeabilities for co-current displacement of resident oil in a two dimensional porous matrix for various geometric and fluidic parameters. This analysis proves the capability of LBM simulations to capture displacement velocities necessary in acquiring relative permeability curves. Also, the dependence of the relative permeability curves on various parameters such as porosity, contact angle, interfacial tension, gravitational influence and aspect ratio of the matrix is studied. Such a relative permeability analysis provides valuable data for further studies related to the estimation of oil recovery.

---

[1]Parts of this chapter have been submitted for publication: *A. Gunde, T. Babadagli, and S. K. Mitra. A generic framework to obtain oil-water relative permeability for capillary driven transport in water-wet fractured porous media by LBM (submitted). Water Resources Research.*

6.1 Experimental and LBM systems

The developed LBM model was validated through comparison with experiments performed by Hatiboglu and Babadagli [5], involving a two dimensional sand pack model having dimensions 5 cm × 5 cm, and comprised of glass spheres as solid grains. The average size of an individual grain was 0.1 mm. The grains were highly water-wet and an ideal equilibrium contact angle of 0° was assumed. In experiments, the sand pack was initially saturated with kerosene and then immersed into water in a vertical position. The two vertically inclined boundaries were closed. Two different sets of experiments were performed with water in contact with both boundaries and only with the bottom boundary, respectively. These configurations are shown in Fig. 6.1. The former arrangement was observed to show a gravity-assisted displacement, while the latter showed a gravity-opposed one. The physical properties of kerosene and water are given in Table 6.1.

Table 6.1: Properties of fluids

Property	Water	Kerosene
Density (g/cm^3)	0.99	0.79
Viscosity (cp)	1	2.9
Interfacial Tension $(dyne/cm)$	46.1	46.1
Bond Number	2.5×10^{-4}	2.5×10^{-4}

In order to obtain a direct comparison with the physical system, the lattice variables are determined by dimensionally scaling them to their respective experimental values. The parameters which are constrained regarding the values they can possess in a LBM simulation are the fluid viscosities (less than 0.166667) and interfacial tension (less than 1.0). The other quantities can be scaled accordingly.

$$
\begin{aligned}
\nu_l &= \nu \frac{\Delta t}{\Delta x^2} \\
\sigma_l^{ift} &= \sigma^{ift} \frac{\Delta t^2}{\Delta m} \\
g_l &= g \frac{\Delta t^2}{\Delta x}
\end{aligned}
\tag{6.1}
$$

Here, ν, σ^{ift} and g are the physical values and ν_l, σ_l^{ift}, and g_l are the
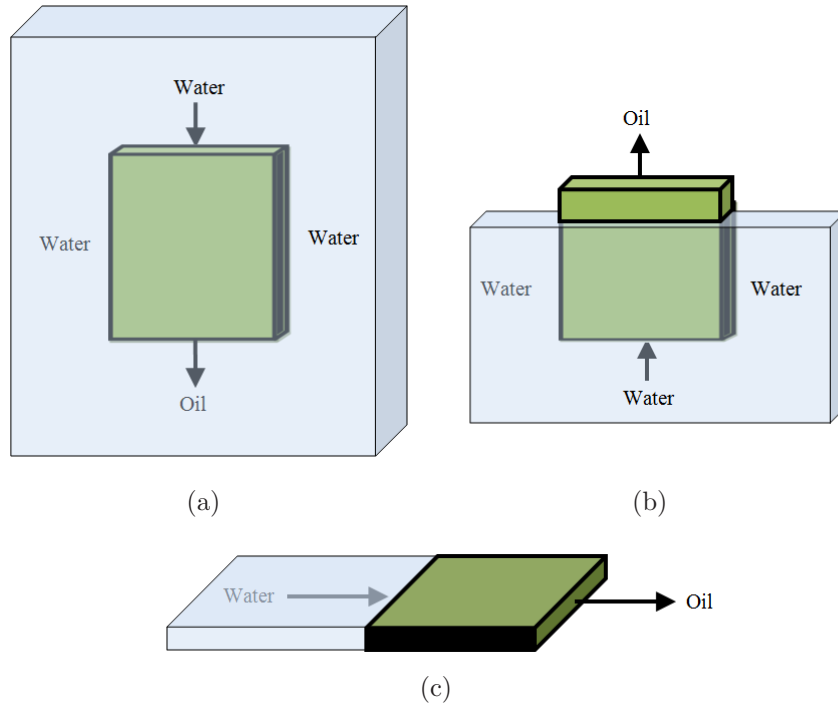
Figure 6.1: A typical (a) gravity-assisted, (b) gravity-opposed and (c) horizontal configuration. Sand pack model is initially saturated with kerosene and then immersed in water. The boundaries experiencing flow (indicated by arrows) are kept open. Water imbibes into the porous matrix due to spontaneous imbibition and/or gravity in co-current fashion.

scaled lattice values of kinematic viscosity, interfacial tension and gravitational constant, respectively. Δt, Δx and Δm are the scaled physical values of length, distance and mass for each of their respective lattice counterpart. In this work, an artificial porous structure was considered for analysis as a generic porous medium. It consists of a two dimensional channel with a certain number of solid grains randomly placed within which gives rise to its porous nature. In this case, while extending such a system to any physical porous medium consisting of packed solids, the geometric parameter of significance is the ratio of characteristic dimensions of the channel and an individual grain. This ratio has to be observed in order to determine the size of the actual porous medium simulated. Further, the average spacing between any two grains is adjusted so that the LBM analysis is numerically stable. Hence, in order to emulate a flow through a typical experimental porous structure, the lattice structure chosen should have these geometric conditions.

6.1.1 Boundary conditions

Solid wall boundaries encountered in the porous domain are dealt with by using the simple bounce-back scheme [70] which applies the no-slip condition. However, in the case of the presence of curved boundary surfaces, interpolated boundary conditions have been used as shown in Fig. 4.1 [72]. Open boundaries at two sides of the matrix in a co-current displacement process are accounted for by applying periodic boundary conditions [69] at the inlet and outlet.

6.1.2 Gravitational force

Gravitational force is numerically included by the addition of an equivalent change in momentum to the fluid velocities. This is calculated as:

$$\mathbf{F}_g = (\Delta \rho_l^{eff}) \mathbf{g}_l \qquad (6.2)$$

Here, $\Delta \rho_l^{eff}$ is the difference between the scaled lattice densities of the wetting and non-wetting phases. Scaled values of effective lattice density and lattice acceleration due to gravity ($\mathbf{g}_l$) are used to calculate the force term as described in section 6.1.3.

6.1.3 Selection of lattice parameters

.

LBM simulations were run for different sizes of the lattice grid and a final lattice discretization was arrived at. In the case of gravity-assisted flow, the computational domain was divided into a uniform grid of 400×400 lattices with a solid grain considered to be 2 lattices in diameter; in order to approach geometric similarity between the physical porous system and the lattice system, and to incorporate the required structural detail, while also taking into account the limitations of computational resources. This lattice discretization is similar to the one used by Hatiboglu and Babadagli [5]. Then, a reasonable time step (about 0.001 s) for the simulation was considered while keeping the lattice viscosity (ν_l) in a stable range. The lattice gravitational constant (g_l) was calculated using these length and time scales from Eq. 6.1. A two dimensional simulation was carried out for an actual three dimensional system. Hence, a typical value of effective density (ρ_l^{eff}) was assumed, which was used

to scale the mass of the system and subsequently, to find the value of lattice interfacial tension (σ_l^{ift}) using Eq. 6.1. Though the matrix was in contact with water from the top and bottom boundaries, it was observed experimentally that the dominance of gravity prevented any imbibition from the bottom side [5]. This was applied by using periodic boundary conditions described in section 3.8.5.

In the case of the gravity-opposed displacement, a smaller domain (200×200 lattices) was chosen to incorporate the large number of time steps (about 1000000) involved. Also, viscosities of the two fluids were assumed to be equal to allow a large value of the time steps. The other parameters were scaled accordingly. The approximations involved in the conversion of units were attempted to be kept to a minimum, with the aim of getting approximate matches of displaced areas with time. However, further improvements are still possible with different methods to obtain more accurate agreements with the literature. The LBM results obtained from this unit conversion are described in sections 6.3 and 6.4.

6.2 Calculation of relative permeability

In this work, in order to calculate the relative permeability from LBM simulations, a method of normalizing the total velocity of a phase to the single-phase velocity at same saturations is used, as suggested by Ramstad et al. [35]. The formulation is given as follows:-

$$k_{r\alpha} = \frac{\pi_\alpha(S_\alpha)}{\pi(S_\alpha = 1)} \frac{p(S_\alpha = 1)}{p(S_\alpha)} \tag{6.3}$$

Here, $k_{r\alpha}$ denotes the relative permeability, $\mathrm{p}(S_\alpha)$ denotes the driving pressure and π_α (S_α) denotes the total phase velocity for saturation S_α of a particular phase α, where $\alpha =$ w and $\alpha =$ nw represent the wetting (water) and non-wetting (oil) phase, respectively. The term π is calculated by summing the velocities at all lattices. The quantities with ($S_\alpha = 1$) denote single phase values obtained by conducting additional simulations. Since it is not possible to directly determine the driving pressure in spontaneous imbibition process cases, an analytical method to determine capillary pressure is used, which is then substituted in Eq. 6.3 to determine the relative permeability. The capillary pressure can be determined by the Leverett function given as [4]:-
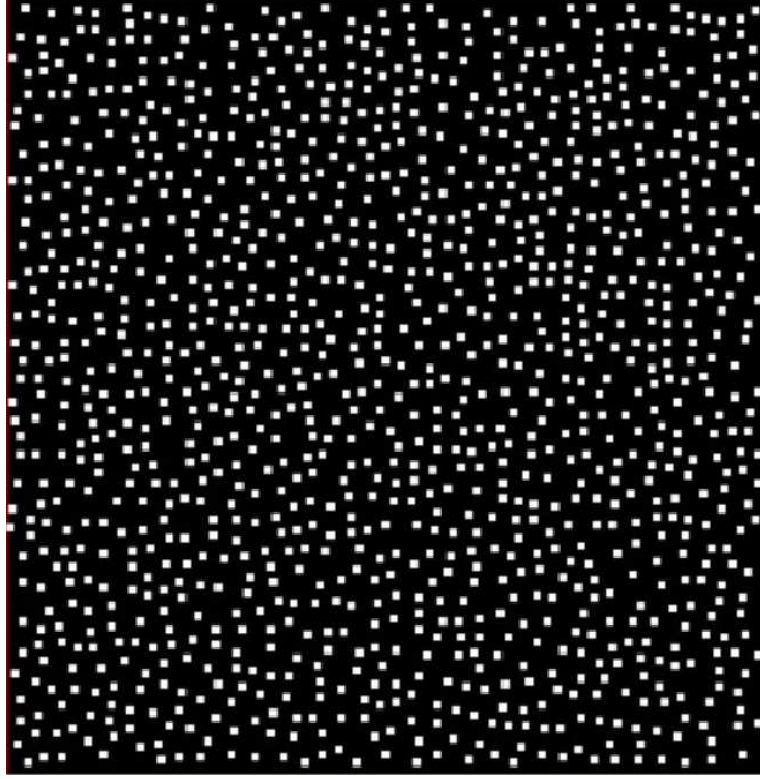
Figure 6.2: Randomly generated porous medium obtained with the constraint of minimum distance between solid grains (white) as 4 lattices (porosity = 79%). Upper and lower boundaries are considered to be solid walls and the medium is assumed to be initially saturated with kerosene with water contact at the left boundary.

$$p_c = p_0 \ \sigma_l^{ift} \ h \tag{6.4}$$

where h depends on saturation, σ_l^{ift} is the lattice interfacial tension scaled according to the method described in section 6.1.3, and p_0 is related to the contact angle (θ_{eq}), porosity (ϕ) and absolute permeability (k) as,

$$p_0 = cos(\theta_{eq})(\frac{\phi}{k})^{1/2} \tag{6.5}$$

The calculation of h is performed by using the power model function of Fatt and Klikoff [18] as shown below:-

$$h = 4.013 - 13.68S_\alpha + 21.313S_\alpha{}^2 - 11.548S_\alpha{}^3 \tag{6.6}$$

The capillary pressure is determined as a function of saturation, which is
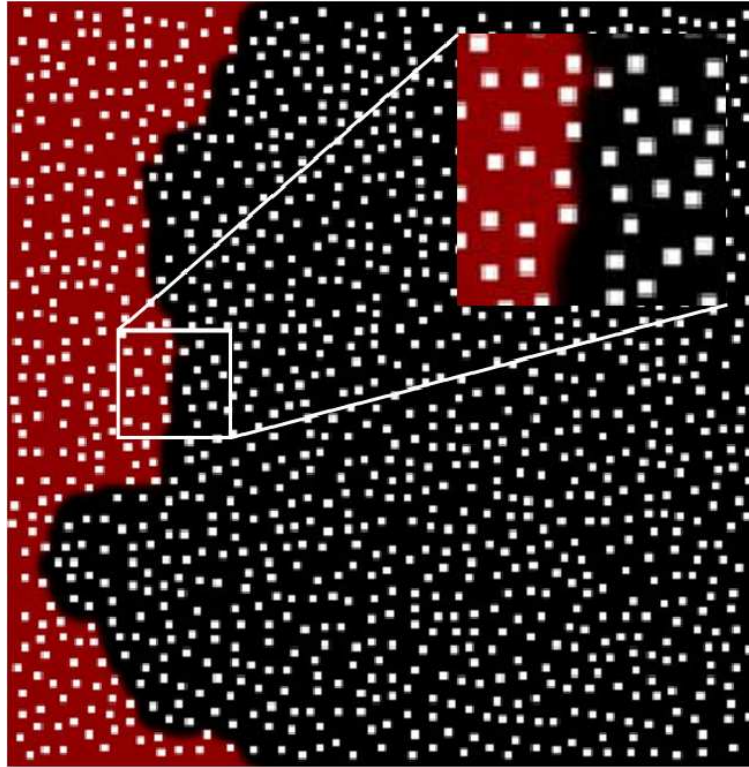
Figure 6.3: Spontaneous imbibition of water (red) into kerosene (black) saturated randomly generated porous medium for a horizontal configuration (porosity = 79%). Flow front observed at a time instant is complete. Absence of residual oil and finger-like profiles due to assumption of equal viscosity for the two fluids and higher porosity.

normalized with single-phase values to obtain the variation of relative permeability with saturation of the wetting and non-wetting phases.

6.3 Solid grain arrangement with porosity 79 %

An initial LBM simulation performed under basic conditions is described in this section. A random arrangement of solid grains in the lattice grid was used to create a porous domain emulating the two dimensional sand pack model. The distance between any two grains (and hence the pore size) was constrained to a minimum value of 4. This kind of regulation is required in order to sustain the stability of the LBM simulation. A typical porous medium obtained by following these considerations is shown in Fig. 6.2. The
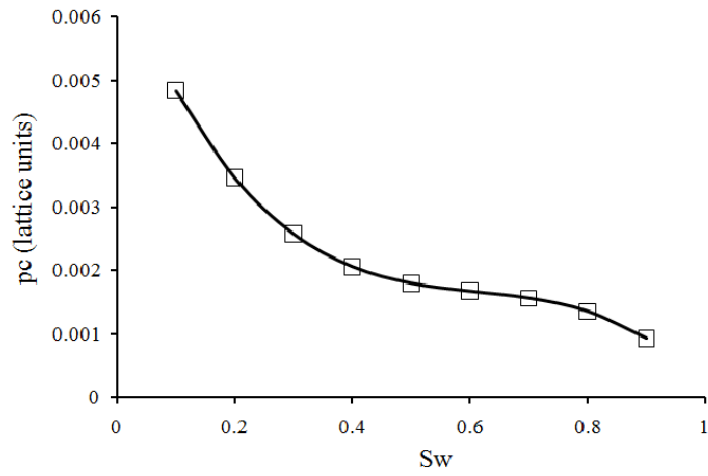
(a)
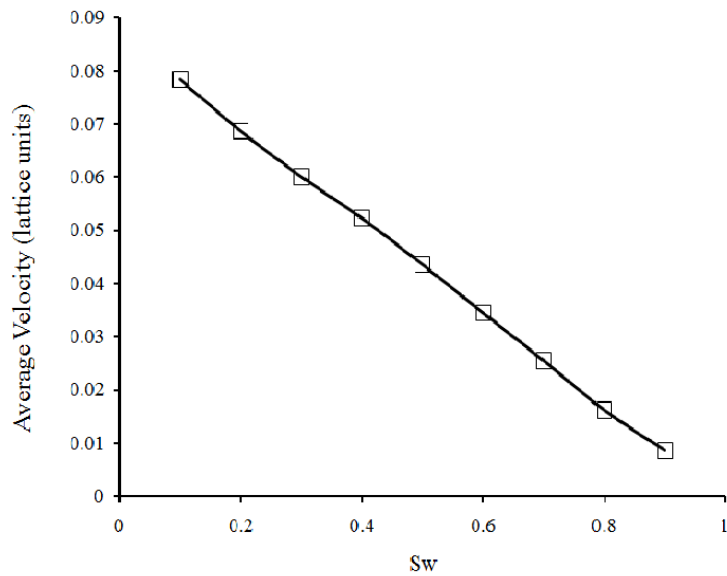
(b)

Figure 6.4: (a)Variation of capillary pressure with respect to saturation of water.(b)Average velocity of wetting fluid shows a continuous decrease with saturation.

viscosities of the two fluids were assumed equal initially for simplicity in the lattice system and scaled to the arithmetic mean of the viscosities of water and kerosene. The geometrical and physical parameters of the fluidic system were scaled accordingly, so as to mimic a co-current displacement with fluidic
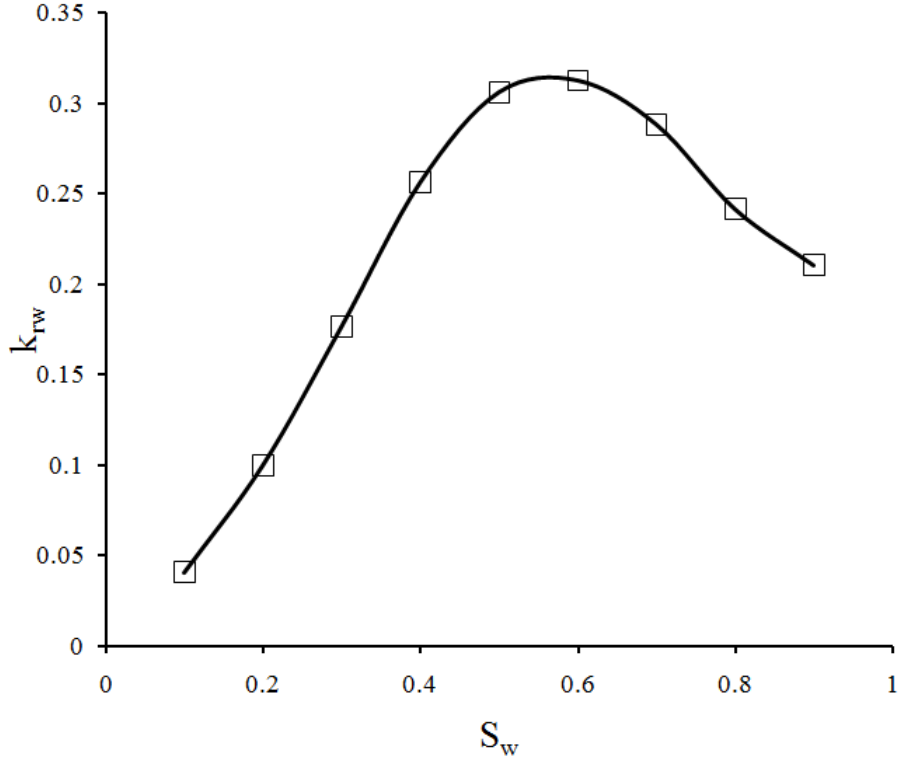
Figure 6.5: Relative permeability curve of wetting fluid (water) for spontaneous imbibition in porous medium (porosity = 79 %)

parameters described in section 6.1.3 without any gravitational force. The consequent simulation was reasonably stable, and a global mass conservation was observed with a final mass increase of 0.0369% confirming the assumption of incompressibility. An example case showing the frontal progress is provided in Fig. 6.3. The LBM simulation shows a continuous kerosene displacement in a co-current fashion. However, an absence of residual oil and finger-like fronts was observed due to relatively high porosity of the medium and the assumption of equal viscosities for the two fluids.

The variation of capillary pressure with water saturation calculated from Eq. 6.4 is illustrated in Fig. 6.4(a). The average velocities of both the components are approximately equal in this case due to the absence of residual oil which results in a complete sweep of kerosene. The average velocity of water shows a continuous decrease with increasing water saturation as observed in Fig. 6.4(b). This value was used to calculate the total phase velocity of water, which was then used in Eq. 6.3 to calculate the water relative permeability
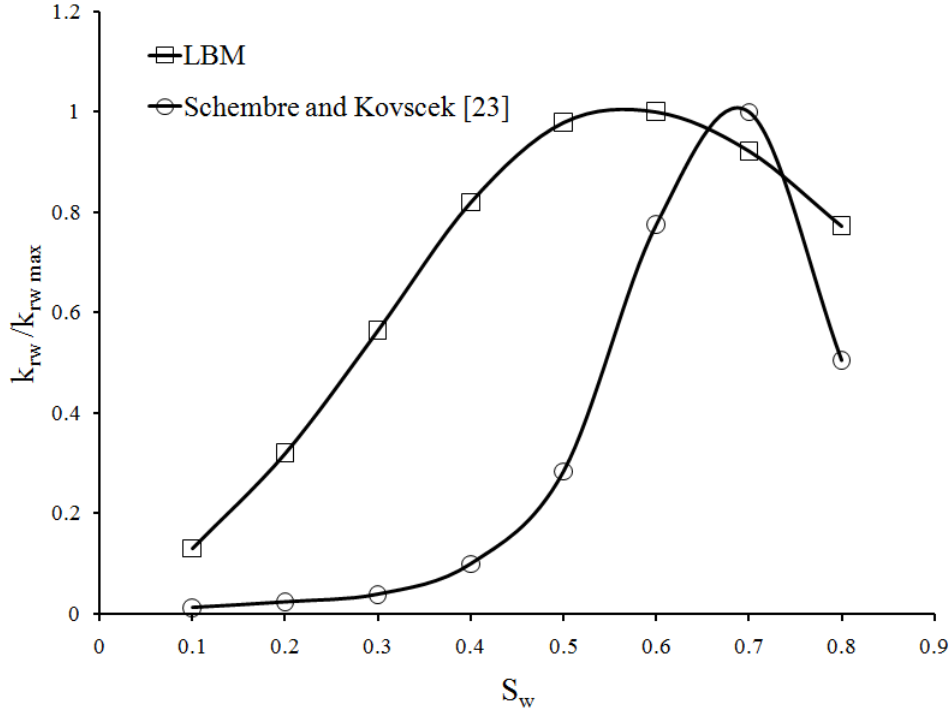
Figure 6.6: Comparison of relative permeability curves of wetting fluid (water) for spontaneous imbibition in porous medium (porosity = 79%), obtained from LBM and literature by Schembre and Kovscek [4]. Decrease in relative permeability in later stages captured by LBM model.

(k_{rw}). The water relative permeability curve is plotted in Fig. 6.5. In spite of the reduction in the rate of decrease of capillary pressure in the later saturation stages, the imbibing velocity did not recover and continued to decrease. This caused the water relative permeability to have a continuous initial increase and a subsequent decrease after a water saturation of 0.75. Such a decrease has been observed in the literature [4] and Fig. 6.6 shows a comparison of the relative permeability trends obtained from LBM simulations and micro-CT experiments for the synthetic oil-water case. In this figure the value of relative permeability k_{rw} has been normalized by $k_{rw\ max}$ which is the maximum water relative permeability observed. The absolute values of relative permeability are different for both cases due to different types of geometrical and fluidic conditions; however, the qualitative trend of relative permeability decrease in later saturation stages has been captured by the present LBM model.

6.4 Solid grain arrangement with porosity 74 %

Results of displacement obtained in section 6.3 showed an absence of residual oil and finger profiles. Further simulations were performed on porous geometry with a further reduced minimum distance between two grains to a value of 3, so as to mimic a more compact arrangement representing the physical system of a two-dimensional sand pack model. A typical porous medium obtained by such a constraint is shown in Fig. 6.7. The simulation was carried out with scaled parameters for gravity-assisted and gravity-opposed displacements. Fig. 6.8 shows a comparison of saturation profiles at same time instants obtained from LBM and experimental results [5]. The LBM simulations were conducted using physical properties of fluids provided in Table 6.1. A reasonable agreement was observed between the two results. The reduction of saturation velocity to very low values during later saturation stages was observed in LBM simulations. Further simulations were carried out for a horizontal orientation of the sand pack model to negate the effect of gravity. It was observed that the penetration of the wetting fluid was primarily in the form of finger-like patterns due to a difference in the viscosities of the two fluids as shown in Fig. 6.9. Also, the presence of trapped oil was observed primarily in large pore regions surrounded by smaller pores, due to the nature of surface tension flows.

Relative permeability curves are plotted for the gravity-assisted and gravity-opposed cases and are shown in Fig. 6.10. It can be observed that the gravity-assisted curves are almost linear in nature due to the addition of a gravitational driving force. However, the gravity-opposed arrangement consisted of surface tension force overcoming the gravitational force and displacing the kerosene. This is reflected in the relative permeability curves, which show a capillary trend. Further curves are plotted for the horizontal configuration for two different viscosity ratios. They are presented in Fig. 6.11. A qualitative and quantitative difference is observed in the trends for the wetting and non- wetting fluids, which is more prominent for viscosity ratio 3, which is defined as the viscosity of oil over water. In this case, the presence of residual oil and viscosity ratio of the two fluids cause the two fluids to possess different velocities for a particular saturation. However, when the viscosities of the fluids were considered equal, the difference in velocities decreased and the relative permeability curves showed markedly less difference. The trend found here is
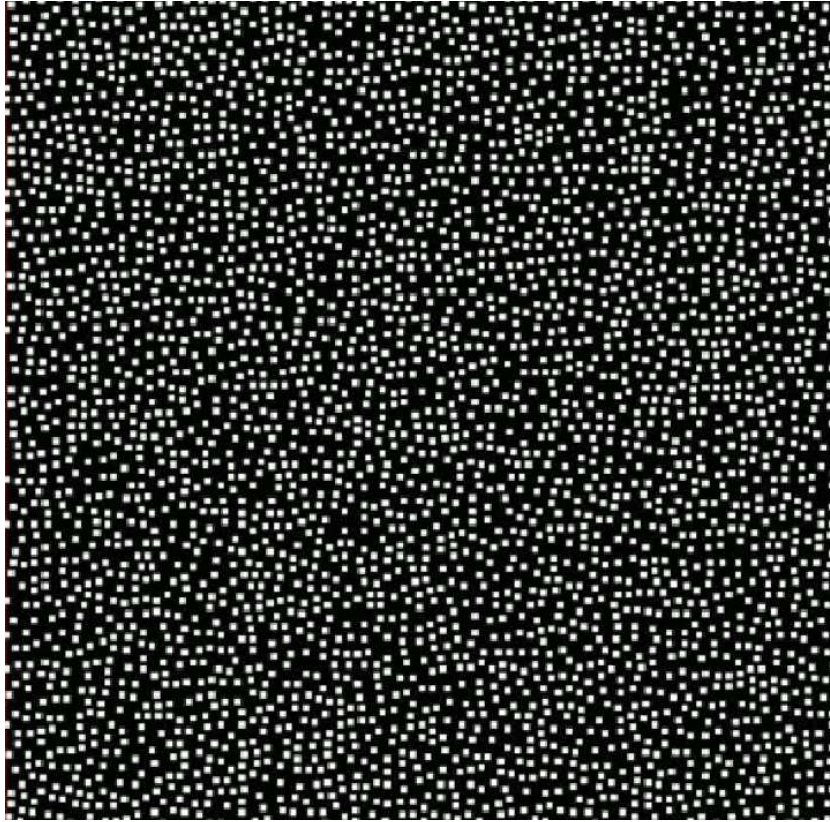
Figure 6.7: Randomly generated porous medium obtained with the maintenance of minimum distance between solid grains (white) as 3 lattices (porosity = 74%). Upper and lower boundaries are considered to be solid walls and the medium is assumed to be initially saturated with kerosene with water contact at the left boundary.

similar to the one observed in the literature for co-current displacement with fluids of different viscosities [35]. In order to observe the dominance of gravity, the curves were plotted for different inclinations of the sand pack, as shown in Fig 6.12. It can be observed that the displacement is gravity dominated in the case of vertical (90°) orientation of the sand pack and that it shows close to linear trends in the relative permeabilities. It gradually becomes surface tension dominated in horizontal (0°) orientation and a 45° orientation shows a variation between these two extremes.
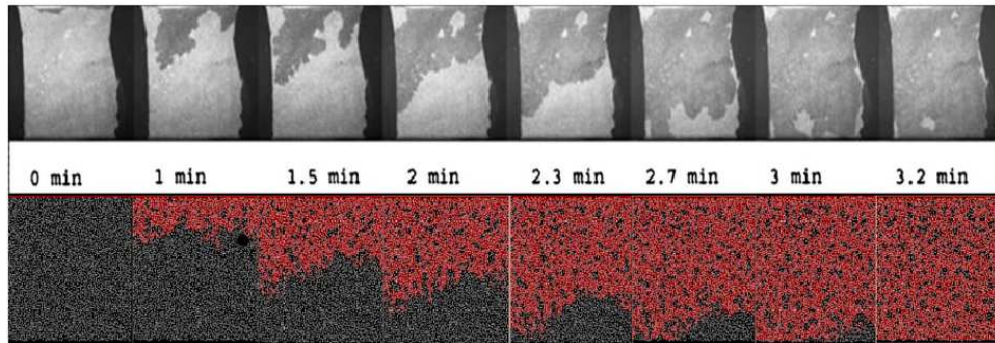
(a)
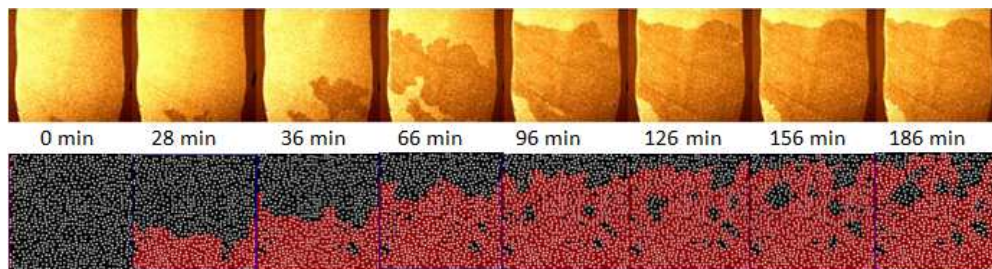
(b)

Figure 6.8: Comparison of saturation profiles at same time instants obtained from LBM and experimental results for (a) gravity assisted and (b) gravity opposed displacements. A reasonable agreement is observed between the sets of two profiles. The darker areas in the experiments (upper images of both cases obtained from literature [5]) represent the imbibing water and lighter areas are oleic phase (2cp kerosene). In the LBM simulations (lower images in both cases) the red (lighter) part is water and black (darker) part is oil.

6.4.1 Relative permeability variation with contact angle and interfacial tension

Simulations were carried out for spontaneous imbibition in a horizontal configuration of the sand pack for three different contact angles and interfacial tension values of the two-component fluid system. The plots are shown in Figs. 6.13 and 6.14. A decrease in interfacial tension or an increase in contact angle caused a corresponding decrease in the capillary pressure for a particular saturation. It can be observed that in both cases there was an increase in relative permeability with a decrease in capillary pressure for both components. This can be explained due to the fact that the drop in velocities of the individual phase components is less than the decrease in capillary pressure.

74

6.5 Solid grain arrangement with different aspect ratios

Further simulations were executed for spontaneous imbibition displacement in a horizontal configuration of the sand pack for two different aspect ratios of the porous matrix, 4:1 and 1:4, respectively. Relative permeability curves for both cases are plotted in Fig. 6.15. The matrix with an aspect ratio of 4:1 showed a typically higher value of relative permeability than that with 1:4. This can be explained by the fact that the lower width of the porous matrix results in higher velocities for the fluids and lower residual oil for similar capillary pressures.

6.6 Solid grain arrangement with different grain distributions

The developed LBM model was applied to three porous matrices with randomly generated solid grains having different grain distributions in order to study the dependence of relative permeability on the distribution of solids in the pore structure. In all the cases, the lattice domain is 400×400 *lattice units* and a minimum distance of 3 *lattice units* is maintained. The model is used to simulate the co-current spontaneous imbibition process for the horizontal case using the fluid propserties given in Table 6.1 and assuming an equilibirum contact angle of 0°. The relative permeability curves obtained for the three different distributions are shown in Fig. 6.16. It can be observed that the curves overlap for all the three cases with a close agreement of the relative permeability values with each other. Thus, the relative permeability is not found to substantially vary with respect to the grain distribution. However, further simulations using different grain and average pore sizes are required to clarify the dependence of relative permeability on pore structures.

6.7 Pore scale observations

Pore-scale modeling of spontaneous displacement from an oil saturated porous medium was performed in the present work using the Lattice Boltzmann method. The simulation results show various pore-scale phenomena captured by the model such as formation of contact angle dependent meniscuses, pres-
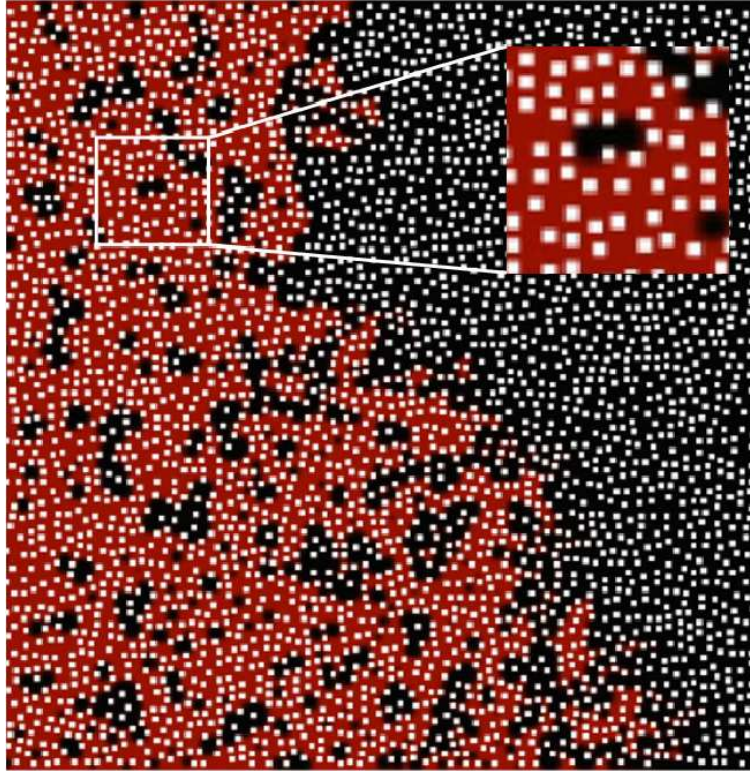
Figure 6.9: Spontaneous imbibition of water (red) into kerosene(black) saturated randomly generated porous medium for a horizontal configuration (porosity = 74%). Prominent presence of residual oil and finger-like profiles due to different viscosities for the two fluids and relatively lower porosity compared to the case shown in Fig. 6.3. A typical oil entrapment in a relatively large pore region surrounded by regions of small pores is observed.

ence of residual oil, and finger-like displacement. The fluid flow profiles obtained from these results yielded a reasonable match with experimental observations on the sand pack model, as described in section 6.4. Some specific observations made related to the two-fluid interface in the pores are described in Table 6.2.

6.8 Summary, remarks and conclusions

6.8.1 LBM modeling

This chapter was a study of multi-component flow through a randomly generated porous medium using a LBM model to analyze the spontaneous imbibition process in a matrix-fracture interaction. The BGK approximation was used
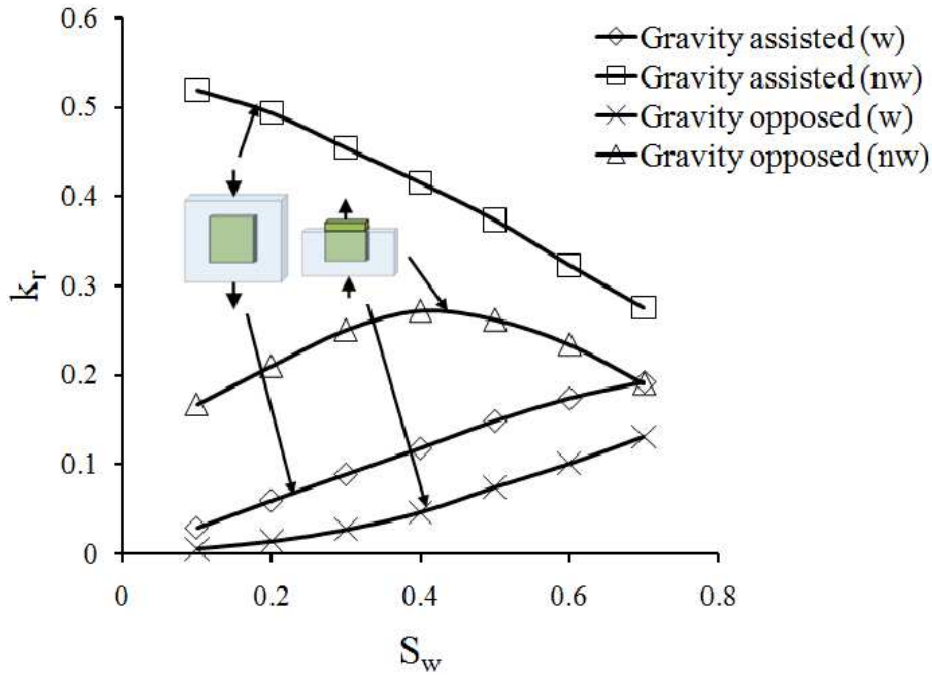
Figure 6.10: Relative permeability curves for gravity-assisted and gravity opposed displacements. The former shows a linear trend due to addition of gravitational force, while the latter shows a capillary trend due to capillary force being the driving force. Here, w and nw refer to the wetting (water) and non-wetting (kerosene) phases, respectively. k_r is the relative permeability with respect to wetting or non-wetting phase as per the given conditions.

to calculate the relaxation parameter. In order to model multi-component flow through the porous region, the two-color LBM model was used, with an interface parameter dependent additional separation scheme to ensure immiscibility of the fluids. Surface tension force was incorporated by preferential coloring of solid wall nodes with density of the wetting fluid. Interpolated and periodic boundary conditions were used to apply a no-slip condition and the conservation of mass respectively. It was found that the displacement in an initial sparse porous matrix (porosity = 79%) with equal fluid viscosities was in the form of a complete sweep without any residual oil. A relative permeability plot for the simulation showed a decrease in the wetting fluid relative permeability in later saturation stages, which was qualitatively validated from the literature.

Further simulations were performed for a compact porous matrix (porosity = 74%) which was assumed to mimic a two-dimensional sand pack model. Saturation profiles obtained for gravity-assisted displacement were found to
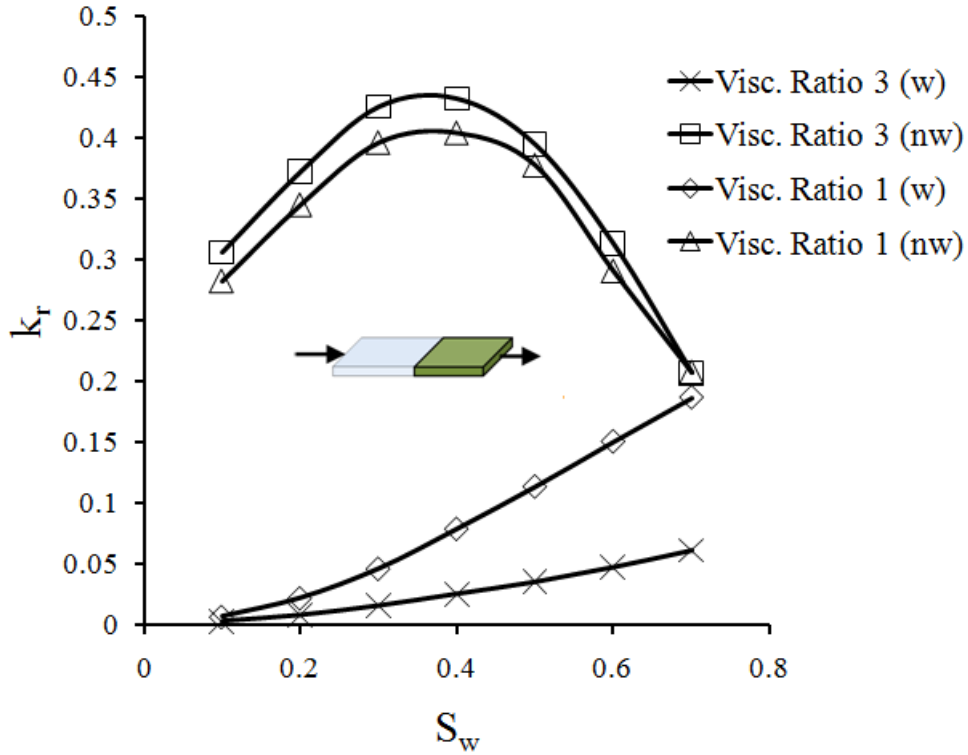
Figure 6.11: Relative permeability curves for horizontal spontaneous imbibition in porous medium (porosity = 74%) for two different viscosity ratios. In case of different viscosities, the curves tend to show a relatively larger difference due to difference in velocities of the two fluids. Here, w and nw refer to the wetting (water) and non-wetting (kerosene) phases, respectively. k_r is the relative permeability with respect to wetting or non-wetting phase as per the given conditions.

reasonably agree with experimental results obtained under similar conditions from the literature. A presence of residual oil and finger-like interface profiles were observed for a horizontal configuration with viscosity ratio 3, which instilled an increased difference in velocities and hence, the subsequently calculated relative permeabilities.

A pore scale analysis of the LBM simulation results led to the observation of various interface processes such as meniscus formation, oil entrapment, and frontal displacement. This kind of analysis can provide a basic understanding of actual phenomena taking place inside a porous structure, which can be subsequently used to calculate relative permeability values and characterize the efficiency of the recovery mechanism.
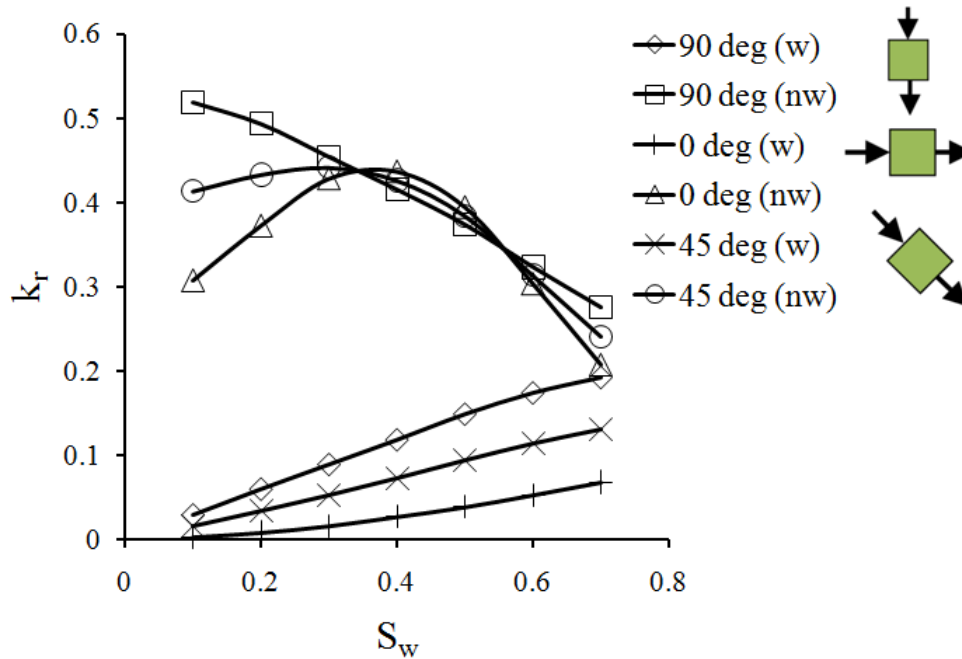
Figure 6.12: Relative permeability curves for spontaneous imbibition in porous medium (porosity = 74%) for different inclinations of the porous matrix. The plot is gravitational trend in case of vertical (90°) inclination and gradually becomes surface forces dominated in horizontal (0°) inclination. The arrows indicate the displacement direction. Here, w and nw refer to the wetting (water) and non-wetting (kerosene) phases, respectively. k_r is the relative permeability with respect to wetting or non-wetting phase as per the given conditions.

6.8.2 Oil-water capillary imbibition relative permeabilities

The variation of relative permeability curves was studied for different inclinations of a sand pack model, showing the gradual dominance of gravity. Further simulations were performed for different contact angles and values of interfacial tension, which showed an increase in relative permeability with decreasing capillary pressure. Additional simulations were performed for porous matrices with two different aspect ratios and the relative permeability plots were observed. The following observations can be extracted from the relative permeability plots given in Figs. 6.10 through 6.15:-

- In all cases, the relative permeability to oil showed a concave shape, i.e. it increases with increasing water saturation (contrary to characteristic
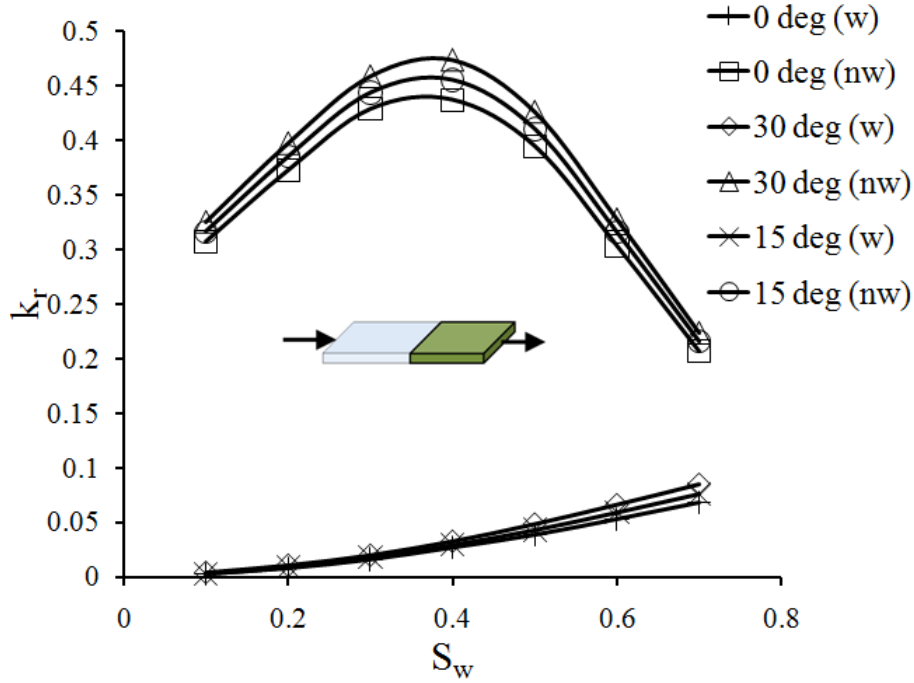
Figure 6.13: Relative permeability curves for horizontal spontaneous imbibition in porous medium (porosity $= 74\%$) for different contact angles. Relative permeability is observed to increase with contact angle, due to the higher corresponding velocities of both components at lower capillary pressures. Here, w and nw refer to the wetting (water) and non-wetting (kerosene) phases, respectively. k_r is the relative permeability with respect to wetting or non-wetting phase as per the given conditions.

relative permeability curves for viscous displacement) and reaches a peak value and declines. This peak value is around 40% of water saturation regardless of the parameters changed (contact angle, aspect ratio, interfacial tension and inclination angle). Once the gravity starts dominating the process strongly (angle 90° in Fig. 6.13), the relative permeability curves become reminiscent of conventional viscous displacement ones (cross shape curves). Note that the intersecting points of the oil and water relative permeability curves are beyond the 50% water saturation point, indicating strong water wettability of the system. All these infer that the curves are controlled by the boundary condition that determines the roles of capillarity and gravity. The system shown in Fig. $5(a)$ is a complex structure (the top and bottom are open but both sides are
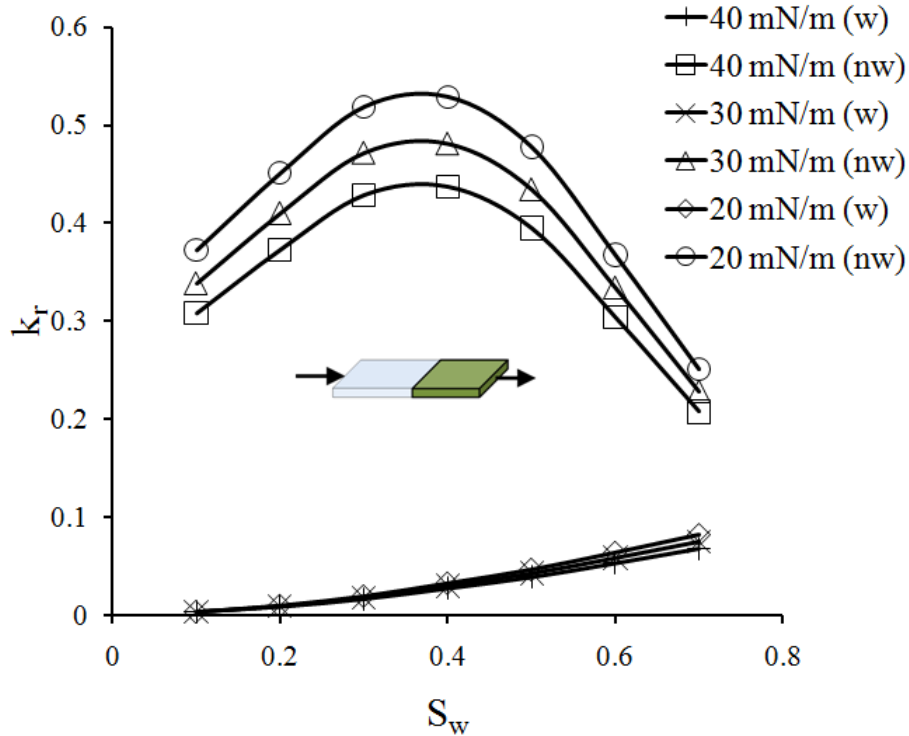
Figure 6.14: Relative permeability curves for horizontal spontaneous imbibition in porous medium (porosity = 74%) for different interfacial tensions. Relative permeability is observed to decrease with interfacial tension, due to the higher corresponding velocities of both components at lower capillary pressures. Here, w and nw refer to the wetting (water) and non-wetting (kerosene) phases, respectively. k_r is the relative permeability with respect to wetting or non-wetting phase as per the given conditions.

in contact with water) for oil-water interaction in presence of capillary forces. This implies that the shape of the oil relative permeability curves is controlled by the dominance of the capillarity and gravity forces on the matrix.

- In three cases (Figs. 6.13, 6.14, and 6.15), the change of water relative permeability curves is not as significant as that of oil relative permeability curves with changing parameters such as contact angle, interfacial tension, and aspect ratio. Water relative permeabilities are more sensitive to the viscosity ratio and inclination angle for the interaction type considered in this study compared to oil relative permeabilities. This is more pronounced in the case of the viscosity ratio. Interestingly, both
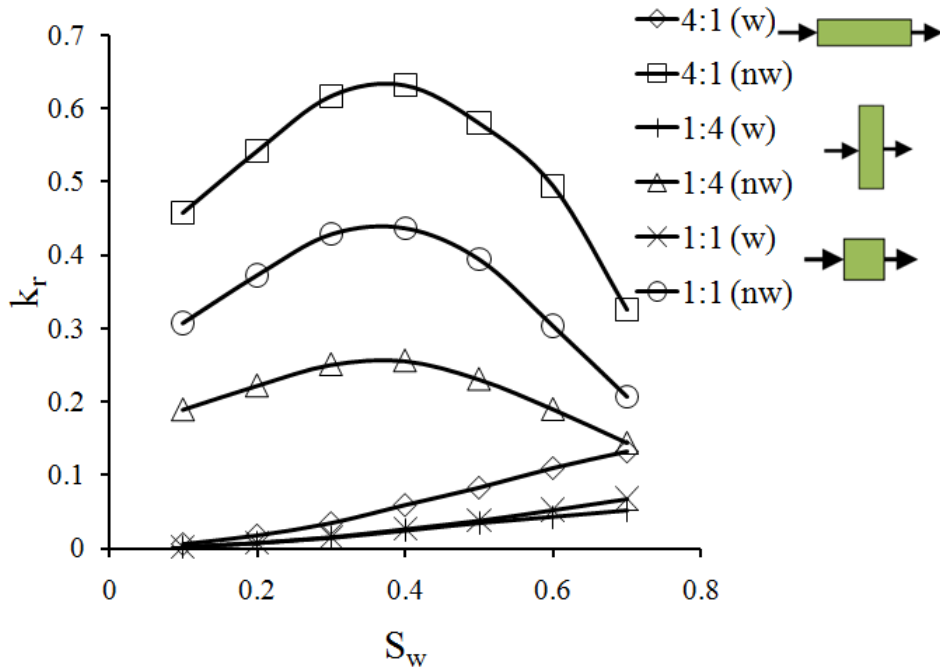
Figure 6.15: Relative permeability curves for horizontal spontaneous imbibition in porous medium (porosity = 74%) for porous matrices with two different aspect ratios. Relative permeability is observed to be higher in case of 4:1 matrix because of lower residual oil. The arrows indicate the displacement direction. Here, w and nw refer to the wetting (water) and non-wetting (kerosene) phases, respectively. k_r is the relative permeability with respect to wetting or non-wetting phase as per the given conditions.

oil and water relative permeabilities increased with changed parameters (given in the plots of Figs. 6.12 through 6.15) except the viscosity ratio case (Fig. 6.11). In this case, the oil relative permeability increased with an increasing viscosity ratio while the water relative permeability decreased and this change in the relative permeabilities for both phases is considerable. In conclusion, the changes on the matrix shape (Fig. 6.15) and interfacial properties (Figs. 6.13 through 6.15) do not affect water relative permeabilities, whereas the change is highly critical with the oil viscosity and inclination angle (gravity vs. capillary dominated displacement). Oil relative permeabilities were highly affected by changing the matrix shape (Fig. 6.15) and interfacial tension.

- The difference among the three curves is not significant and within the given range of contact angle (0-30°) there exists strong capillary suction
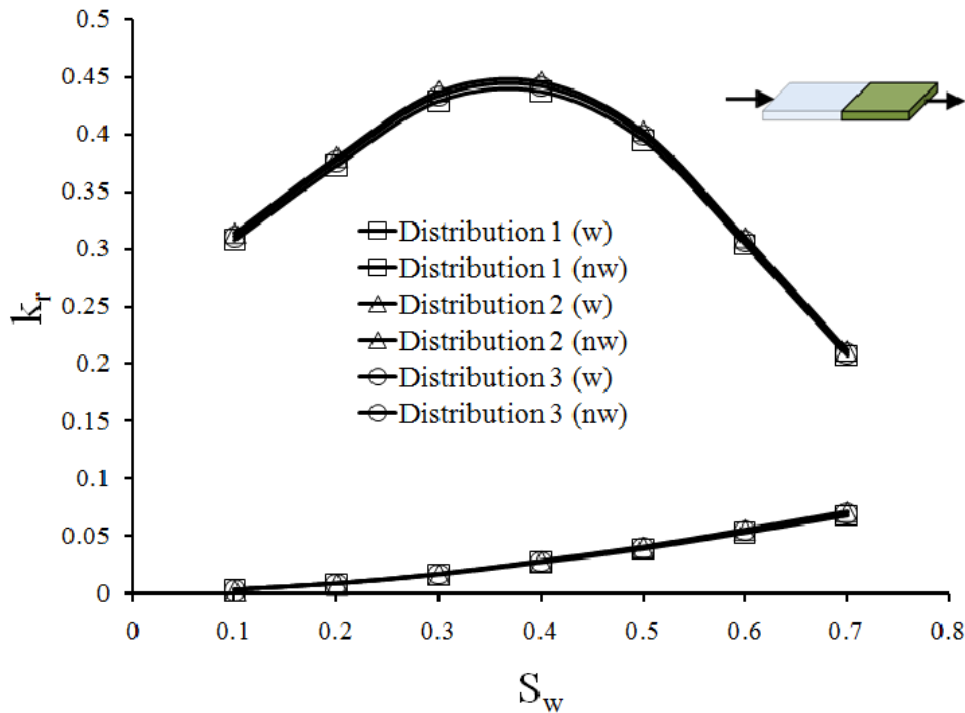
Figure 6.16: Relative permeability curves for horizontal spontaneous imbibition in porous medium (porosity = 74%) for three porous matrices with different solid grain distributions. Relative permeability is not observed to be dependent on grain distribution, since the curves are in close agreement with each other. Here, w and nw refer to the wetting (water) and non-wetting (kerosene) phases, respectively. k_r is the relative permeability with respect to wetting or non-wetting phase as per the given conditions.

to initiate the process. The change in the relative permeability curves is trivial when the contact angle is changed within the range of (0-30°). Further change in the contact angle substantially impact spontaneous imbibition and hinders any water intrusion into the system even if less than 90°.

The curves presented in this chapter are very different to the characteristic curves obtained for viscous displacement cases. The characteristics of the capillary imbibitions relative permeability curves that distinguish them from that of viscous displacement relative permeability curves, i.e., the curved shape of oil relative permeability curves and the simultaneous increase of both relative permeabilities with changing parameters up to a certain water saturation as well as matrix shape and size dependency, are summarized above. We also

showed that one may obtain typical relative permeability curves if the system is controlled greatly by gravity (intersecting curves as represented by square symbol for a 90° angle in Fig. 6.12). In addition to the concave shape relative permeabilities, the dependency of the curves on the shape and boundary conditions of the matrix block was an interesting outcome of this research.

This study presented an extensive analysis of capillary driven displacement (spontaneous imbibition) coupled with gravity displacement at pore scale and the results were presented as relative permeability curves. This data is useful for simulation studies done for performance estimation in any naturally fractured reservoir system. Interesting and promising observations are highly encouraging for further studies and clarification on the effect of matrix boundary conditions such as comparison with counter-current displacement which is done in the next chapter.

Table 6.2: Various interface shapes observed at the pore scale for the horizontal configuration

No.	Pore scale image	Description
1		wetting fluid penetrates through smaller pore region, but forms a meniscus and stays for large pore for 0° contact angle.
2		wetting fluid spreads over solid grain surfaces displaying high spreading and tends to achieve 0° contact angle.
3		wetting fluid spreads over solid grain and forms inclined meniscus for 0° contact angle.
4		wetting fluid forms a meniscus for 70° contact angle and fails to penetrate further due to achievement of equilibrium contact angle.
5		wetting fluid forms an inclined lower meniscus for a contact angle of 40°
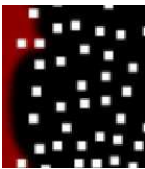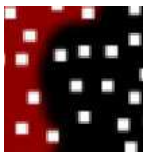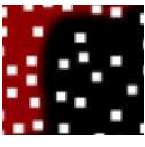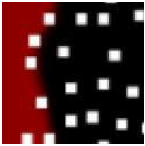
Chapter 7

Counter-current spontaneous imbibition by LBM [1]

This chapter applies the LBM model developed in Chapter 5 to perform simulations of counter-current imbibition in a fractured porous medium and compares the obtained saturation profiles with experimental results from literature [5]. The two-color model with the interface diffusion parameter [9] is used, along with the wettability method proposed by Latva-Kokko and Rothman [3]. The pore-scale interfacial profiles are studied in order to understand the basic physics of the counter-current capillary displacement process. The simulation is performed on two porous matrices of different sizes in order to study variability of counter-current and co-current displacement processes. A two-phase relative permeability curve is obtained to quantify the displacement process. The relative permeability curves are then plotted for different values of contact angles and interfacial tensions and their respective variation is analyzed. This study can provide a basis for further simulations of counter-current flows by LBM and understanding the physical processes involved in such displacement mechanism.

---

[1]Parts of this chapter have been submitted for publication. *A. Gunde, T. Babadagli, S. Roy, and S. K. Mitra. Pore-scale interfacial dynamics and oil-water relative permeabilities of capillary driven counter-current flow in fractured porous media (submitted).*

7.1   Experimental and LBM systems

A counter-current displacement of resident oil by water due to capillary imbibition is simulated by the LBM model described in Chapter 5. The LBM simulations are compared with an experimental data of counter-current displacement obtained from the literature [5]. Schematics of co-current and counter-current displacement are shown in Fig.7.1. The porous medium used in the experiment involves a two dimensional sand pack made up of highly water-wet spherical glass beads compressed together between two acrylic sheets to form a 5 cm × 5 cm porous matrix. The average grain size and the equilibrium contact angle were assumed to be 0.1 mm and 0°, respectively. Three boundaries of the sand pack are closed leaving only one open boundary. The porous matrix is initially saturated with kerosene and then immersed in water in a horizontal position, as shown in Fig. 7.2. The water beside the open boundary behaves as a fracture fluid. The resident kerosene is observed to be displaced by imbibing water due to capillary imbibition. The physical properties of kerosene and water are given in Table 7.1.

Table 7.1: Properties of fluids

Property	Water	Kerosene
Density (g/cm^3)	0.99	0.79
Viscosity (cp)	1	2.9
Interfacial Tension $(dyne/cm)$	46.1	46.1
Bond Number	2.5×10^{-4}	2.5×10^{-4}

A LBM simulation of this counter-current displacement is performed by choosing a two dimensional 200 × 200 sized lattice grid. Some lattices in the grid are randomly assigned to be solid lattices, so that a porous medium analogous to the experimental set-up is created. An average distance of 3 lattices is maintained between any two solid lattices in order to perform a stable LBM simulation. The three boundaries of the computational domain are assumed to be closed and a channel flow with a width of 10 lattice units is maintained at the inlet boundary. This channel can be assumed to be a fracture in contact with the porous matrix. The lattice porous system is shown in Fig. 7.3. The fracture channel has an inlet and outlet in order to maintain a supply of water, which also expels the displaced kerosene from the system. The distribution functions in the pore lattices are assigned to be that

of kerosene; and the ones in the fracture and the solid boundaries to be that of water. In order to obtain a realistic comparison of saturation areas (fractions of the porous matrix occupied by both phases) of the experimental system and the numerical solutions, the values used in the LBM simulations are scaled from the experimental data using an appropriate dimensional analysis, which has been described in section 6.1.3. A viscosity ratio of 3 is maintained in accordance with the physical values. The time scale used in these simulations is adopted from the following correlation given by Ma et. al. [73]:

$$ t_D = t \sqrt{\frac{k}{\phi} \frac{\sigma_{o-w}}{\sqrt{\mu_w \mu_o}} \frac{1}{L_c^2}} \tag{7.1} $$

Here, t_D is the dimensionless time, k is the absolute permeability, ϕ is the porosity, σ_{o-w} is the oil-water interfacial tension, μ_w and μ_o are the viscosities of water and oil, respectively. The characteristic length L_c, is considered to be the average size of a solid grain, and k is the the absolute permeability of the physical system calculated by using the Kozeny-Carman relation [74]. The time required for the complete displacement of oil is $t = 120\ min$. Based, on Eq. 7.1, the corresponding lattice time t_l is 2.5×10^5. Initial simulations showed an accumulation of displaced oil in the fracture channel which prevented the further imbibition of water in the porous medium. Hence, for the oil to be removed from the porous matrix, a velocity inlet is maintained at the fracture inlet. Interpolated bounce-back scheme is used for the solid boundaries of the grains within the porous matrix.

LBM simulation is performed for the calculated lattice parameters and the evolution of the oil-water interface is studied at different time steps. The resident kerosene is observed to be displaced by the water in the fracture due to capillary imbibition. Water enters the porous matrix through the smaller pores and displaces the kerosene through the relatively larger pores into the fracture, which is further convected out of the porous matrix through the fracture at the outlet. Figure 7.4(a) shows the oil-water interface development in the system after $1.2\ mins$. A section is selected at the fracture-matrix boundary in order to observe the imbibition process in the pore-scale, which is shown in Fig. 7.4(b). It can be observed that the capillary imbibition of water takes place through smaller pores (regions with relatively small distance between solid grains) and corresponding kerosene is displaced out through the larger pores. Such simultaneous displacements of kerosene and water through
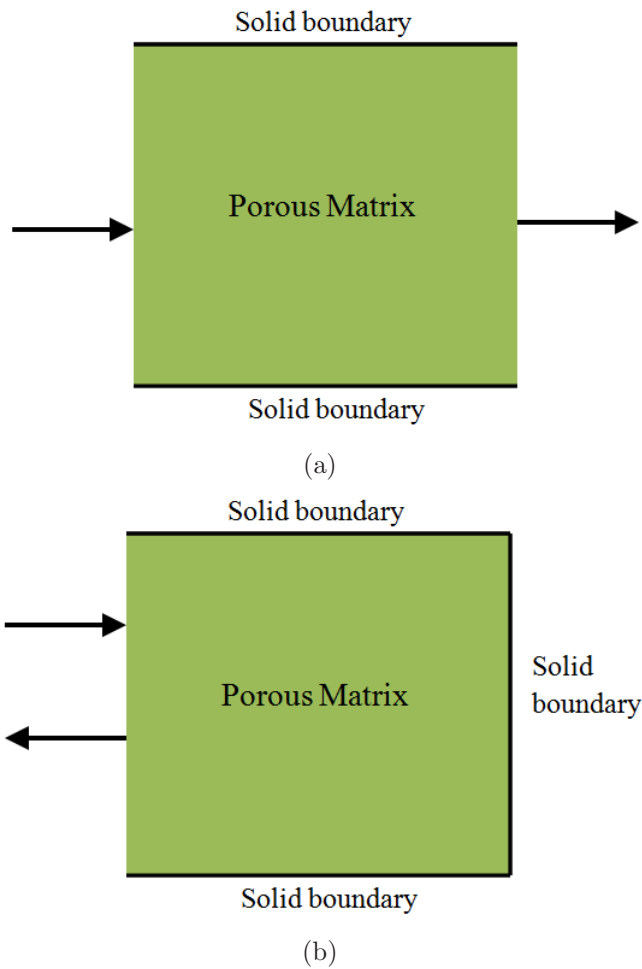
Figure 7.1: (a) A schematic showing a typical co-current displacement system. The wetting phase enters the porous matrix from one boundary and displaces the resident phase from the opposing one. (b) A schematic showing a typical counter-current displacement system. The wetting and resident phases enter and exit out of the porous matrix from the same boundary, since all the other boundaries are closed.

the same boundary maintains mass conservation of the overall porous matrix.

Similar observation can be made in Fig. 7.5, which shows a velocity vector plot for the selected section, shown in Fig. 7.4(a). The vectors denote the direction of bulk fluid velocity, however the size of the individual vectors does not scale with the velocity magnitude. The selected section involves a relatively large pore (pore 1) beside a series of smaller pores (pores 2, 3, 4, and 5). The velocity vectors for pore 5 represents water imbibition into the porous matrix. Similar, observations can be made for pores 4, 3 and 2, where the
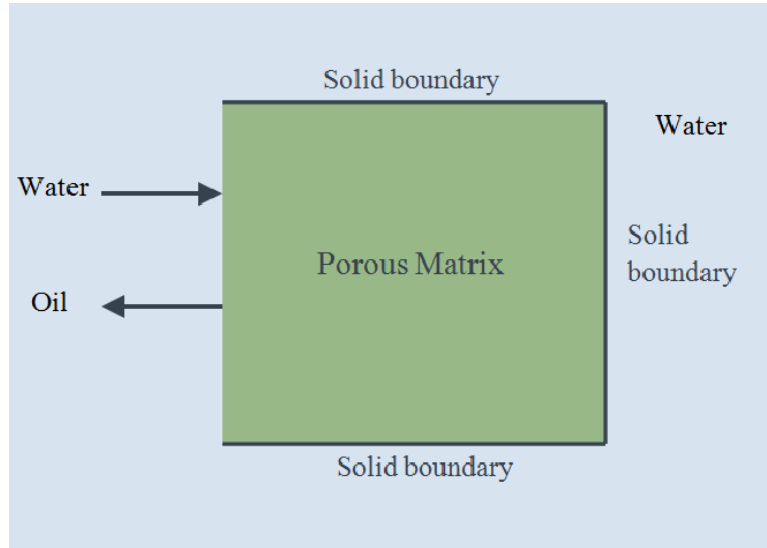
Figure 7.2: Schematic showing the configuration of experiments [5] involving counter-current displacement of kerosene from a horizontal sand pack by water acting as wetting phase. The porous matrix is initially saturated with kerosene and then immersed in water.

velocity vectors point towards a dominant in-flow of water in these small pores. However, for the pore 1 it is observed that the velocity vectors are steadily directed out of the matrix into the fracture. This indicates that the kerosene is expelled from a relatively large pore. This can also be verified from the oil-water interface in Fig. 7.4(b) which shows kerosene (red) accumulated in the fracture from pore 5, in contrast to water entering from the adjacent pores. These observations are qualitatively similar to the displacement process observed by Rangel-German and Kovscek [24]. The present simulation shows that the flow is reversing its direction, along with the formation of a large number of re-circulations in the porous matrix which is a typical characteristic of the counter-current displacement process.

Figures 7.6(a) and 7.6(b) show the interface developments for the whole fracture-matrix system at $t = 30 \ mins$ and $t = 60 \ mins$. The gradual flooding of the porous medium by water with the expulsion of kerosene from the fracture outlet can be observed. The water saturation eventually forms a single finger-like profile which reaches the opposite boundary and starts the reverse displacement of kerosene from the pore to the fracture.

In order to obtain qualitative validation of the capillary displacement simulated by the LBM model, the obtained displacement profiles are compared
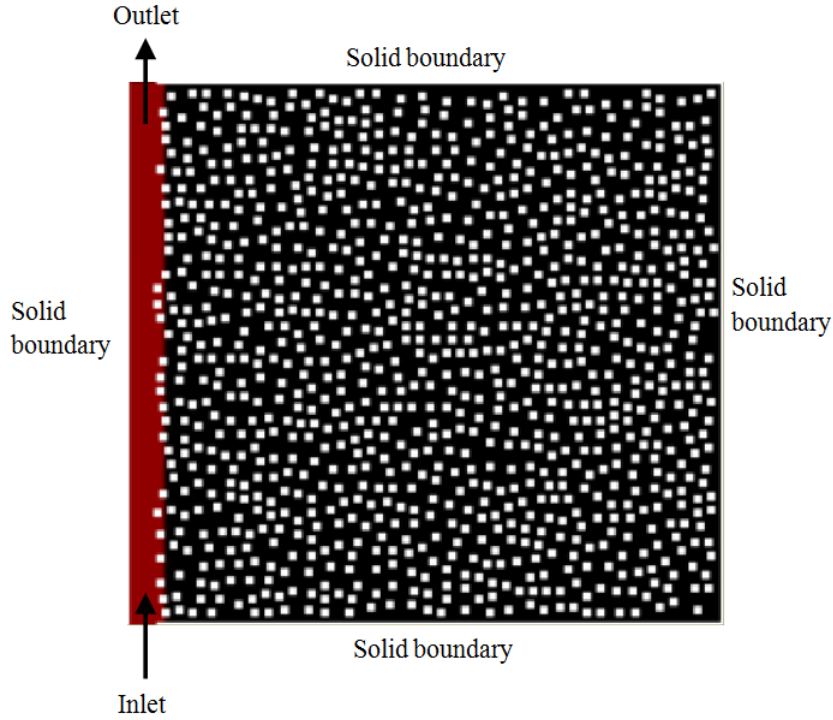
Figure 7.3: The lattice porous system for counter-current simulation. The pores are initially saturated with kerosene (black) with water (red) lying in a fracture in contact with the porous matrix. White color denotes the solid grains, which are randomly generated. A constant velocity is maintained at the fracture inlet in order to keep a continuous supply of water and expel the displaced kerosene from the fracture.

with the core-scale experimental results. Figure 7.7 shows a comparison of the simulated displacement profiles with the experimental profiles at different time steps. The experimental results show a finger-like growth of the imbibing water entering the matrix in a non-uniform manner whereby displacing the kerosene. A similar profile can be found in the later stages of the LBM simulation (after 50 *mins*) where a finger-like profile in the center and the displacement of kerosene from either side are observed. Further matching of the simulated profiles with the experimental data can be realized accurately if an exact representation of the physical porous media is used for the simulation.

An additional LBM simulation of the counter-current displacement process is performed for a larger porous medium of dimension 10 *cm* × 10 *cm* using similar physical properties as in the previous one. The capillary displacement profiles at different water saturations are shown in Fig. 7.8. Here, the water saturation, S_w, in the porous matrix is calculated as:

(a)   (b)
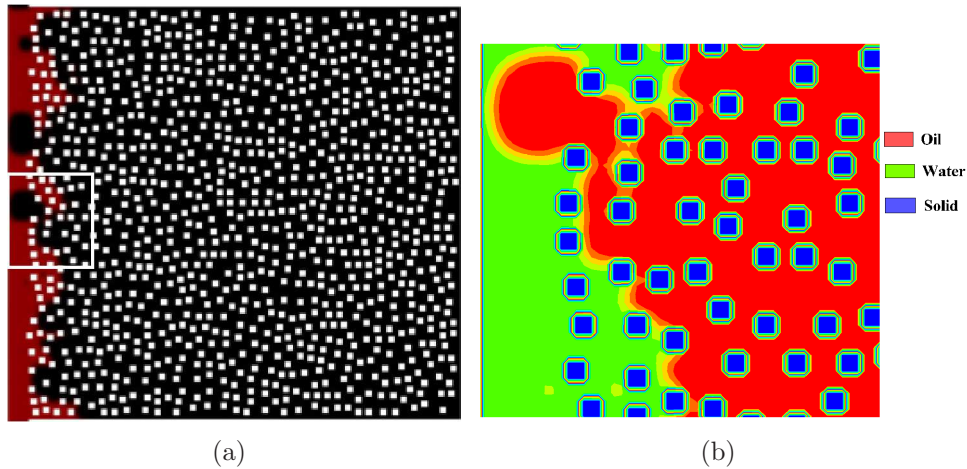
Figure 7.4: (a) Oil-water interface development at $t = 1.2\ mins$. Water (red) imbibes into the porous matrix due to capillary forces and resident kerosene (black) is displaced out. A section is chosen to observe the interface development in the pores. (b) Pore-scale representation of the oil-water interface in the selected section. It can be observed that water (green) imbibes into the porous matrix through small pores, while kerosene (red) is displaced from a large pore i.e., a region with a relatively large distance between the solid grains.

$$S_w = \frac{n_{lp,w}}{n_{lp}} \tag{7.2}$$

where $n_{lp,w}$ is the number of pore lattices occupied by water phase, and n_{lp} is the total number of pore lattices. It can be observed that the interfacial development in the porous matrix is more uniform in nature compared to the previously simulated smaller porous medium. Similar observations were obtained by Bourbiaux and Kalaydjian [6], where they have observed a stable saturation growth for counter-current displacements in a relatively large porous medium.

7.2   Relative permeability analysis

A two-phase relative permeability curve was obtained for the counter-current simulations based on the method described in section 6.2. The relative permeability curves for the $5\ cm \times 5\ cm$ porous medium are shown in Fig. 7.9. In case of counter-current displacement, the relative permeability curves show
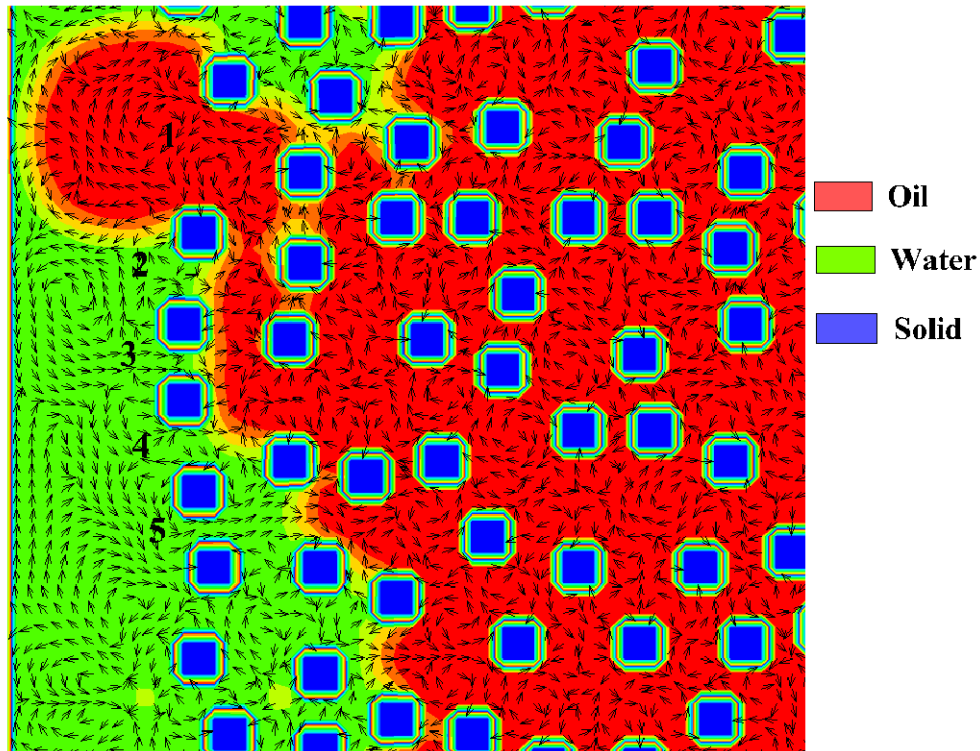
Figure 7.5: A plot of velocity vectors in a countercurrent displacement corresponding to the enlarged section shown in Fig. 7.4(a). Displacement of kerosene (red) takes place by water (green).

a gradual increasing trend for the wetting phase (water) and a concave trend for the non-wetting phase (kerosene). The oil relative permeability increases with S_w up to a certain point (peak point) and then decreases steadily. Similar trends were observed for co-current displacement in Chapter 6. A quantitative comparison between the relative permeability values of the non-wetting phase (kerosene) shows that the values for the counter-current case are approximately 50 % that of the corresponding co-current case. This can be explained by the fact that the capillary pressure, which is calculated in an empirical manner, is numerically same for both the process. However, in a co-current displacement process, the non-wetting phase has the flexibility to move towards the two open boundaries of the porous medium, causing simultaneous displacements from both the boundaries. This movement is restricted to only one boundary in the counter-current case, which results in diminished velocity values for the same capillary pressure and hence reduced relative permeabilities. Thus, the location of the peak point in the relative permeability curve is dictated by the boundary opposite to the inlet of the porous matrix.
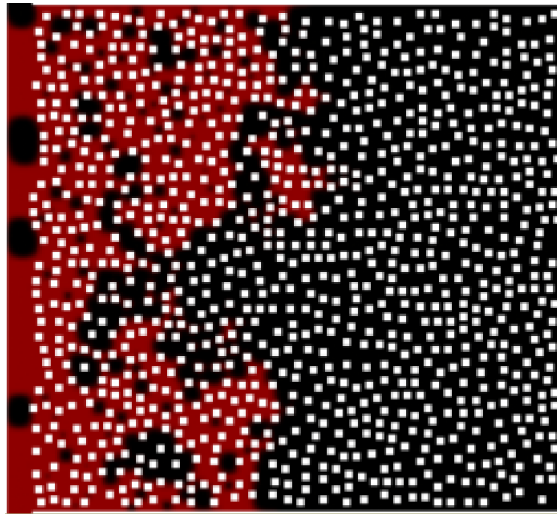
(a)
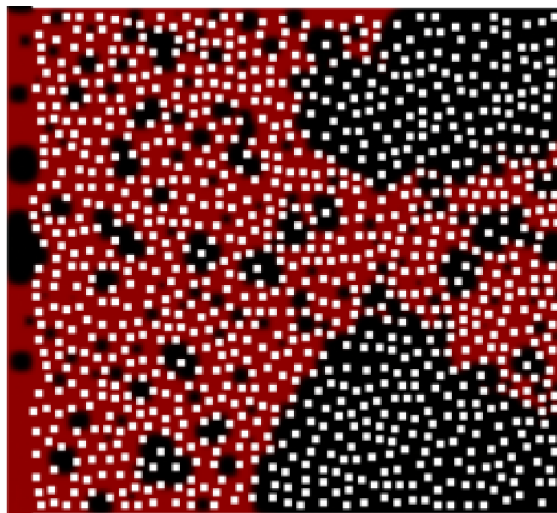
(b)

Figure 7.6: (a) Oil-water interfacial profile in the counter-current displacement of kerosene (black) by water (red) at $t = 30\ mins$. (b) Oil-water interfacial profile at $t = 60\ mins$.

It can be observed from Fig. 7.9 that the oil relative permeabilities are profoundly affected by the boundary conditions compared to the water relative permeabilities. Counter-current interaction significantly reduces the oil permeability for the same rock and fluid properties, whereas the effect on water relative permeabilities is much less pronounced. Bourbiaux and Kalydjian [6] observed a similarly significant reduction in oil relative permeability in counter-current case compared to the co-current case. However, they observed
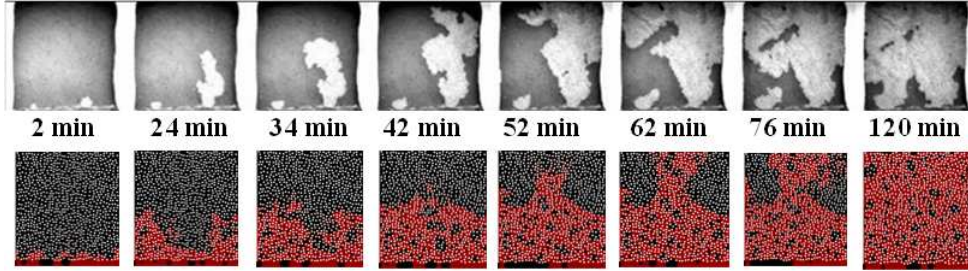
Figure 7.7: Comparison of saturation profiles for horizontal counter-current displacement process from experimental and simulation results at equal time instants in a 5 cm × 5 cm porous matrix. Upper snapshots show the saturation profiles of oil(dark) and water(light) obtained from experiments in literature [5], while the lower snapshots show profiles of oil(black) and water(red) obtained from LBM simulations. Both the profiles show a reasonable agreement. The finger-like displacement profile encountered in the experimental case is seen in the LBM simulation in later saturation stages (after 50 $mins$).

a decrease in the water relative permeability as well. The water relative permeability is found to increase for counter-current displacement in this case, though the relative change is insignificant.

Further relative permeability curves are plotted for different values of contact angles and interfacial tensions for the 5 cm × 5 cm porous medium, which are shown in Figs. 7.10(a) and 7.10(b). It can be observed that the relative permeability increases with the increase in the equilibrium contact angle for the wetting phase. It is also found that the relative permeability increases with the decrease in the interfacial tension. This is similar to the trends observed for co-current displacement, which has been recently reported by the authors [75].

7.3   Conclusion

The presented work involves a pore-scale analysis of interface development and saturation profile for a capillary driven counter-current displacement process in a two-dimensional fracture porous matrix using the Lattice Boltzmann method (LBM). The LBM model is validated against the core-scale experimental data related to the displacement of kerosene by water for a water wet sand pack. The LBM model uses the two-color method developed by Latva-Kokko and Rothman [9] [3] to simulate the multi-phase capillary driven flow in a randomly generated porous lattice system. The kerosene-water interface is

S_w=0.1 S_w=0.2 S_w=0.3 S_w=0.4 S_w=0.5 S_w=0.6
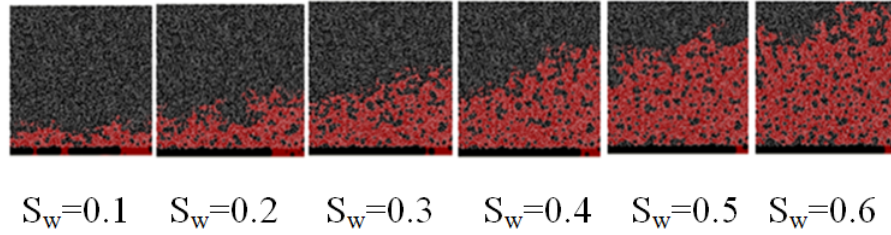
Figure 7.8: Saturation profiles for a horizontal counter-current displacement of oil(black) by water(red) from LBM simulation in a 10 cm × 10 cm porous matrix for different water saturation values. Upper snapshots show the saturation profiles of oil(dark) and water(light) obtained from experiments [5], while the lower snapshots show profiles of oil(black) and water(red) obtained from LBM simulations. Water saturation profile shows a very stable growth as observed in literature [6].

obtained at the pore scale in order to study the mechanism of counter-current displacement in such cases. The saturation profiles are studied at the core-scale and compared with those obtained from experiments. Further, a relative permeability analysis is performed by plotting the curves for both phases and compared with the corresponding co-current displacement process. The major conclusions made are:

- Counter-current displacement process takes place in a kerosene saturated water-wet porous matrix by the capillary imbibition of water through smaller pores and the simultaneous displacement of kerosene through the relatively larger pores.

- Core-scale comparison of the saturation profiles of both phases between the simulation and the experiments shows a reasonable agreement in terms for the displaced volume of kerosene. The experimental results show the displacement in the form of a finger-like profile of imbibing water, which can be observed in the LBM simulations at a later time instant (after 50 $mins$).

- A counter-current simulation performed for a larger porous medium (10 cm × 10 cm) shows a stable saturation growth as compared to the co-current process.

- Relative permeability trends for the wetting and non-wetting phases in counter-current displacement are similar to those in co-current displacement. The relative permeability of non-wetting (oleic) phase shows a
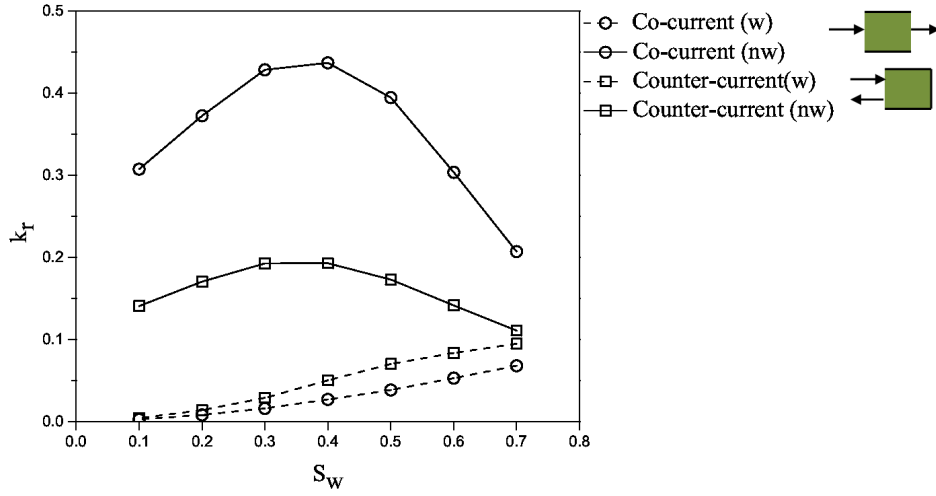
Figure 7.9: Two-phase relative permeability analysis of counter-current displacement process. Here, w and nw refer to the wettable (water) and non-wettable (kerosene) phases, respectively. k_r is the relative permeability with respect to wetting or non-wetting phase as per the given conditions. The relative permeability values for the non-wetting phase are approximately 50 % of the corresponding values for the co-current case.

concave nature i.e., initial increase followed by a subsequent decrease. Such a trend can be explained by the fact that the resident oil is displaced more easily in the initial water saturation stages till the peak of the relative permeability curve, after which the presence of water hinders further displacement of the trapped oil. However, the relative permeability value of the non-wetting phase in counter-current displacement case is significantly reduced (approx. 50 %) as compared to the corresponding value for the co-current displacement case. Similar reduction has been observed in literature [6]. The relative permeability value of the wetting phase for the counter-current case is greater than the corresponding value for the co-current case, but the change is not significant.

- The relative permeability increases with an increase in the equilibrium contact angle for the wetting phase. It is also found that the relative permeability increases with the decrease in the interfacial tension. This trend is similar to the case of co-current displacement process.

The LBM simulations provide valuable insight to the pore-scale counter-current capillary displacement process in fractured porous matrix. With the

advances in experimental techniques, such pore-scale velocity simulations can be compared with the pore-scale experimental data [76].
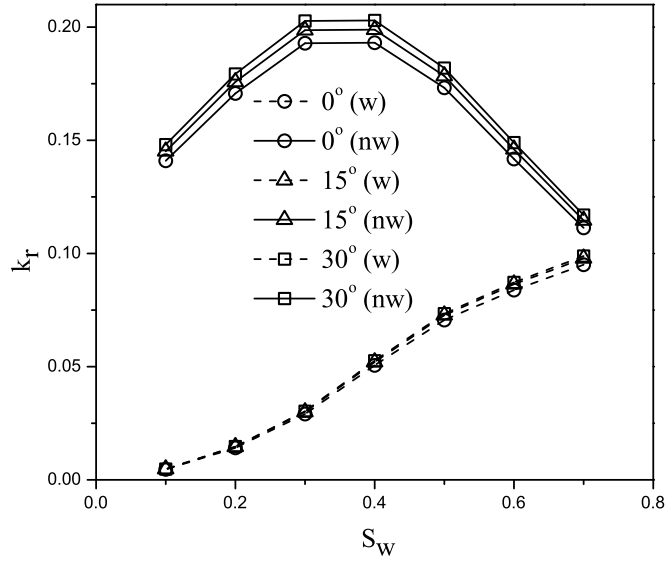
(a)
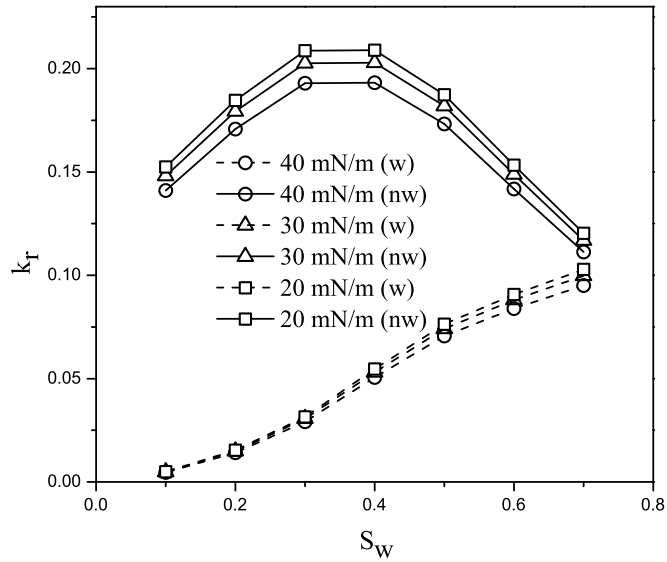
(b)

Figure 7.10: Two-phase relative permeability analysis of counter-current displacement process for different (a) equilibrium contact angles and (b) interfacial tensions. Here, w and nw refer to the wettable (water) and non-wettable (kerosene) phases, respectively. k_r is the relative permeability with respect to wetting or non-wetting phase as per the given conditions.

Chapter 8

Conclusions and future work

In the presented work, multi-phase flow simulations of solvent diffusion and spontaneous imbibition oil recovery processes were carried out using LBM. The developed LBM models used randomly generated porous structures to represent sand packs. The major conclusions of the simulations are given below:

8.1 Solvent diffusion process

- The LBM algorithm was found to be computationally stable for the viscosity ratios encountered in the fluids used for the simulations (3.0 to 25.0).

- For the simulations performed for static conditions, the areas swept by the pentane in the porous matrix with time were in reasonable agreement with those obtained from corresponding experiments in literature [1]. However, the non-uniform nature of the diffusion front observed in the experimental results was not reproduced in the simulations.

- For the simulations performed under dynamic conditions, the saturation profiles of pentane in the pore matrix were found to be in excellent agreement in experiments from literature [2]. The time required for the recovery of light mineral oil was found to be more than that for kerosene, which can be explained by the difference in viscosities of the fluids. The simulations showed the tendency of lighter pentane to stay on top of the heavier oleic phases in case of vertically oriented sand pack. However, the LBM model did not show the finger formation observed in

the experiments. Though, the LBM provided provided a basis to study miscible oil recovery processes, a further development of the model is required to apply the model in practically relevant situations such as the injection of CO_2 and carbon sequestration.

8.2   Spontaneous imbibition process

- Though the model is naturally unsuitable to deal with fluids of different viscosities, a viscosity ratio of 3.0 for the two fluids was accommodated by assigning a value of 0.85 to the interface parameter.

- For the co-current case, pore-scale observations showed the imbibition of water in the pore matrix to displace kerosene. The interface development reflected the wettability of water (contact angle 0°), which gradually entered the porous medium by forming various concave meniscii on the solid grains. The non-uniform nature of the imbibition front lead to residual oil trapped in the pore regions.

- The saturation profiles of the phases were compared with experimental results from literature [5] for the gravity-assisted and gravity-opposed cases, and a reasonable agreement was observed in both.

- Relative permeability curves were obtained for both phases by determining the capillary pressure from an empirical formulation [18]. The relative permeabilities of kerosene (non-wetting) showed a concave trend, while those of water (wetting) increased with water saturation. The intersection of both the relative permeabilities was predicted for the higher water saturation values, which in an indicative of the capillary driven nature of the process [4]. The difference in the relative permeabilities was observed to decrease for a case with equal viscosities of both fluids.

- The gravity-assisted configuration showed the oil relative permeability curve to approach a linear nature, due to the action of gravitational pressure gradient. This change is also observed when the curves the plotted for different matrix orientations. The relative permeabilities of both phases were found to increase with contact angle and decrease with interfacial tension. The water relative permeability for a specific case of

porous matrix with high porosity showed a decrease in later water saturation stages, which was in agreement with an experimental observation from literature [4].

- In the simulations of counter-current displacement process, the water imbibition was observed to take place from relatively smaller pores, while the oil was expelled out of the matrix from larger pores. The core-scale observation showed a finger-like profile of water in later water saturation stages, which was absent in the case of a larger porous matrix (10 cm × 10 cm). The relative permeability curves showed a similar trend when compared with co-current case, but the values were significantly reduced for oil. The relative permeability showed an increase with contact angle and a decrease with interfacial tension, analogous to the co-current case.

Further developments are possible by improving the LBM model and using actual porous structures for such simulations.

8.3   Contributions

The major contributions of the performed work are listed below:

- The performed work uses a Lattice Boltzmann framework to capture the pore-scale physical interaction of two fluids in a porous medium, which can be used to study miscible and immiscible oil recovery from fractured porous media. A methodology to determine the relative permeability for the spontaneous imbibition process is proposed, which is found to reflect the physical conditions of the porous matrix and fracture, and can be used for field-scale oil-recovery predictions.

- The developed LBM model is applied to simulate the counter-current spontaneous imbibition process and the complex interactions in this capillary driven displacement are successfully captured at the pore-scale, which leads to a further understanding of this oil-recovery mechanism.

8.4 Future work

Some of the recent and ongoing developments in the LBM and its application are described below:

- The LBM can be extended to model fluid flow in three-dimensional domains by using the D3Q15 and D3Q19 models described in Chapter 3. This model can be used to simulate the oil recovery processes from realistic three-dimensional rock structures. These simulations will aid in the understanding of pore-scale physical interactions. Also, they can be further extended to measure the relative permeabilities in different directions, and analyze the anisotropy in the relative permeability for different physical conditions [35] [40].

- Multiple relaxation times have been used in recent LBM simulations in the collision step, instead of a single viscosity-dependent relaxation time [64] [77]. The incorporation of this scheme makes the simulation more dynamic by calculating the relaxation time at each time step and has been found to increase the accuracy of the results.

- An inherent advantage of the LBM is that the collision step, which usually requires the most computational time, is spatially independent, i.e., the knowledge of variables in the adjacent lattices is not required for the application of collision equation at a particular lattice. This makes the LBM an excellent prospect for parallel computing, wherein the computation of the entire lattice grid can be distributed to multiple processing systems. However, this advantage is reduced in the case of multi-phase flow modeling, wherein the collision step involves the determination of fluid-fluid interface and hence, deals with calculations relating adjacent lattices. [78]

- An interesting technique to perform simulations in porous rocks is the application of multi-scale modeling techniques by using the LBM in conjunction with a macro-scale continuum model [79]. In this case, the core-scaled porous structure can be divided into zones and pore-scale simulations can be performed by LBM to find the rock properties for each zone. Then, a continuum model can be used to perform a macro-scale simulation of the entire structure by treating each zone as a single

element having properties determined from the LBM simulations. This approach can prove to be applicable in the case oil recovery simulations, since the size of flow domains has a wide range in these cases.

Bibliography

[1] C. U. Hatiboglu and T. Babadagli. Lattice-boltzmann simulation of solvent diffusion into oil-saturated porous media. *Physical Review E - Statistical, Nonlinear, and Soft Matter Physics*, 76(6), 2007.

[2] V. Er and T. Babadagli. Miscible interaction between matrix and fracture: A visualization and simulation study. *SPE Reservoir Evaluation and Engineering*, 13(1):109–117, 2010.

[3] M. Latva-Kokko and D. H. Rothman. Static contact angle in lattice boltzmann models of immiscible fluids. *Physical Review E - Statistical, Nonlinear, and Soft Matter Physics*, 72(4):1–7, 2005.

[4] J. M. Schembre and A. R. Kovscek. Direct measurement of dynamic relative permeability from ct monitored spontaneous imbibition experiments. pages 1351–1361, 2001.

[5] C. U. Hatiboglu and T. Babadagli. Pore-scale studies of spontaneous imbibition into oil-saturated porous media. *Physical Review E - Statistical, Nonlinear, and Soft Matter Physics*, 77(6), 2008.

[6] B. J. Bourbiaux and F. J. Kalaydjian. Experimental study of cocurrent and countercurrent flows in natural porous media. volume SIGMA, pages 209–222 18283, 1988.

[7] E. G. Flekkoy. Lattice bhatnagar-gross-krook models for miscible fluids. *Physical Review E*, 47(6):4247–4257, 1993.

[8] A. K. Gunstensen, D. H. Rothman, S. Zaleski, and G. Zanetti. Lattice boltzmann model of immiscible fluids. *Physical Review A*, 43(8):4320–4327, 1991.

[9] M. Latva-Kokko and D. H. Rothman. Diffusion properties of gradient-based lattice boltzmann models of immiscible fluids. *Physical Review E - Statistical, Nonlinear, and Soft Matter Physics*, 71(5):1–8, 2005.

[10] G. A. Pope. The application of fractional flow theory to enhanced oil recovery. *SOC. PET. ENGRS. J.*, 20(3 , Jun. 1980):191–205, 1966.

[11] P. Biggs and C.A. Koch. Waterflooding of oilfields in wyoming to 1968. *U S Bur Mines, Rep Invest 7469*, 1970.

[12] F.F. Craig. *The reservoir engineering aspects of waterflooding.*, volume 3 of the Henry L. Doherty Ser.). 1971.

[13] N. Mungan. Enhanced oil recovery using water as a driving fluid. *World Oil*, 193(4), 1981.

[14] V.Y. Konoplyov and A.F. Zazovsky. Numerical simulation of oil displacement in pattern floods with fractured wells. volume Sigma, pages 481–488, 1991.

[15] N. Hadia, L. Chaudhari, S. K. Mitra, M. Vinjamur, and R. Singh. Experimental investigation of use of horizontal wells in waterflooding. *Journal of Petroleum Science and Engineering*, 56(4):303–310, 2007.

[16] V. Santhosh, S.K. Mitra, M. Vinjamur, and M.S. Kumar. Flow visualization of waterflooding with horizontal and vertical wells. *Petroleum Science and Technology*, 26(15):1835–1851, 2008.

[17] Y. Ghomian, G.A. Pope, and K. Sepehrnoori. Reservoir simulation of co2 sequestration pilot in frio brine formation, usa gulf coast. *Energy*, 33(7): 1055–1067, 2008.

[18] I. Fatt. Application of the network model to gas diffusion in moist porous media. *Science*, 131(3394):158–159, 1960.

[19] M.J. Blunt. Flow in porous media - pore-network models and multiphase flow. *Current Opinion in Colloid and Interface Science*, 6(3):197–207, 2001.

[20] A.C. Gunde, B. Bera and S.K. Mitra. Investigation of water and co_2 (carbon dioxide) flooding using micro-ct (micro-computed tomography)

images of berea sandstone core using finite element simulations. *Energy*, 35(12):5209–5216, 2010.

[21] C.C. Mattax and J.R. Kyte. Imbibition oil recovery from fractured, water-drive reservoir. *Society of Petroleum Engineers Journal*, 1962.

[22] T. Babadagli. Dynamics of capillary imbibition when surfactant, polymer, and hot water are used as aqueous phase for oil recovery. *Journal of Colloid and Interface Science*, 246(1):203–213, 2002.

[23] P. V. Indel'man and R. M. Katz. On countercurrent capillary imbibition in a hydrophilic porous medium. *Fluid Dynamics*, 15(2):290–293, 1980.

[24] E. R. Rangel-German and A. R. Kovscek. A micromodel investigation of two-phase matrix-fracture transfer mechanisms. *Water Resources Research*, 42(3), 2006.

[25] D. Silin and T. Patzek. On barenblatt's model of spontaneous counter-current imbibition. *Transport in Porous Media*, 54(3):297–322, 2004.

[26] M. Zeybek, G. Gurakin, A. Donmez, and M. Onur. Effects of capillary heterogeneities on spontaneous imbibition. volume Sigma, pages 779–793, 1995.

[27] H. Behbahani and M. J. Blunt. Analysis of imbibition in mixed-wet rocks using pore-scale modelling. *SPE Journal*, 10(4):466–473, 2005.

[28] E. Unsal, G. Mason, N. R. Morrow, and D. W. Ruth. Co-current and counter-current imbibition in independent tubes of non-axisymmetric geometry. *Journal of Colloid and Interface Science*, 306(1):105–117, 2007.

[29] K. S. Schmid, S. Geiger, and K. S. Sorbie. Semianalytical solutions for cocurrent and countercurrent imbibition and dispersion of solutes in immiscible two-phase flow. *Water Resources Research*, 47(2), 2011.

[30] L. W. Holm. Status of CO_2 and hydrocarbon miscible oil recovery methods. *JPT, Journal of Petroleum Technology*, 28:76–84, 1976.

[31] L. Paterson. Fingering with miscible fluids in a hele shaw cell. *Physics of Fluids*, 28(1):26–30, 1985.

[32] A. Danesh, D. Krinis, G. D. Henderson, and J. M. Peden. Pore-level visual investigation of miscible and immiscible displacements. *Journal of Petroleum Science and Engineering*, 2(2-3):167–177, 1989.

[33] J. Trivedi and T. Babadagli. Scaling miscible displacement in fractured porous media using dimensionless groups. *Journal of Petroleum Science and Engineering*, 61(2-4):58–66, 2008.

[34] A.C. Gunde, T. Babadagli and S.K. Mitra Lattice-boltzmann method to estimate relative permeabilities for matrix-fracture interaction in naturally fractured reservoirs. *SPE Eastern Regional Meeting*, 138255-MS, 2010.

[35] T. Ramstad, P. Oren, and S. Bakke. Simulation of two-phase flow in reservoir rocks using a lattice boltzmann method. *SPE Journal*, 15(4): 923–933, 2010.

[36] S. Wolfram. Cellular automaton fluids 1: Basic theory. *Journal of Statistical Physics*, 45(3-4):471–526, 1986.

[37] D. D'humiares and P. Lallemand. Lattice gas automata for fluid mechanics. *Physica A: Statistical Mechanics and its Applications*, 140(1-2): 326–335, 1986.

[38] G. R. McNamara and G. Zanetti. Use of the boltzmann equation to simulate lattice-gas automata. *Physical Review Letters*, 61(20):2332–2335, 1988.

[39] S. Succi, R. Benzi, and F. Higuera. The lattice boltzmann equation: A new tool for computational fluid-dynamics. *Physica D: Nonlinear Phenomena*, 47(1-2):219–230, 1991.

[40] S. Succi, A. Cancelliere, C. Changa, E. Foti, M. Gramignani, and D. Rothman. Direct computation of the permeability of three-dimensional porous media. pages 129–136, 1990.

[41] R. Benzi, S. Succi, and M. Vergassola. The lattice boltzmann equation for turbulence. *Nuclear Physics B (Proceedings Supplements)*, 17(C):708–711, 1990.

[42] Y. Qian, D. d'Humiares, and P. Lallemand. Diffusion simulation with a deterministic one-dimensional lattice-gas model. *Journal of Statistical Physics*, 68(3-4):563–573, 1992.

[43] P. L. Bhatnagar, E. P. Gross, and M. Krook. A model for collision processes in gases. i. small amplitude processes in charged and neutral one-component systems. *Physical Review*, 94(3):511–525, 1954.

[44] S. Succi, D. d'Humiares, Y. Qian, and S. A. Orszag. On the small-scale dynamical behavior of lattice bgk and lattice boltzmann schemes. *Journal of Scientific Computing*, 8(3):219–230, 1993.

[45] S. Succi. Lattice boltzmann equation: Failure or success? *Physica A: Statistical Mechanics and its Applications*, 240(1-2):221–228, 1997.

[46] D. H. Rothman. Cellular-automaton fluids: A model for flow in porous media. *Geophysics*, 53(4):509–518, 1988.

[47] S. Chen, Z. Wang, X. Shan, and G.D. Doolen. Lattice boltzmann computational fluid dynamics in three dimensions. *Journal of Statistical Physics*, 68(3-4):379–400, 1992.

[48] E. Aharonov and D. H. Rothman. Non-newtonian flow (through porous media): a lattice-boltzmann method. *Geophysical Research Letters*, 20 (8):679–682, 1993.

[49] D.W. Grunau, T. Lookman, S.Y. Chen, and A.S. Lapedes. Domain growth, wetting, and scaling in porous media. *Physical Review Letters*, 71(25):4198–4201, 1993.

[50] B. Ferreol and D. H. Rothman. Lattice-boltzmann simulations of flow through fontainebleau sandstone. *Transport in Porous Media*, 20(1-2): 3–20, 1995.

[51] A.W.J. Heijs and C.P. Lowe. Numerical evaluation of the permeability and the kozeny constant for two types of porous media. *Physical Review E*, 51(5):4346–4352, 1995.

[52] R.S. Maier, D.M. Kroll, H.T. Davis, and R.S. Bernard. Simulation of flow in bidisperse sphere packings. *Journal of Colloid and Interface Science*, 217(2):341–347, 1999.

[53] N.S. Martys and H. Chen. Simulation of multicomponent fluids in complex three-dimensional geometries by the lattice boltzmann method. *Physical Review E - Statistical Physics, Plasmas, Fluids, and Related Interdisciplinary Topics*, 53(1 SUPPL. B):743–750, 1996.

[54] R.D. Hazlett, S.Y. Chen, and W.E. Soll. Wettability and rate effects on immiscible displacement: Lattice boltzmann simulation in microtomographic images of reservoir rocks. *Journal of Petroleum Science and Engineering*, 20(3-4):167–175, 1998.

[55] E. Eker and S. Akin. Lattice boltzmann simulation of fluid flow in synthetic fractures. *Transport in Porous Media*, 65(3):363–384, 2006.

[56] A.S. Joshi, K.N. Grew, A.A. Peracchio, and W.K.S. Chiu. Lattice boltzmann modeling of 2d gas transport in a solid oxide fuel cell anode. *Journal of Power Sources*, 164(2):631–638, 2007.

[57] J. Park, M. Matsubara, and X. Li. Application of lattice boltzmann method to a micro-scale flow simulation in the porous electrode of a pem fuel cell. *Journal of Power Sources*, 173(1):404–414, 2007.

[58] M.A. van Doormaal and J.G. Pharoah. Determination of permeability in fibrous porous media using the lattice boltzmann method with application to pem fuel cells. *International Journal for Numerical Methods in Fluids*, 59(1):75–89, 2009.

[59] Q. Kang, P. C. Lichtner, H. S. Viswanathan, and A. I. Abdel-Fattah. Pore scale modeling of reactive transport involved in geologic co_2 sequestration. *Transport in Porous Media*, 82(1):197–213, 2010.

[60] D.H. Rothman and J.M. Keller. Immiscible cellular-automaton fluids. *Journal of Statistical Physics*, 52(3-4):1119–1127, 1988.

[61] B. Dong, Y.Y. Yan, W. Li, and Y. Song. Lattice boltzmann simulation of viscous fingering phenomenon of immiscible fluids displacement in a channel. *Computers and Fluids*, 39(5):768–779, 2010.

[62] J. Tolke, M. Krafczyk, M. Schulz, and E. Rank. Lattice boltzmann simulations of binary fluid flow through porous media. *Philosophical Transactions of the Royal Society A: Mathematical, Physical and Engineering Sciences*, 360(1792):535–545, 2002.

[63] J. G. Zhou. A lattice boltzmann method for solute transport. *International Journal for Numerical Methods in Fluids*, 61(8):848–863, 2009.

[64] H. Yoshida and M. Nagaoka. Multiple-relaxation-time lattice boltzmann model for the convection and anisotropic diffusion equation. *Journal of Computational Physics*, 229(20):7774–7795, 2010.

[65] R.L. Panton. *Incompressible flow*. Wiley-India, 2006.

[66] J.H. Ferziger and M. Peric. *Computational methods for fluid dynamics*, volume 2. Springer Berlin, 1999.

[67] W.F. van Gunsteren and Berendsen. Computer simulation of molecular dynamics: Methodology, applications, and perspectives in chemistry. *Angewandte Chemie International Edition in English*, 29(9):992–1023, 1990.

[68] E.S. Oran, C.H. Oh, and B.Z.Cybyk. Direct simulation monte carlo: Recent advances and applications 1. *Annual Review of Fluid Mechanics*, 30(1):403–441, 1998.

[69] A. A. Mohamad. *Applied lattice Boltzmann method for transport phenomena, momentum, heat and mass transfer*. Sure Print, 2007.

[70] S. Succi. *The Lattice Boltzmann Equation: For Fluid Dynamics and Beyond*. Clarendon Press, 2001.

[71] Dieter A. Wolf-Gladrow. *Lattice-Gas Cellular Automata and Lattice Boltzmann Models: An Introduction*. Springer, 2000.

[72] C. Pan, L. S. Luo, and C. T. Miller. An evaluation of lattice boltzmann schemes for porous medium flow simulation. *Computers and Fluids*, 35 (8-9):898–909, 2006.

[73] S. Ma, N. R. Morrow, and X. Zhang. Generalized scaling of spontaneous imbibition data for strongly water-wet systems. *Journal of Petroleum Science and Engineering*, 18:165–178, 1997.

[74] G. Jin, T. W. Patzek, and D. B. Silin. Direct prediction of the absolute permeability of unconsolidated and consolidated reservoir rock. pages 1287–1301, 2004.

[75] A. Gunde, T. Babadagli, and S. K. Mitra. A generic framework to obtain oil-water relative permeability for capillary driven transport in water-wet fractured porous media by lbm (submitted). *Water Resources Research.*

[76] D. Sen, D. Nobes, and S.K. Mitra. Optical measurement of pore scale velocity field inside micro porous media. *Microfluidics Nanofluidics*, 2011.

[77] X. Shan and H. Chen. A general multiple-relaxation-time boltzmann collision model. *International Journal of Modern Physics C*, 18(4):635–643, 2007.

[78] C. Pan, J. F. Prins, and C. T. Miller. A high-performance lattice boltzmann implementation to model flow in porous media. *Computer Physics Communications*, 158(2):89–105, 2004.

[79] R.I. Borja, J.T. Fredrich, J.A. White. Calculating the effective permeability of sandstone with multiscale lattice boltzmann/finite element simulations. *Acta Geotechnica*, 1(4):195–209, 2006.

Appendix A

A.1 LBM algorithm

The fluid flow simulations described in this work were computationally performed by the developed Lattice Boltzmann model using the FORTRAN 90 programming language. The algorithms of the single- and multi-phase LBM models are given in Figs. A.1 and A.2 respectively.
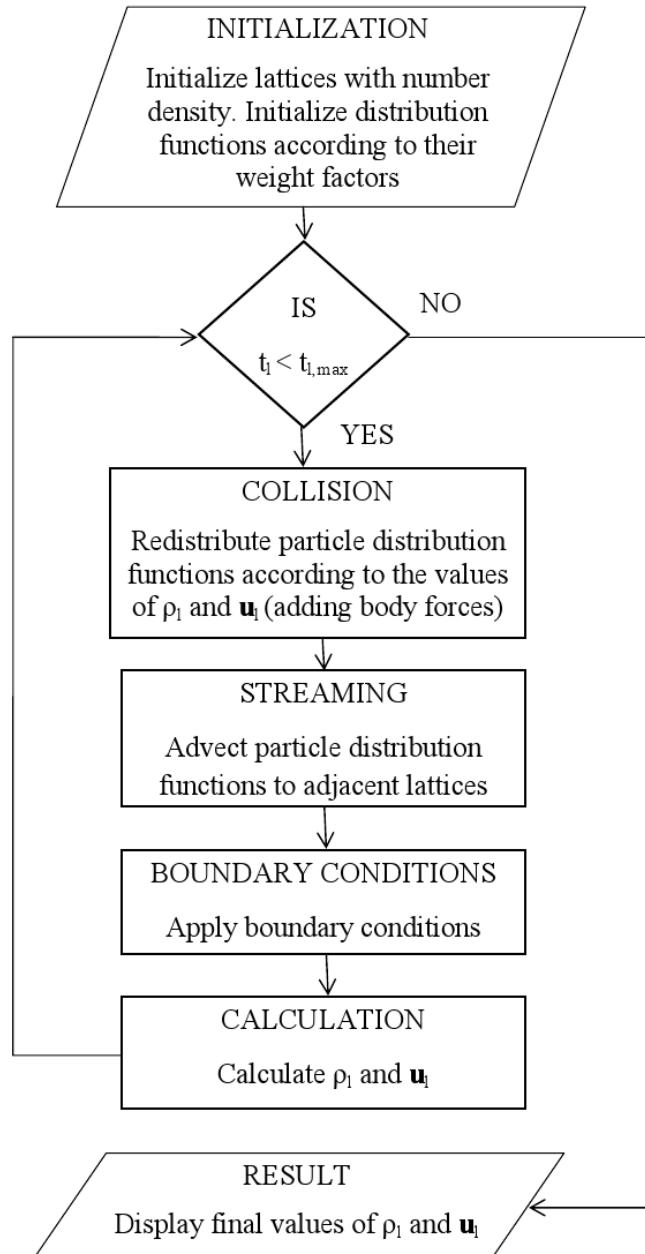
Figure A.1: Flowchart of single-phase LBM algorithm. Here, t_l is the current time step, t_l, max is the maximum number of time steps, ρ_l is the number density of the fluid, $\mathbf{u}_l$ is the velocity.
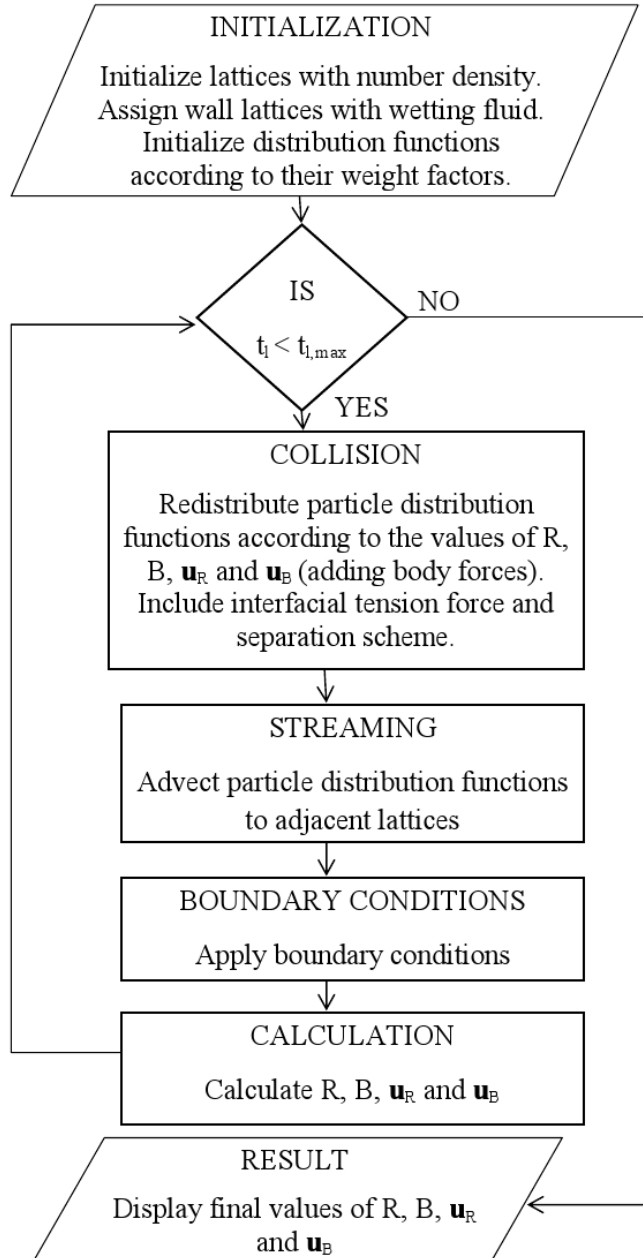
Figure A.2: Flowchart of immiscible multi-phase LBM algorithm. Here, t_l is the current time step, t_l, max is the maximum number of time steps, R (or B) is the number density of the Red (or Black) fluid, $\mathbf{u}_R$ (or $\mathbf{u}_B$) is the velocity of the Red (or Black) fluid.